A BASIS FOR MOLECULAR FACTORIES: MULTIFUNCTIONALITY AND IMMOBILIZATION OF BIOMOLECULE-POLYMER ASSEMBLIES

Inauguraldissertation

Zur Erlangung der Würde eines Doktors der Philosophie

vorgelegt der Philosophisch-Naturwissenschaftlichen Fakultät der Universität Basel

von

Viktoria Mikhalevich

aus

Deutschland

Basel, 2023

Genehmigt von der Philosophisch-Naturwissenschaftlichen Fakultät auf Antrag von

Prof. Dr. Wolfgang Meier und Prof. Dr. Corinne Nardin.

Basel, den 30.03.2021 Prof. Dr. Marcel Mayor, Dekan

Table of contents

Nothing in this world that's worth having comes easy.

-Dr. Kelso, Scrubs

Acknowledgements

I would like to use the opportunity and thank all the amazing people who supported me during this journey.

My deepest gratitude goes to my PhD supervisor Prof. Dr. Wolfgang Meier who gave me the opportunity to do my doctorate studies in his laboratory. Dear Wolfgang, thank you for your time and patience. You always gave me the opportunity to try out the weirdest ideas and that is not self-evident. I had a great time during my work.

A special thank goes to Prof. Dr. Cornelia G. Palivan, who has always supported me with her optimistic approach and great advices. Dear Cornelia, I greatly appreciate all your effort and never took you for granted. Without you, this thesis would not have worked out.

I am very grateful to Prof. Dr. Corinne Nardin for accepting to be my co-referee for this thesis, thank you very much!

In general, I would like to thank the committee for taking the time and reading this thesis.

I want to thank especially my family, my mom and the greatest brother, a woman can have. And of course, my heartfelt thanks to my grandparents and dad, who unfortunately haven´t lived long enough to witness my defense, but who are always in my heart.

A personal thank you to my close friends, who always have been there for me during these times and beyond and who grew very close to my heart: Amal Hasnaoui, Melisande Fischer, Christina Gabriel, Karolina Strauss, Sabrina Wilk, Isabel Borchert.

Of course, I want to thank all former and current team members of the Meier and Palivan groups, who were responsible for the nice working atmosphere.

Especially, my thanks goes to Justyna Haller (Kowal), who introduced me to the planar membranes and is my co-partner on two papers. Thank you, for being a friend. I wish you the best of luck!

My great co-author Camelia Draghici, who taught me so much, thank you! I owe you a lot and I appreciated working with you, your diligence, wisdom and patience.

Thanks also to my other co-authors who made the papers possible and to my students Alessia and Clemens who helped me during their internship.

Svetlana Stolarov, thank you for your company and friendship. It would not have been the same without you and I am very happy that I found a friend like you.

Thank you, Gesine Gunkel-Grabole, for your patient and smart advices. I hope that you are rocking Merck.

My heartfelt thanks to Saziye Yorulmaz for reading the thesis. Also, thanks to Martina Garni, Adi Dinu, Christina Zelmer, Anja Car, Luisa Zartner, Juan Wu and the ones, I might have forgotten to mention, but who supported me during the four years.

And finally, I want to thank the NCCR MSE and the Swiss National Science Foundation, not only for providing the financial support, but especially for the great courses and seminars I was allowed to attend. I met amazing fellow scientists, who taught me a lot.

List of Abbreviations

2D	two-dimensional
4-MP	4-methoxyphenol
ΔF_n	resonance frequency
ΔD_n	Energy Dissipation
AFM	atomic force microscopy
APTES	aminopropyltriethoxysilane
ATRP	atom transfer radical polymerization
BAM	Brewster angle microscopy
BCA	bicinchoninic acid (assay)
BSA	bovine serum abumin
CA	Contact angle
CLSM	confocal laser scanning microscopy
Đ	Dispersity
DMP	2,6-dimethoxyphenol
EM	electron microscopy
EPR	electron paramagnetic resonance
FITC	Fluoresceinisothiocyanat
FTIR	Fourier transform infrared spectroscopy
G	gaseous

GUVs	giant unilamellar vesicles
LB	Langmuir-Blodgett
LC	liquid-condensed
LE	liquid-expanded
LS	Langmuir-Schaefer
LSM	laser scanning microscopy
MBTH	3-methyl-2-benzothiazolinone hydrazone hydrochloride
MCOs	multicopper oxidases
Mw	molecular weight
PAA	poly(acrylic acid)
PB	poly(butadiene)
PBS	phosphate buffer saline
PDMAEMA	poly[(2-dimethylamino) ethyl methacrylate]
PDMS	poly(dimethylsiloxane)
PEG	poly(ethylene glycol)
(PEG-*b*-PMCL-*b*-PDMAEMA)	poly(ethylene glycol)-*block*-poly(γ-methyl-ε-caprolactone)-*block*-poly[(2-dimethylamino) ethyl methacrylate]
PEO	Poly(ethylene oxide)
PL	photoluminescence
PMOXA	poly(2-methyl oxazoline)

PMOXA-*b*- PDMS-b-PMOXA	poly(2-methyl-2-oxazoline) -block-poly(dimethylsiloxane)-*block*- poly(2-methyl-2-oxazoline)
PS	polystyrene
PS-b-PAA	polystyrene-b-poly(acrylic acid)
RMS	rough mean square
Ra	average roughness
S	solid
SDS	sodium dodecyl sulfate
Tg	glass transition temperature
QCM	Quartz crystal microbalance
QCM-D	Quartz Crystal Microbalance with dissipation
XPS	x-ray photoelectron spectroscopy

List of Publications/Reviews/Book Chapters

For some chapters, images and excerpts were used which have been published in the following publications:

- How do the properties of amphiphilic polymer membranes influence the functional insertion of peptide pores?

  A. Belluati, V. Mikhalevich, S. Yorulmaz Avsar, D. Daubian, I. Craciun, M. Chami, W. Meier, C.G. Palivan

  Biomacromolecules, 2020, 21(2), 701-715. (Shared first authorship)

- Functional Surfaces, Bio-hybrid Membranes for Biosensing

  C. Draghici, V. Mikhalevich, G. Gunkel-Grabole, J. Kowal, W. Meier, C. G. Palivan

  G.I.T. Laboratory Journal., 2019.

- Biomimetic Planar Polymer Membranes Decorated with Enzymes as Functional Surfaces

  C. Draghici, V. Mikhalevich, G. Gunkel-Grabole, J. Kowal, W. Meier, C. G. Palivan

  Langmuir., 2018, 34, 9015-9024. (Shared first authorship)

- Amphiphilic peptide self-assembly: Expansion to hybrid materials

  V. Mikhalevich, I. Craciun, M. Kyropoulou, C. G. Palivan, W. Meier

  Biomacromolecules, 2017, 18(11), 3471–3480.

- "Active surfaces" as Possible Functional Systems in Detection and Chemical (Bio) Reactivity

  C.E. Housecroft, C.G. Palivan, K. Gademann, W. Meier, M. Calame, X. Zhang, V. Mikhalevich, E. Piel, M. Szponarski, A. Wiesler, A. Lanzilotto, E.C. Constable, A. Fanget, R.L. Stoop

  Chimia, 2016, 6, 402-413.

- Chapter: Bio-inspired polymer membranes

  V. Mikhalevich, C. Zelmer, A. Car, C.G. Palivan, W. Meier, in ***Bio-inspired polymers***

  [Publisher: RSC Publishing, 2016, 221-258, ISBN 978-1-78262-413-4].

- Hybrid polymer-lipid films as platforms for directed membrane protein insertion

  J. Kowal, D. Wu, V. Mikhalevich, C.G. Palivan, W. Meier

  Langmuir, 2015, 31(17), 4868-4877.

List of Figures

Summary

Bio-inspired planar polymer membranes are synthetic membranes designed to be combined with biomolecules such as proteins, enzymes or peptides. These membranes provide both an increased mechanical stability as well as an environment to preserve the functionality of the biomolecules. In this thesis, two different kinds of planar membrane systems are demonstrated. In the first project, a sensor for phenolic compounds based on a bio-inspired polymer membrane was developed. Functional surfaces were generated by combining enzymes with polymer membranes composed of an amphiphilic, asymmetric block copolymer. Firstly, polymer films which were formed at the air-water interface were transferred onto silica solid support, by using the Langmuir-Blodgett method. The films were characterized according to their properties, including film thickness, wettability, topography, and roughness. The most promising membranes were used for enzyme attachment. Two model enzymes, laccase and tyrosinase, were adsorbed to the surface and their activity regarding the conversion of phenolic compounds was measured. This project is described in Chapter 1 in detail. In the second project, the interaction of the model pore-forming peptide melittin was studied in combination with a planar synthetic membrane. The investigation focused the interaction of melittin with amphiphilic block copolymer-based synthetic planar membranes as well as the insertion of melittin into these membranes to induce pore formation. Some specific molecular properties of the block copolymers and of the resulting membranes were selected for the investigation, such as hydrophilic to hydrophobic block ratio, membrane thickness and surface roughness. Through melittin addition to the synthetic membranes, melittin insertion requirements were better understood. This project is described in Chapter 2 in detail. Each chapter contains a separate introduction, material and methods section and conclusion and outlook specific to the project.

In summary, in this thesis the properties of different combinations and applications of polymer-based membranes with biomolecules were investigated to a deeper level.

1 Introduction

Within this chapter, different kinds of membranes will be presented, followed by preparation and investigation techniques.

1.1 Biological membranes

The biological membrane surrounds every living cell and separates the cell inside from the outside environment. In eukaryotic cells in addition to the outer membrane, numerous subcellular membranes can be found that divide the cytoplasm into multiple organelles, allowing different functions to occur in different parts of the cell. Many cellular processes are dependent on this semi-permeable barrier, such as intracellular metabolism. The membrane allows and regulates the traffic of nutrients and small molecules in and out of the cell and cellular compartments and is responsible for sensing the environment.[1] The consensual model to describe the membrane structure and its function is called as the "fluid mosaic model".[2] Formulated by Singer and Nicolson in 1972, this model describes membranes built up of lipids, proteins and carbohydrates (Figure 1). The main lipid membrane components are phospholipids. These molecules are amphiphilic, having a polar part attracted by water (hydrophilic) and a nonpolar component repelled by water (hydrophobic). When diluted in water, amphiphiles spontaneously assemble in the most thermodynamically stable molecular structure, namely the one that maximizes both hydrophilic and hydrophobic interactions.[3]

In this lipid bilayer, biological molecules, such as membrane proteins and glycoproteins, arrange depending on their chemical nature. Some proteins (integral) are embedded in the lipid bilayer matrix where they are able to establish hydrophobic and hydrophilic interactions with their respective lipid counterparts. Other proteins (peripheral), can also be associated with membrane surfaces through weaker interactions. In addition, carbohydrates can be parts of proteins or lipids, resulting in glycoproteins and glycolipids.[4]

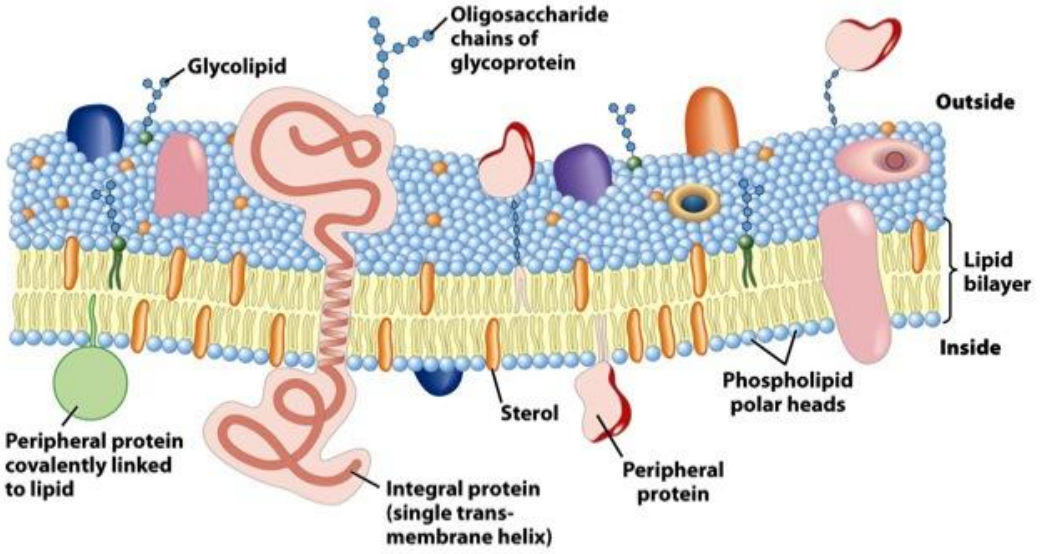

Figure 1. Fluid mosaic model of a cell membrane. [5]

An important characteristic of the membrane is its fluidity. In 2D fluids, individual biological molecules (both lipids and proteins) can rotate and move in lateral directions. This fluidity is a critical property of membranes and is determined by both temperature and lipid composition. For example, the interactions between shorter fatty acid chains are weaker compared to the ones between longer chains, so membranes containing shorter fatty acid chains are less rigid and can remain fluid at lower temperatures. Lipids containing unsaturated fatty acids similarly increase membrane fluidity because the presence of double bonds introduces kinks in the fatty acid chains, which makes them more difficult to be packed together.[6]

Membranes are currently of interest for many studies in order to understand the functions of membrane proteins and other membrane-related processes. For example, because transmembrane proteins are important targets for drugs. [7] A famous example is the drug

"Pantoprazole" which is a medication used for the treatment of several gastrointestinal diseases by inhibiting a proton pump and with that blocking the final step in gastric acid production.[8]

One of the current challenges is to reconstruct an artificial membrane with equal or even superior functionality to the biological membrane. While searching for new opportunities and investigating membrane-related processes, membrane mimics have been developed. Such artificial membranes can also find industrial applications, e.g., as filtering membranes, or as biosensors.[9, 10]

1.2 Biomimetic membranes

1.2.1 From lipids to polymers

The structural and functional complexity of biomembranes has challenged researchers to develop simpler artificial models to mimic their properties. The simplest model is the lipid bilayer. When added to water, lipids as amphiphilic molecules are self-assembling in different ways depending on the system and their chemical nature. Bilayers made of lipids have many advantages, being non-toxic and biocompatible. Additionally, they possess thin membranes and are dynamic, fluid systems. However, they suffer several limitations, such as high permeability, low stability of phospholipids, which can undergo oxidation, and are difficult to be chemically modified.[11] In order to address these limitations, amphiphilic block copolymers are of particular interests, because of the dual environmental affinity that is associated with covalently bound hydrophobic and hydrophilic blocks. These strive to minimize their contact, and therefore drive self-assembly into assemblies with different architectures. [12] By adjusting the chemical synthesis steps, different block copolymer structures can be achieved. The most common ones, are the AB, ABA and ABC block copolymers, shown in Figure 2. AB are diblock copolymers, consisting of two different blocks, one hydrophilic, the other one hydrophobic. Both, ABA and ABC are triblock copolymers. ABA is a so-called symmetric block copolymer, where the hydrophobic block B is the

middle block, with hydrophilic identical end blocks A. ABC, an asymmetric block copolymer, consists of three distinct copolymer blocks, with hydrophilic A and C and hydrophobic B blocks.

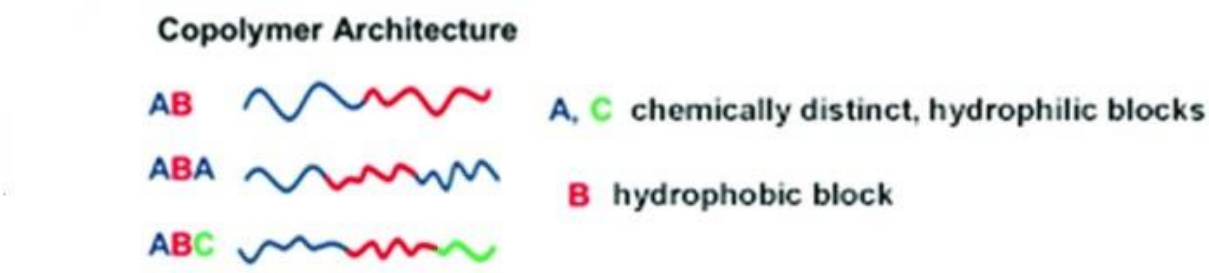

Figure 2. Illustration shows different block copolymer architectures.[13]

Based on their chemical specificity, as for example hydrophilic-to hydrophobic ratio, amphiphilic block copolymers can self-assemble in dilute aqueous solutions into micelles, vesicles, tubes, wire-like structures, or nanoparticles or planar membranes at a water-air interface. [14, 15]

Synthetic membranes have greater mechanical stability than phospholipids, because of the higher molecular weight (Mw) of amphiphilic block copolymers, and thus they are thicker and stiffer than lipid bilayers.[16]

Thereby, these amphiphilic block copolymers are able to assemble in different ways and combined with biomolecules, various biomimetic systems can be achieved (Figure 3).

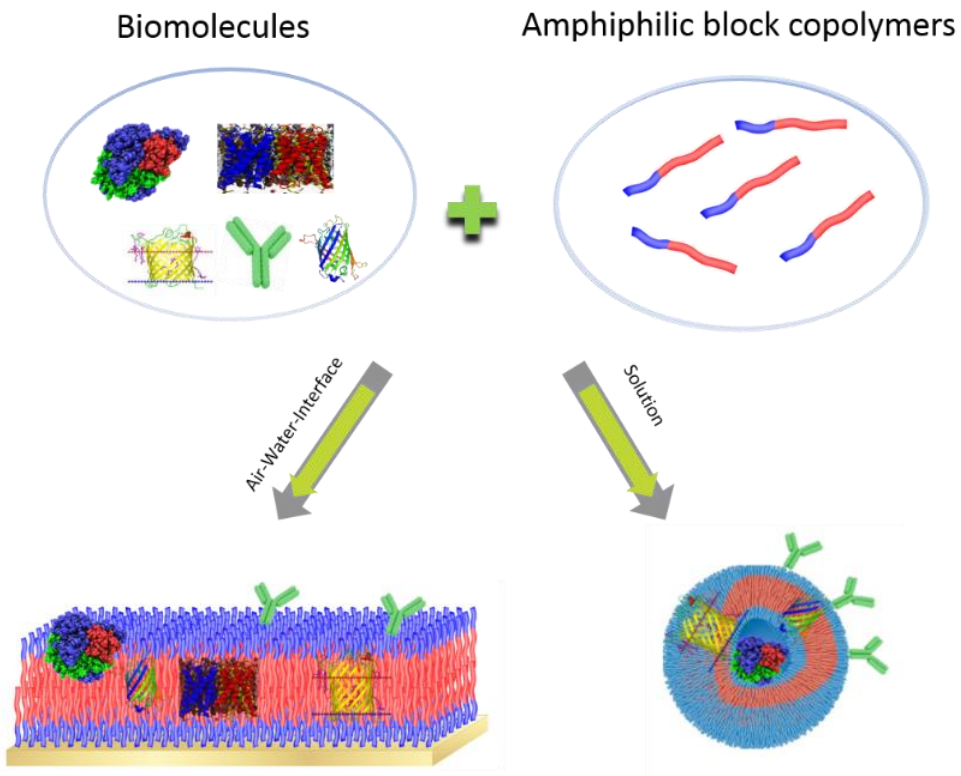

Figure 3. Conceptual overview of bioinspired polymer vesicles and planar polymer membranes on solid support.[16]

1.2.2 Properties of copolymers that form bioinspired and biomimetic membranes

The amphiphilic copolymers most frequently used in bioinspired strategies consist of hydrophilic blocks, such as poly(acrylic acid) (PAA), poly(ethylene oxide) (PEO), or poly(2-methyl oxazoline) (PMOXA) and a hydrophobic block, such as polystyrene (PS), poly(butadiene) (PB), or poly(dimethylsiloxane) (PDMS). [17, 18] The chemical nature of the blocks is a crucial factor for introducing into an artificial membrane the properties required in biomimetic approaches. [19] Variation in block copolymer compositions and M*w* will influence the architecture and also the size of the supramolecular assembly and the membrane thickness, whilst the glass transition and crystallinity of the hydrophobic block influence the flexibility and fluidity of the membrane. [20] Most often characterized in the literature are polystyrene-b-poly(acrylic acid) (PS-b-PAA) polymersomes.[21] Despite of their excellent mechanical stability they cannot be used as a model

membrane system. The reason is that the glassy core is consisting of polystyrene (Tg PS = ∼100 °C) which makes their membrane is relatively rigid in contrast to the fluidic character of biological membranes. A very promising candidate is a block copolymer (AB or ABA) made of PDMS and PMOXA (Tg = −124 °C, depending on the length and ratio) which is much more flexible and thus closer mimic the dynamic mechanical response of biological membranes.[22, 23] A key parameter for further biomolecule conjugation is the flexibility of the membrane. It plays a crucial role in the insertion of biomolecules and the preservation of their function. Therefore, the choice of amphiphilic copolymer and the architecture of the supramolecular membrane assembly need to be exactly chosen to each application.[24]

1.2.3 3D- amphiphilic block copolymer membranes

Several three-dimensional structures can form spontaneously by self-assembly out of amphiphilic molecules, such as micelles, vesicles and worms. The formation of these structures depends on the hydrophobic and hydrophilic ratio of the molecule and can be determined by the so-called packing parameter, which is defined as following:

$$p_0 = \frac{v_0}{a l_0} \qquad (1)$$

Thereby, v_o is the volume and l_o the length of the hydrophobic tail, and a is an optimal area of the hydrophilic head group. The dimensionless value of P characterize the morphology of the self-assemblies: spherical micelle ($0 < P \leq 1/3$), cylindrical micelle ($1/3 < P \leq 1/2$), or bilayer structure, such as vesicle ($1/2 < P \leq 1$).[25, 26]

Polymer vesicles, the so called polymersomes, are of great interest, because of their unique architecture which involves an enclosed membrane with a central aqueous compartment, similar to that of biocompartments. [27] They can have several sizes staring at nanometer-scale and when achieving cell-size, they are called giant unilamellar vesicles (GUVs). Polymersomes provide three different regions for combination with active molecules: the aqueous cavity (for encapsulating hydrophilic molecules), the membrane (for insertion of hydrophobic molecules), and the boundary of the membrane with the environment (for functionalization with specific molecular groups to serve as targets or for immobilization on solid supports). [28] The internal cavity of

polymersomes serves as a container, either for the application as a drug delivery system, or as a nano-space for reactions in so-called nanoreactors. A key parameter for *in situ* catalytic reactions is permeability of polymersome membranes to allow exchange of substrates/products with the environment. Therefore, selection of the amphiphilic copolymer and the type of the corresponding supramolecular assembly has to match both the selected biomolecule and the intended application.[16]

1.2.4 2D-amphiphilic block copolymer membranes

Various models of planar membranes exist and are being investigated regularly: monolayers at the water-air interface (Langmuir monolayers), free-standing bilayers, and solid-supported membranes (Figure 4). Langmuir Films are thin organic films of a thickness of just one molecule which are often formed spontaneously by amphiphilic molecules of a certain structure at the air-water interface. When transferred to a solid-support, different architectures such as monolayers or bilayers are possible. The techniques which are used for such a transfer are for example Langmuir- Blodgett (LB) or vesicle fusion. Free-standing bilayers are traditionally formed across apertures in Teflon or other plastic septa, by painting the apertures with lipid or amphiphilic copolymers dissolved in organic solvent (usually *n*-decane). The solvent spontaneously drains toward the septum, finally forming a bilayer.[29]

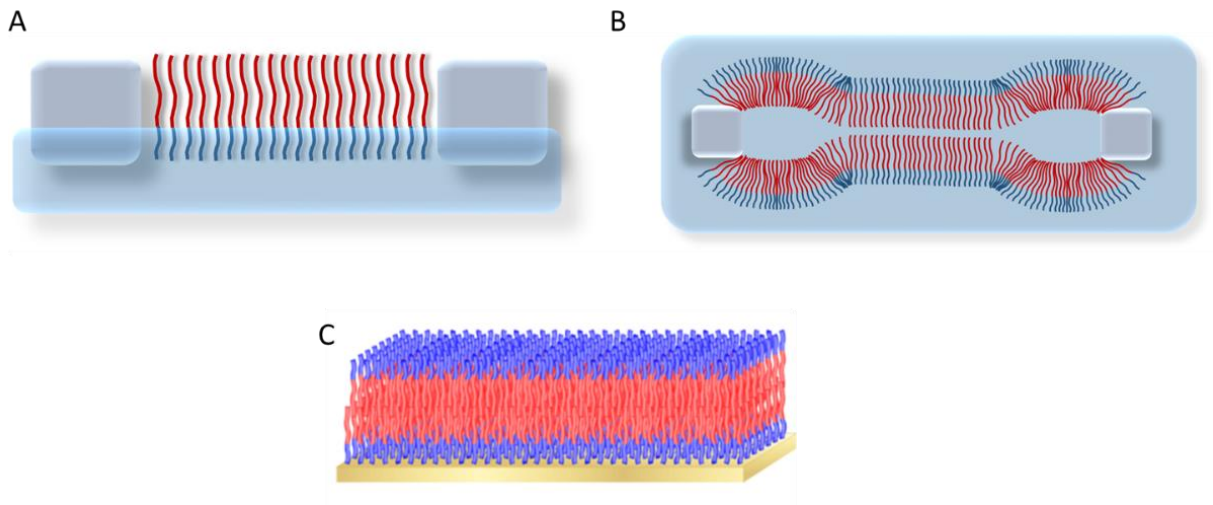

Figure 4. Models for planar membranes. A) Monolayer at air-water interface, B) free-standing membrane and c) solid-supported planar membrane.

The most stable model is the solid supported membrane. However, the other two models have a great advantage of being more dynamic and closer to a biological system.

1.2.5 Decoration of planar membranes with biomolecules

There are several examples of combination of planar membranes with biomolecules, such as proteins or enzymes.[9, 30-32] The functionality of proteins in natural membranes depends on their mobility in the matrix, and this is therefore an essential prerequisite for artificial membranes to mimic the dynamic environment of biomembranes to serve as templates for biomolecules. [20] Therefore, the building blocks forming a bioinspired membrane need to possess high flexibility to compensate the hydrophobic mismatch between the size of the biomolecules, and the membrane thickness. [33] In addition, a variety of membrane properties (thickness, polarity, and surface charge) have to be considered for successful insertion/attachment of biomolecules. Decoration of polymer membranes with biomolecules, either on their surfaces or inside the bilayers, can be achieved by various approaches, such as physical adsorption, insertion, and

covalent binding. [34] Surface modification of planar membranes is a focus for the development of active surfaces for biosensing and diagnostic purposes. [16, 35]

1.3 Preparation of solid supported membranes

1.3.1 Strategies for the preparation of solid-supported membranes

Several techniques exist for the preparation of solid-supported membranes. The use of solid supports for membrane immobilization provides mechanical stability, even in the dry state.[36] The most common methods used for the formation of solid-supported membranes are (i) vesicle fusion (ii) LB and LS techniques and (iii) solvent-assisted bilayer formation. All these methods are based on physical interactions (hydrophobic/hydrophilic) between the lipid, the polymer, and the substrate, which drive their self-assembly into membranes.[37] One of the easiest procedures to obtain synthetic solid-supported membranes, is the fusion and spreading of polymersomes onto the support (*i.e.* gold, silica or glass surfaces). Moreover, in order to attain stronger attachment, it is possible to promote the chemical bond formation between reactive groups on the surface and reactive end groups of the polymer, or by physisorption of block copolymers.[38, 39] Due to the different parameters, like for example as pH, ionic strength, the chemical composition of the polymer, or size and distribution of the vesicles, it is very difficult to control the properties of the films obtained using this method.[37] The solvent-assisted lipid bilayer method consists of the deposition of a lipid dissolved in an organic solvent on a solid support, followed by an exchange of the solvent with an aqueous buffer.[40] The LB and LS method are based on the self-assembly of the amphiphilic molecules on the air-water interface. [41] These techniques are going to be explained in the following sections.

1.3.2 Langmuir monolayers

The mechanism of monolayer formation and organization of molecules at the air-water interface has been developed by Irving Langmuir.[42, 43] Langmuir monolayers are usually prepared on the surface of an aqueous subphase, such as buffer or water, in a trough, called

Langmuir trough, through spreading of solutions of water-insoluble amphiphilic molecules, such as lipids or amphiphilic block copolymers. Langmuir troughs are usually equipped with barriers (usually of Teflon) which can be used to compress monolayers in the way that the area occupied by each amphiphile molecule is varied. During this process, surface pressure changes of the monolayer can be monitored in situ using a surface balance. The most commonly used balance is of the Wilhelmy-type in which a thin rectangular plate of glass or filter paper of dimensions 1 cm × 2 cm is hung from a force sensor and is partially immersed in the subphase. The area occupied by a single amphiphile molecule (*A*) can be calculated from the geometrical area of the surface occupied by Langmuir monolayer and the number of amphiphile molecules in the monolayer. The most common evaluation of Langmuir monolayers is the measurement of the surface pressure-molecular area (π-*A*) isotherm where surface pressure (π) is measured as a function of molecular area (*A*), at constant temperature. The surface pressure (π) can be calculated from the difference between the surface tension of pure water (γ_0) and the surface tension after addition of a substance that adsorbs to the water surface (γ) (equation 2). [44]

$$\pi = \gamma_0 - \gamma \qquad (2)$$

By measuring π during compression of the total surface area, Langmuir compression isotherm can be obtained. Although the shape of π-*A* isotherms varies drastically depending on the nature of amphiphiles and the temperature, a typical isotherm can be described as follows: at molecular areas larger than 20–30 nm^2/molecule, monolayers are in a two-dimensional gaseous (G) phase. Compression of the monolayer induces a phase transition to a liquid-expanded (LE) phase through the G-LE coexisting region, or to the liquid-condensed (LC) phase through the G-LC coexisting region, depending on temperature or on the structure of the amphiphile used. Further compression results in transition of the LE phase to the LC phase, finally leading to a two-dimensional solid (S) phase. [45] At the moment when molecules are fully packed and no more free space between molecules is available, the monolayer collapses and a multilayer is formed (**Figure 5**).[46]

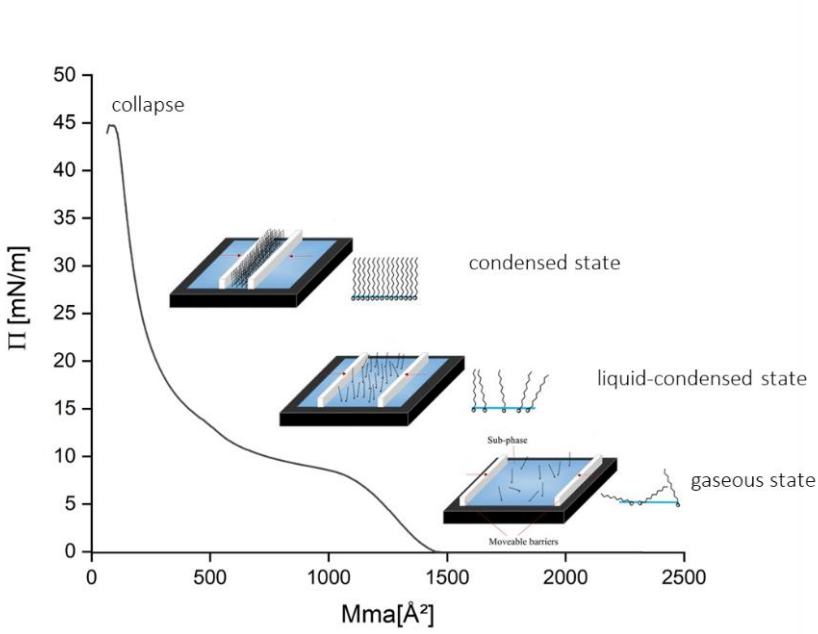

Figure 5. A schematic representation of a Langmuir Isotherm, showing the different states of the monolayer during compression with π= surface pressure and Mma= mean molecular area.

1.3.3 Langmuir-Blodgett and Langmuir-Schaefer technique

The LB trough that was used for the experiments in this thesis is shown in Figure 6.

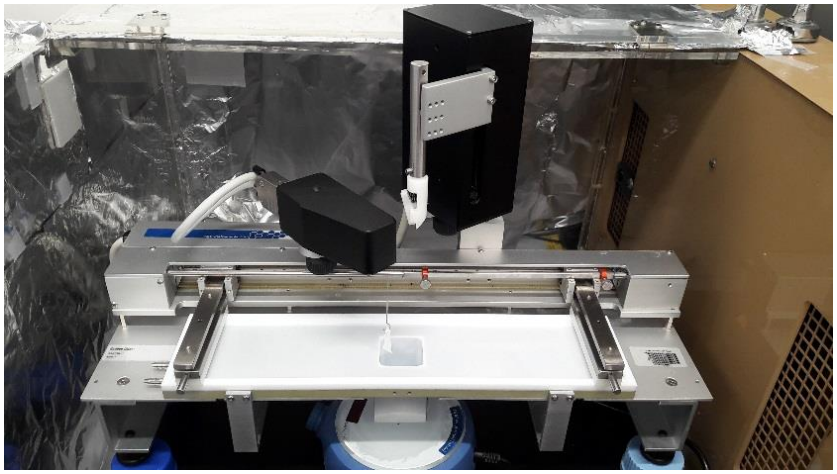

Figure 6. Langmuir trough for Langmuir-Blodgett (LB) and Langmuir-Schaefer (LS) depositions.

It consists of a Teflon container for the liquid (water) subphase, moveable barriers for compressing the surface area and devices for measuring the surface pressure and for transferring the monolayer to a solid substrate. The term, "Langmuir–Blodgett film", refers to a monolayer or a multilayer of an amphiphilic material that has been transferred from the water surface to a solid substrate such as, silicon or glass.[47] Usually, deposition is done at a constant surface pressure and at a constant transfer rate (0.5-5 mm/min). The film adsorbs to the substrate through hydrophilic/hydrophobic interactions and is characterised by the deposition (transfer) ratio.

The monolayer is transferred to the support with the hydrophobic tail side of the monolayer facing the support in the initial down lift. On the subsequent uplift, the monolayer is transferred with the opposing orientation, this means with hydrophilic head-side of the monolayer facing the support. This transfer method is called the vertical dipping method, or LB. When monolayer transfer occurs on both down stroke and upstroke, head-to-head and tail-to-tail orientations of the monolayers are achieved (Y-type). In cases where the monolayer is only transferred during the down stroke of the solid support, the transfer mode is called X-type. Similarly, transfer only during the upstroke provides Z-type modes. X films and Z films often result in LB films with asymmetric orientations.[44]

It is also possible to get such transferred films by using the LS technique. The difference here is the orientation of the solid support. Both methods are shown in Figure 7.

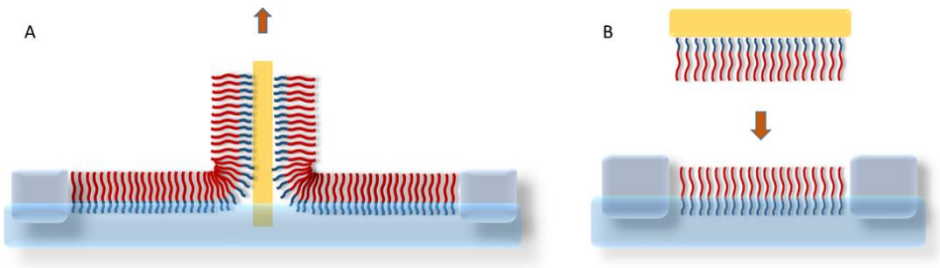

Figure 7. A) Langmuir-Blodgett technique and B) Langmuir-Schaefer technique.

1.4 Characterization of solid-supported membranes

For the characterization of the solid supported membranes, several analytical methods can be used. Common are, for example standard spectroscopic techniques which are typically used for identification and analysis of organic compounds, like Fourier transform infrared spectroscopy (FTIR). Depending on the composition and the predestined properties of the layers, the characterization can include surface-specific methods, e.g., x-ray photoelectron spectroscopy (XPS) or electron-spin sensitive techniques, e.g., electron paramagnetic resonance (EPR). If the obtained layer contains a fluorophore or exhibits electroactive properties, the characterization is typically complemented by light-emission sensitive methods, such as photoluminescence (PL), fluorescence spectroscopy or absorption and or emission in UV-vis. Other methods commonly applied for the surface observations of different membranes and films are for example electron microscopy (SEM) and atomic force microscopy (AFM). [37] In this thesis, techniques such as ellipsometry, contact angle measurements, laser scanning microscopy (LSM), quartz crystal microbalance (QCM) and AFM were used.

1.4.1 Brewster Angle Microscopy (BAM)

Brewster angle microscopy (BAM) is a technique which allows real-time visualization of Langmuir monolayers. It is possible to investigate the lateral organization of these films, including phase separation and the formation of domains. Those can be of different sizes and shapes depending on the properties of the monolayer. Even small changes within a molecule such as the molecule's length or presence of a double bond can change the monolayer's lateral organization that is usually undetected using surface pressure-area isotherms. It goes for different molecules. These changes can be clearly observed using BAM in real-time, especially under full hydration, which is an experimental advantage in many cases. BAM can be used for investigation of biological materials and systems including the visualization of amphiphilic molecules, proteins, drugs,

extracts, DNA, and nanoparticles at the air-water interface.[48] BAM was developed independently by two groups.[49, 50] The experimental set-up and principle are shown in Figure 8.

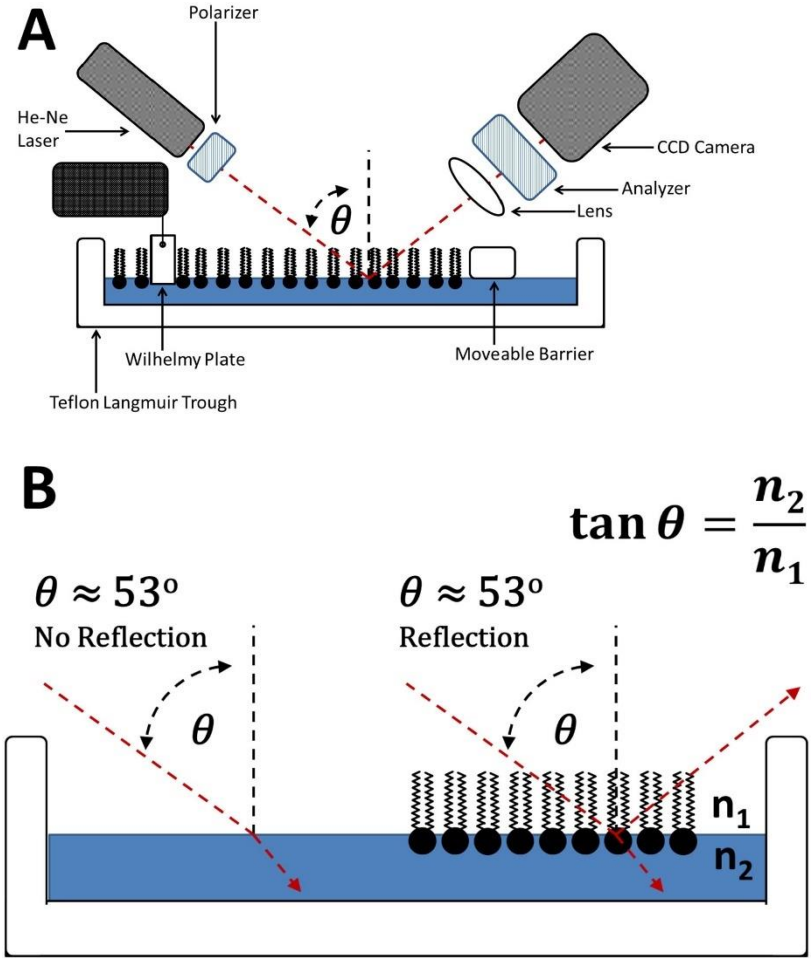

Figure 8. Experimental set up of Brewster angle microscopy (A). Principle of Brewster angle microscopy (B).[48]

The technique is based on the so-called Brewster angle. This is the angle at which light of a certain polarisation will not reflect off a surface. A laser beam is polarized in the parallel plane and directed at the Brewster angle, which is approximately 53° for water, onto the air water interface shown in Figure 8 A. Under these conditions the light is not reflected, how shown in Figure 8 B. When molecules are added at the air-water interface the refractive index changes, resulting in light reflection off the films into a camera that provides real-time images of the interface. For the experimental set-up, a Langmuir trough is necessary. It provides additional

information on film packing by recording changes in surface pressure upon reduction of the molecular area changes. These are displayed as pressure-area isotherms. In addition, portions of the monolayer that stick up from the surface appear brighter and this information is also useful to analyze the phase behavior of the monolayers.[48, 51]

1.4.2 Ellipsometry

Ellipsometry is an optical technique that allows very precise and accurate analysis of the optical properties of various thin film systems, including film thickness and dielectric constants. Ellipsometry relies on the changes in the polarization state of light upon reflection from monolayer and multilayer systems.[52]

The principle of ellipsometry works due to the fact that the different polarization states of an electric field, parallel E_p and perpendicular E_s to the plane of incidence, are reflected with different intensities. Therefore, the resulting polarization state is generally elliptic. This elliptically polarized light is described by using the so-called ellipsometric angles Ψ and Δ. They are defined by Fresnel reflection coefficients r_p und r_s:

$$r_p r_s = (\tan \Psi_p / \tan \Psi_s) \exp[i(\Delta_p - \Delta_s)] =: \tan \Psi \exp(i\Delta) \qquad (1)$$

In this case, Δ corresponds to the phase shift of the electrical fields in p- and s- direction and tanΨ describes the corresponding change of the amplitude ratios.[53] The set-up is shown in **Figure 9**.

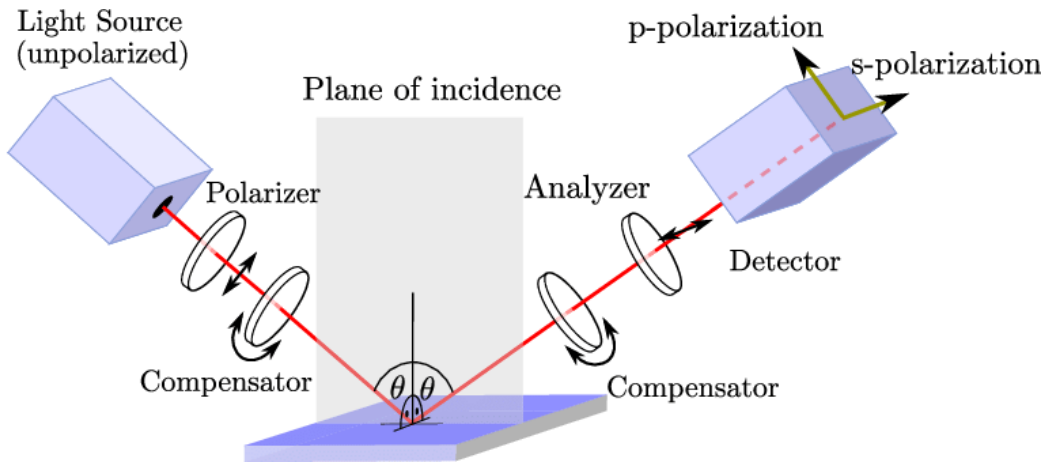

Figure 9. Typical set-up of an ellipsometer [54]

First, the unpolarized light coming from a light source is linearly polarized through a polarizer. When the light interacts with the sample surface, the polarization state changes to elliptic. The analyzer rotates and modulates the intensity of the reflected light with twice the rotation frequency. The calculation is done by using the Fourier analysis of amplitude and phase of the detected signal the ellipsometric angles Ψ and Δ.

Ellipsometry is an indirect measuring method, therefore it is necessary to model the optical response of the investigated sample. Here, all fitting parameters like film thickness or optical constants are varied in an iterative process until matching the experimental data. Only exception exists, if there is the case of an isotropic sample, where only the air-sample interface is considered (for example bulk materials). In this case the optical constants can directly be calculated from the angles Ψ and Δ.[53]

1.4.3 Atomic Force Microscopy (AFM)

The invention of AFM in 1986 was a milestone in the history of nanotechnology and created new opportunities in physics, chemistry, biology and medicine.[55-57] AFM imaging is performed not by an incident beam as in classical microscopes, but rather by sensing the force between a probe

and the sample surface.[58] Therefore, an AFM image is generated by recording the force changes while scanning the probe (or sample) in the *x* and *y* directions. The sample is fixed on a piezoelectric scanner, which ensures three-dimensional positioning with high resolution. The force is monitored by attaching the probe to a cantilever, which acts as a spring, and measures the bending or the so-called "deflection" of the cantilever. The bigger the cantilever deflection, the higher the force that will be experienced by the probe. Most instruments today use an optical method to measure the cantilever deflection with high resolution; a laser beam is focused on the free end of the cantilever, and the position of the reflected beam is detected by a position-sensitive detector (photodiode). AFM cantilevers and probes are usually made of silicon or silicon nitride by microfabrication techniques. Figure 10 is showing the basic principles of AFM in the most common operation modes. In contact mode, the cantilever deflection is kept constant (constant force) by adjusting the relative height between tip and sample. A topographic height change alters the cantilever deflection, which a feedback loop corrects by adjusting the tip–sample distance. The dynamic or tapping mode oscillates the cantilever close to or at resonance frequency. Height changes alter the cantilever oscillation, which is used to adjust the tip–sample distance.[57]

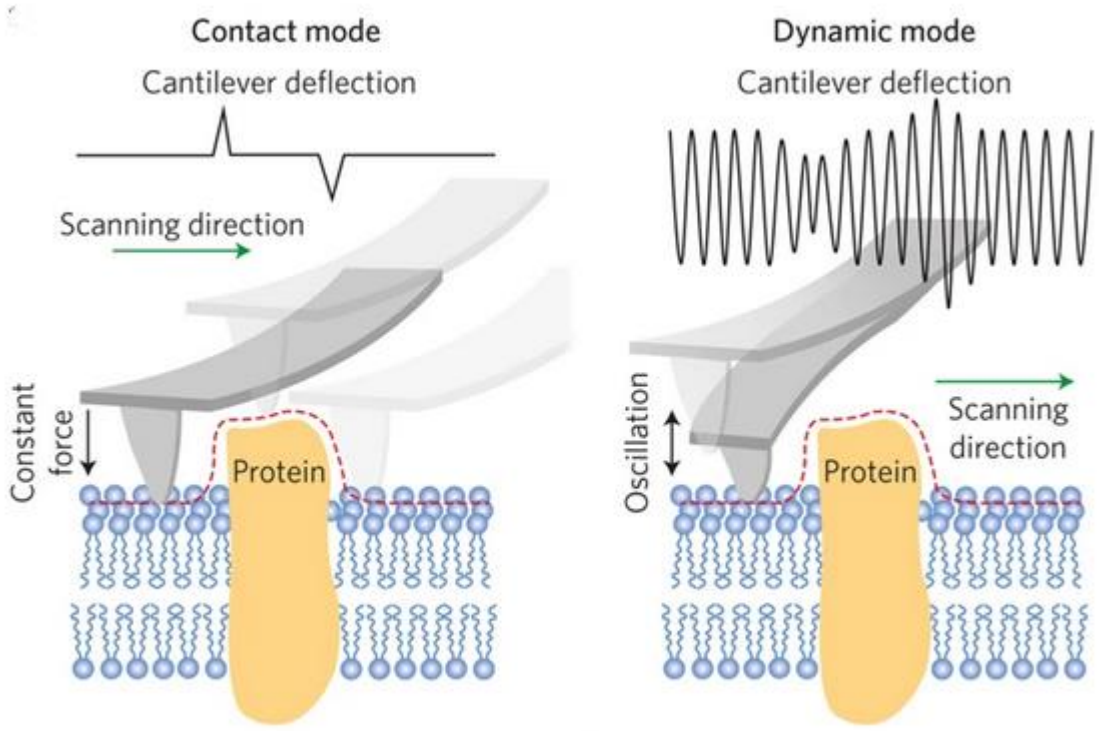

Figure 10. Basic principles of contact (left) and dynamic (right) AFM imaging modes.[57]

An advantage of AFM is its ability to describe quantitative surface quality by determining roughness coefficients. The quantitative analysis of the surface topography of layers can be carried out based on surface roughness parameters. The most commonly used parameters describing surface topographies are RMS (rough mean square) and Ra (average roughness) parameter. The RMS parameter is defined as the standard deviation from the mean value calculated from the area based on the point grid (characterized by the height of Zi). Formula 3 where *n* is the number of points, *Zi* is the height of each point for the z coordinate, and *Z* is the average value of the sample height for the z coordinate, describes the RMS value.[59]

$$RMS = \sqrt{\frac{1}{n} \times \sum_{i=1}^{n} (Zi - Z)^2} \qquad (3)$$

In addition, AFM also allows thickness measurement of thin layers, which can be convenient especially for soft materials. The usual methods that use the determination of layer thickness based on measurement of optical properties require complex calculations or are relatively time-

consuming. With AFM, the thickness measurement is simpler and faster. During the measurement the material of the layer up to the substrate material is removed. Then, the measurement of surface topography at the boundary of the layer and the substrate is performed. Through the linear analysis of the height change value in the topographic profile, it is possible to specify the layer thickness. However, the accuracy of the test should depend on the total exposure of the substrate and the selection of a representative place thickness test. Therefore, it is necessary to perform measurements several times in order to determine the statistical average.[59]

1.4.4 Quartz Crystal Microbalance with dissipation (QCM-D)

In 1959 Sauerbrey established the linear relationship between the deposited mass and the frequency response. This formed the fundamental basis of the QCM methodology.[60] Nevertheless, QCM was first just used as a mass detector in vacuum or air. This changed in the beginning of 1980s when scientists realized that a quartz crystal can be excited with a stable oscillation in a viscous liquid medium, such as buffer.[61] Afterwards, the applications of QCM were used in many research areas such as biology, chemistry, physics, medicine, polymer science, and environmental science.[62] Energy dissipation can be measured together with the frequency change oscillator using QCM-D. The principle of QCM-D is based on the measurement of the change (reduction) in oscillating frequency of a quartz crystal corresponding to the adsorption amount of material based on the Sauerbrey equation (formula X). With Δm being the mass change, C the constant and Δf_n the frequency change observed at the overtone number *n.*

$$\Delta m = -C\frac{\Delta f_n}{n} \qquad (x)$$

The amplitude of oscillation goes down by cutting off the electric current for the oscillator. An abrupt decay of amplitude can be found for adsorbed soft viscoelastic materials, while hard adsorbed materials with lower viscoelasticity keep oscillation with slow decay. Therefore, dissipation is a useful indicator to represent rheological properties of the adsorbed material, for example higher viscoelasticity is larger in dissipation (Figure 11).

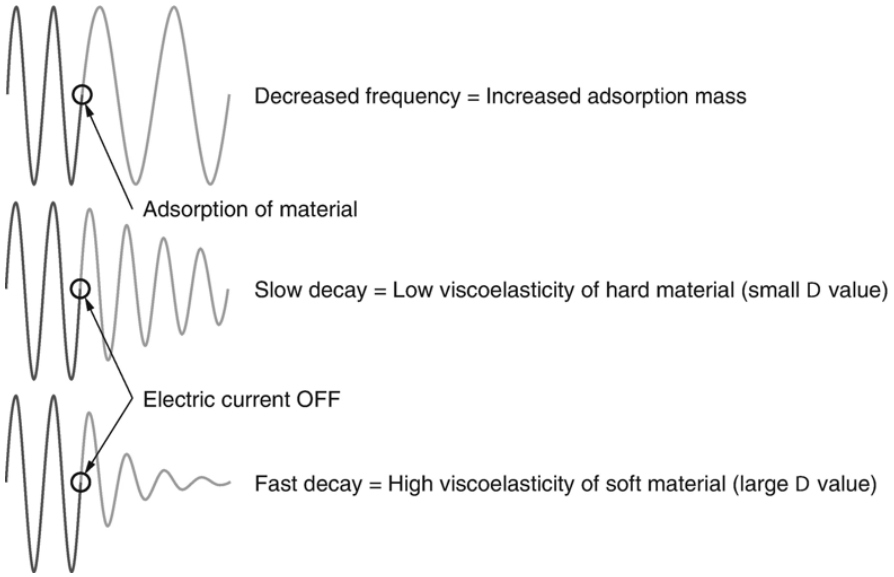

Figure 11. Schematic representation of QCM-D measurements: frequency and dissipation change in reliance to the material properties.[63]

QCM-D is a highly sensitive instrument which is capable to detect small amounts of adsorption, but it should be noted that results could be easily interfered due to additional factors.[63]

1.4.5 Contact angle (CA)

The characterization of the wettability of solid surfaces is of significant importance. Wettability is often characterized by measuring the contact angle formed between a liquid drop and a solid surface. Contact angle, θ, describes a quantitative measure of the wetting of a solid by a liquid. The instrument used to measure contact angles is an optical tensiometer. A force tensiometers can also be used. Both optical and force tensiometers enable static and dynamic contact angle measurements.[64] The contact angle between liquid and an ideal solid surface, which is for example a chemically homogeneous surface, is defined using the Young equation(Figure 12).

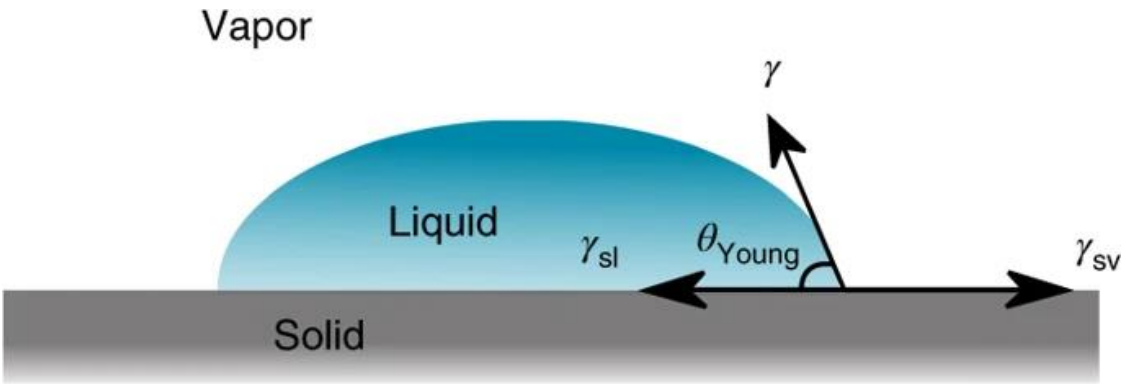

Figure 12. Drop of water on an ideal solid substrate.[65]

Thereby, ϑ_{Young} is the Young contact angle, γ_{sv} and γ_{sl} the solid–vapor and solid–liquid interfacial tensions, respectively, and γ is the surface tension of the liquid. This equation shows that a solid surface with high surface energy) tends to have a low contact angle, whereas a low-energy surface exhibits a high contact angle.

$$cos\theta_{Young} = \frac{\gamma_{sv} - \gamma_{sl}}{\gamma} \qquad [x]$$

A high-quality silicon wafer can be considered a real surface which is close to ideal. It is smooth at the atomic level and can be chemically homogeneous when handled in clean environment. However, even silicon wafers, both chemically unmodified and coated ones with high-quality smooth films with various surface energies, have a range of stable static contact angles. The method of measuring contact angles is called sessile-drop goniometry. [65]

1.4.6 Confocal Laser Scanning Microscopy (CLSM)

In comparison to conventional optical microscopy, CLSM has a number of advantages for the study of materials. For example, the property of three-dimensional reconstruction function allows to perform three-dimensional imaging of materials and with this enabling the accurate

analysis of the spatial structure of materials. On the other hand, CLSM has an improved lateral and axial resolution, which is beyond conventional light optical microscopy. At this moment, two different variants of CLSM are used to characterize material structures, reflectance-mode CLSM and fluorescence-mode CLSM. Reflectance-mode CLSM is used to characterize the surface texture or roughness of material surfaces. Fluorescence-mode CLSM is the most commonly used technique, which relies on the excitation of fluorophores to generate image contrast.[66] CLSM consists of a laser light which acts as a light source and at the same time an electronic system which processes the image. The resolution of the images can be obtained in very thin sections (0.5-1.5 µm). In addition it eliminates the interference produced by light arising from the different optical fields across the sample section.[67]

2 Scope of the Thesis

Engineering molecular systems is one of the most ambitious research goals for the near future. Access to tools and devices for the creation of artificial cellular systems or molecular factories would set a new path for several research fields, such as diagnostics, environment or medicine. In order to achieve this, it is essential to understand and to be capable of mimicking biological systems such as living cells, in particular their protection shield and transport system- the biological lipid membrane. For this reason, planar artificial membranes which are based on amphiphilic block copolymers are of special interest due to their potential medical applications, but also sensing, separation properties and others. These synthetic membranes are used to mimic biological membranes. They are able to provide high robustness and stability compared to lipid membranes. In the past years, solid-supported polymer membranes were investigated to a certain extent, however their interactions with biomolecules are still not fully understood.

The scope of this thesis is, therefore, the development of stable solid-supported membranes and the understanding of the insertion and attachment of biomolecules.

These main goals were approached through:

i) the development of solid-supported membranes having a bilayer-like structure, with hydrophilic-hydrophobic- hydrophilic parts

ii) the functional insertion of a model pore-forming peptide into such polymer membranes

iii) the preparation of asymmetric polymer membranes decorated with active enzymes for potential applications in sensing.

Different Polymers were used for this work, including poly(2-methyl-2-oxazoline -block- poly(dimethylsiloxane)-*block*-) (PMOXA-*b*- PDMS-b-PMOXA) and poly(ethylene glycol)-*block*-poly(γ-methyl-ε-caprolactone)-*block*-poly[(2-dimethylamino) ethyl methacrylate] (PEG-*b*-PMCL-*b*-PDMAEMA).

First, those copolymers were investigated with respect to their behavior at the air-water interface. For this, a Langmuir trough with compressing barriers was used together with BAM. The films were deposited on different solid supports (silica wafers and glass). This was achieved by using the LB- method, by transferring Langmuir monolayers, which provide formation of reproducible defect-free films, on the solid supports. Afterwards, deposited films were characterized by different methods, such as AFM, ellipsometry and contact angle and later on functionalized by introduction of pore-forming peptides and enzymes. Insights about the morphology and thickness of the obtained systems was gained through this characterization. The activity and presence of the biomolecules was proven by using activity assays, and CLSM.

Overall, this work provides insight into the preparation of stable solid-supported polymer membranes in a controllable and reproducible way. In addition, different strategies for the introduction of biomolecules into such systems are presented, resulting in functional systems for different applications, such as sensing and molecule transport. This thesis brings fundamental understanding and development of functional membranes. Such synthetic functional membranes can be further adapted for potential applications and may one day become a part of synthetic cells.

3 Chapter 1: Biomimetic Planar Polymer Membranes Decorated with Enzymes as Functional Surfaces

3.1 Introduction

3.1.1 Biomimetic planar membrane-based biosensors

Recently, a number of techniques to create biomimetic membranes have widened the field of applicability of biomimetic membrane systems, which now includes artificial cells, drug delivery systems, nanoreactors, and water purification. [68-72] A very important domain is the usage of such biomimetic membrane system as biosensing platforms. Amongst sensor devices, polymers are the most commonly used materials and do not cease to be the topic of intensive investigations.[73] Planar polymer membranes represent a simpler alternative to study biological membrane without having to deal with the complexity of biological structures. Different methods to develop distinctive planar polymer membrane-based biosensors have been established and are still in preparation and optimization. Polymer based biosensors allow to probe numerous chemical or biological analytes, such as ions or bigger molecules like phenols.[9, 74] In this regards, the polymer membrane plays a major role in the recognition efficiency of the sensing device. Planar polymer membranes can be used to immobilize active species or improve the sensitivity through an improved signal transduction. [75] In particular, the creation of biomimetic membranes integrated with functional proteins and enzymes has been of great interest in relation to physiological studies and sensing platforms.[9, 74-77]

3.1.2 Environmental impact of phenolic compounds on wastewater

A particularly appealing field for applying protein-polymer membranes are the environmental sciences, especially with respect to high water quality where the detection and removal of high-risk pollutants is a major challenge. Phenolic compounds belong to a class of organic compounds with one or more hydroxyl group(s) directly bonded to one or more aromatic rings. The most common member of chemicals belonging to this category of organic compounds is the actual phenol molecule, also known as carbolic acid, benzophenol or hydroxybenzene with the chemical formula of C_6H_5OH. All other members of the group are derivatives of phenol. Phenolic compounds are grouped in mono, bi and polyphenols depending on the number of phenol groups present in the molecule. Polyphenols can be subdivided into other groups such as flavonoids, phenolic acids, tannins, stilbenes and lignans. [78] The efficient detection and removal of phenols and phenol derivatives, that are high toxicity pollutants even at low concentrations is of particular interest. Discharge of these compounds may lead to health risks for humans and animals and endangers aquatic systems. The toxicity levels are usually in the range of 9-25 mg L^{-1} for both humans and aquatic life. [79] Most phenolic compounds can easily permeate skin and can readily be absorbed from the gastrointestinal tract of humans. When entering the system, they undergo metabolism and transform to various reactive intermediates. These quinone moieties can easily form covalent bonds with proteins, resulting in their ability to exert toxic effects on humans. In addition, phenolic compounds present in water have high inclinations of interacting or reacting with other components of the aquatic environment. Such components are for example inorganic compounds and microorganisms.

The existence of phenolic compounds in water is due to both, natural and man-made activities. Natural sources of phenolic compounds in water pollution include decomposition of dead plants and animals (organic matter) in the water. However, they are also synthesized by microorganisms and plants in the aquatic environment. The most important anthropogenic reasons are due to industrial, domestic, agricultural and municipal activities.[78] Considering the threat caused by phenolic derivatives in waste water, it is highly desirable to develop effective tools for their sensing and follow-up removal or neutralization.

3.1.3 Laccase and Tyrosinase

Both enzymes, tyrosinase and laccase are known for their ability to oxidize phenolic compounds. Both belong to the class of copper-containing enzymes. In general, copper-containing proteins are almost all extracellular. They are widely distributed in nature, where they participate in oxygen transport and activation and electron(s) transfer in redox processes. Laccase is one of the first enzymes ever described and was discovered in 1883. It belongs to the superfamily of multicopper oxidases (MCOs)—a group of enzymes containing many proteins with different substrate specificities and different biological functions. MCO´s contain the so-called cupredoxin-like domains. The presence of these domains allows all MCOs to reduce oxygen to water without producing harmful byproducts. The amino acid sequences of all MCOs contain a small, 10–20 kDa, cupredoxin-like domain and possess relatively simple 3D structures, primarily composed of beta sheets and turns. Mainly, they serve as electron transfer proteins.[80] Laccase is found in many plants, microorganisms and mushrooms. Tyrosinase on the other hand, belongs to the binuclear Cu proteins. [81] Tyrosinases have been isolated and purified from different sources, for example plants, animals, humans and microorganisms. Although many of them have been sequenced, only few of them have been characterized on a deeper level. Among different sources of tyrosinase, mushroom tyrosinase from *Agaricus bisporus* is a major and cheap source of tyrosinase with high similarity and homology compared to human tyrosinase.[82]

3.1.4 Biomimetic membranes as sensing platforms for phenolic compounds

Different combinations of enzymes with nanomaterials have been proposed to offer solutions for detection of phenols and their derivatives: horseradish peroxidase inserted into a self-assembled peptide hydrogel with three-dimensional network of nanofibers [83], laccase immobilized on nano-structured materials, such as carbon nanoparticles, fullerene, multi-walled carbon nanotubes and graphene oxide [84], tyrosinase at a graphene-silk peptide composite nanointerface [85] or tyrosinase immobilized on gold nanoparticles incorporated in a thin polymer film of poly(2-hydroxyethyl methacrylate-co-n-butyl acrylate) copolymer. [86] [86] Lipid films combined with laccase and

tyrosinase served for phenol biosensing [87, 88], but the preferred films for such applications are composed of polymers due to the increased chemical and mechanical stability. [89-91] For example, tyrosinase incorporated in a LB film of arachidic acid and lutetium bisphthalocyanine allowed to decrease the sensitivity towards the phenol derivatives in the order of diphenols > triphenols > monophenols [92], while an amperometric biosensor was obtained by tyrosinase immobilization in a conducting polypyrrole film. [93]

Several types of nanomaterial-based biosensors have been proposed for detection of phenolic compounds by using either electrochemical or optical detection methods. [94, 95] Electrochemical sensors have advantages regarding quick responses, simplified operation and cost efficiency, but a main disadvantage is the degradation of the electrode surface by continuous flow. In contrast, optical nanomaterial-based biosensors achieved lower limits of detection and longer stability, but they were normally engineered as elaborate multi-step assays and associated with higher costs. [96] Importantly, the use of solid supported polymer membranes is associated with lower costs due to the straightforward generation of such films. For example, laccase immobilized on monolayers resulting from LB transfer of amphiphilic triblock copolymers preserved its bio-activity upon immobilization and indicated that a flexible polymer membrane is able to protect the enzymes, whilst allowing them to act for local sensing of phenols derivatives. [9]

3.2 Motivation

This work presents an approach to generate solid supported mono- and bilayer films of asymmetric

triblock copolymers and to combine them with enzymes to serve as functional membranes for efficient detection of phenol derivatives, in particular for the production of high quality drinking water. In a previous study, a group of six poly(ethyleneglycol)-*block*-poly(γ-methyl-ε-caprolactone)-*block*-poly[(2-dimethylamino)ethylmethacrylate] (PEG_{45}-*b*-$PMCL_x$-*b*-$PDMAEMA_y$) asymmetric amphiphilic triblock copolymers were investigated in terms of their behavior at the air–water interface, formation of films on a solid support, and ability to adsorb laccase, which was used as a model enzyme. The asymmetric amphiphilic ABC triblock copolymer PEG_{45}-*b*-

$PMCL_{101}$-*b*-$PDMAEMA_{27}$ (A_{45}-B_{101}-C_{27}) was now selected as it was previously shown that it forms uniform films with a high degree of molecular ordering for attachment of laccase. [9] Due to its asymmetry, this triblock copolymer has the advantage of two different hydrophilic blocks, specifically a PEG domain that is protein repellent and a pH responsive PDMAEMA domain with tertiary amino groups that is expected to serve for attachment of enzymes. Well-organized polymer mono- and bilayer films have been prepared by film transfer techniques. In the previously reported study of laccase attachment on PEG-*b*-PMCL-*b*-PDMAEMA monolayers it was not possible to evaluate the accessibility of the immobilized enzymes and the influence of film roughness on the enzyme immobilization. However, this is very important to understand the exact properties of such sensing platforms. Therefore, it was necessary to go one step further in order to optimize such functional surfaces based on enzyme-polymer membranes on solid support. [9] Thus, this thesis focuses on following questions: (a) the orientation of the asymmetric amphiphilic ABC block copolymer at air-water interface; (b) the parameters influencing the mono- and bilayer film formation by the block copolymer at air-water interface and the parameters influencing the transfer to silica solid support using the LB- technique; (c) the structural properties, which determine the block copolymer film formation and their availability for enzyme immobilization, and (d) the stability, accessibility and reactivity of the active surface of the enzyme-polymer film. A systematic evaluation at molecular level provides detailed understanding of film properties that are necessary to build effective biosensors for phenol derivative detection. In addition, this is the first time that solid supported polymer bilayer membranes based on asymmetric amphiphilic copolymers are used for enzymes immobilization in order to engineer active surfaces. This provides new understanding for membrane formation and how it is influenced by the functional groups interacting with proteins. Active surfaces like the ones developed here, open new perspectives for biosensing applications and can easily be modified for other applications by adapting the biomolecules. Here, for example medical device applications would be an appealing topic.

3.3 Materials and Methods

3.3.1 Materials

The amphiphilic asymmetric ABC block copolymer, poly(ethyleneglycol)-*block*-poly(γ-methyl-ε-caprolactone)-*block*-poly[(2-dimethylamino)ethylmethacrylate], was synthesized as previously described.[97] Briefly, ring-opening polymerization of γ-methyl-ε-caprolactone was performed using PEG as a macroinitiator. The modified PEG-b-PMCL diblock copolymer contained an atom transfer radical polymerization (ATRP)-initiating group. It was used for synthesis of the third, PDMAEMA block. Polished silicon wafers were obtained from Si-Mat Silicon Materials, Germany. Laccase from *Trametes versicolor*, tyrosinase from Mushroom (*Agaricus Bisporus*), 2,6-dimethoxyphenol (DMP), 4-methoxyphenol (4-MP) and solvents (of highest purity grade) were purchased from Sigma-Aldrich. The standard phosphate buffer saline solution (PBS), sodium dodecyl sulfate (SDS) and 3-methyl-2-benzothiazolinone hydrazone (MBTH), Na_2HPO_4 7 H_2O and NaH_2PO_4 used to prepare the phosphate buffer were from Sigma-Aldrich. Bovine serum albumin (BSA) was purchased from Thermo Fisher.

3.3.2 Methods

3.3.2.1 Polymer Film Transfer on Solid Support

Polymer films were formed at the air-water interface by closing the LB barriers, which was monitored as previously described by an EP^3SW system (Nanofilm Technologie GmbH, Göttingen, Germany) equipped with a Nd-YAG laser (λ = 532 nm), long distance objective (Nikon, 20x) and monochrome CCD camera.[9] The size of the BAM image is 220 x 250 μm^2, with a resolution of 1 µm. The transfer of the block copolymer films onto the silica solid support was performed using the LB technique, using a Mini-trough (KSV Instruments, Finland). The silica slides were cut into pieces of approx. 1 cm^2 and then cleaned by ultrasonication in chloroform (three times, 15 minutes each time). For the “down” transfer, the silica slides were placed in the air subphase, the

polymer film was formed and transferred onto the silica slide by dipping the LB dipper into the water. In order to avoid uncontrolled film deposition or contamination the water surface was cleaned after “down” dipping transfer prior to lifting the silica slides from the water subphase.

3.3.2.2 Copolymer Monolayer and Bilayer Films Characterization

The dry thickness of the polymer monolayer and bilayer films were measured on two different slides (at least five individual measurements on each) and average values with standard deviation were calculated for values determined with a mean squared error (MSE) below 1. Film thickness was measured with EP^{3}SW imaging ellipsometer (Nanofilm Technologie GmbH, Göttingen, Germany). The thickness of the silicon dioxide layer (~ 2 nm) was taken into account and measurements were performed for ten incident angles ranging from 55° to 75°, with 1.5 refractive index value used for the polymer, using the nk_fix model. The wetting properties of the polymer films were investigated with a contact angle goniometer, CAM 100 (LOT quantum design) using a CDD camera with 50 mm optics. The measurements were performed by placing droplets of ultrapure water with a micro-syringe on the solid supported films, images were then recorded and analyzed by automatic curve fitting performed by the instrument software. The drop volume was kept constant for all measurements, measurements were taken on two different slides (five different areas on each) and average values and standard deviation were calculated. The topography of the polymer films on silica slides was investigated by AFM using a JPK NanoWizard® 3 AFM (JPK Instruments AG). All measurements were carried out in the AC mode in air, using silicon cantilevers (PPP-NHCR, Nanosensors) with a nominal spring constant of 10-130 N m^{-1} and a resonance frequency of 300 kHz. The images were analyzed with the data analysis software JPK Data Processing (v. 5.0).

3.3.2.3 QCM Measurements of Enzyme Adsorption on Polymer Films

The adsorption of the enzymes on polymer films was studied with a quartz crystal microbalance with dissipation (QCM-D) system Q-Sense E1 (Biolin Scientific, Sweden). The block copolymer

monolayer and bilayer films were first transferred to silicon dioxide QCM-D sensor chips (5 MHz quartz crystal q-sense, Biolin Scientific) by the LB technique using the mini-trough and then placed in the QCM-D chamber. The QCM-D sensor was stabilized under buffer flow until the frequency signal fluctuation was below ± 1 Hz. After system stabilization, solutions of 0.5 μg mL^{-1} laccase (in phosphate buffer, pH 7) or 0.5 μg mL^{-1} tyrosinase (in PBS, pH 7) were introduced into the QCM-D chamber with the flow speed of 100 μL min^{-1}. The enzyme was allowed to adsorb for 1-2 hours until signal fluctuations were less than ± 1 Hz, incubated for further 30 min before washing thoroughly with the appropriate buffer solution. The enzyme adsorption and desorption stages (washing) are performed under the same constant slow flow (100 μL min^{-1}) of enzyme solution and buffer, respectively, for several hours. The change in resonance frequency value (Δf) measured with overtone 5 is used to calculate the mass (Δm) adsorbed onto the polymer film, based on Sauerbrey equation ($\Delta m = - C\Delta f$, where C = 17.7 ng cm^{-2} Hz^{-1} is a constant, depending on the quartz QCM-sensor properties.[98]

3.3.2.4 Enzyme Adsorption on Polymer Films.

Immobilization of enzymes on polymer films was performed after the film transfer onto the solid support, in conditions similar to that used for the QCM-D experiments (enzyme adsorption, incubation and desorption). Silica slides with transferred mono- or bilayers of block copolymer were immersed in enzyme solutions (0.5 μg mL^{-1} for both laccase and tyrosinase, the first in in phosphate buffer 50 mM, pH 7, the second in PBS buffer pH 7) for 2 h under shaking (dynamic regime), incubation for 30 min without shaking (static regime), then rinsed with the buffer for 1 h (dynamic regime).

3.3.2.5 Bicinchoninic Acid Assay

The concentrations of enzymes adsorbed on polymer films were determined by a bicinchoninic acid assay (BCA assay, Micro BCA™ Protein Assay Thermo Fisher). Prior to the assay, the enzymes were desorbed from the polymer films by incubation with sodium dodecyl sulfate (SDS, 5 wt%) under shaking for 2 h, adapted from Gunkel et al.[99] The enzyme concentration of the supernatant solution was determined using a calibration curve obtained with bovine serum abumin (BSA, 0.5–

20 µg mL^{-1}). As the enzyme concentration in solution was 0.1-0.3 µg mL^{-1}, the surface area was increased by using two silica plates with polymer films (8.75 cm^2/ plate) for one measurement. The amounts of desorbed proteins were quantified, calculating averages determined with the two silica plates and from 4 repeated measurements.

3.3.2.6 Activity of Free and Immobilized Enzymes

The enzymatic activity of laccase in solution (0.1-0.3 µg mL^{-1}) was studied using 2,6-dimethoxyphenol (DMP) as substrate (0.1 mM DMP in 50 mM phosphate buffer, pH 7). DMP forms an oxidation product that allows spectrophotometric detection at λ_{max} = 470 nm. [100] Similarly, the laccase-polymer functionalized surfaces were placed into 24 well plates and a solution of 0.1 mM DMP (in 50 mM phosphate buffer, pH 7) was added. Enzymatic activity was monitored by spectrophotometric measurements of the supernatant solution. Four replicates of different solid supported films were used. The activity of tyrosinase in solution (0.1-0.3 µg mL^{-1}) was investigated spectrophotometrically with 0.2 mM 4-methoxyphenol (4-MP) as a substrate and 2.5 mM 3-methyl-2-benzothiazolinone hydrazone hydrochloride (MBTH) as a dye at λ_{max} = 492 nm. The tyrosinase-polymer functionalized surfaces were placed into 24 well plates and a solution of 0.2 mM 4-MP and 2.5 mM MBTH (in 50 mM phosphate buffer, pH 7) was added and the activity was measured using the supernatant. For the calculation of the end concentration of the product, the substrates (DMP and 4-MP, respectively) were reacted with an excess of the enzyme (laccase and tyrosinase, 0.2 mg/ml). The product formation was monitored by UV-vis to determine full conversion. Subsequently, the product solution was diluted to the concentrations used in the calibration curve. For the calculation of enzyme activity, the washing solutions after enzyme immobilization were collected and the activity was measured and subtracted from the activity of the start solution. The difference was then assumed to be enzyme immobilized on the surface and compared to measured activity of the immobilized enzymes. UV–Vis spectra were recorded at λ_{max} = 492 nm or λ_{max} = 470 nm in the wavelength range 200–800 nm (with an accuracy of 1 nm) using Quartz cuvettes on a Specord 210 Plus (Analytik Jena Edition 2010) and a Thermo Scientific NanoDrop 2000c.

All other reagents and methodologies are detailed in the text, figures legends or tables footnotes.

3.4 Results and Discussion

3.4.1 Formation of asymmetric polymer membranes on solid support

Planar polymer membranes on solid support were prepared with an amphiphilic asymmetric ABC triblock copolymer PEG_{45}-*b*-$PMCL_{101}$-*b*-$PDMAEMA_{27}$, poly(ethyleneglycol)-*block*-poly(γ-methyl-ε-caprolactone)-*block*-poly[(2-dimethylamino)ethylmethacrylate] (Figure 13).

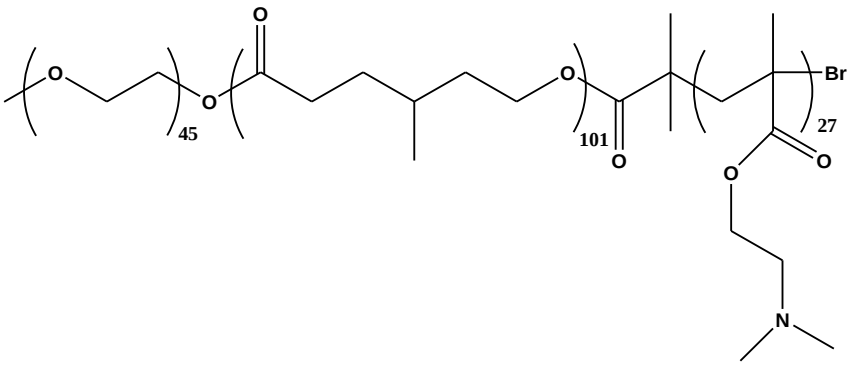

Figure 13. Structure of ABC triblock copolymer poly(ethylene glycol)-b-poly(γ-methyl-ε-caprolactone)-b-poly[(2-dimethylamino) ethyl methacrylate] (PEG_{45}-$PMCL_{101}$-$PDMAEMA_{27}$).

The morphology and properties of the mono- and bilayer polymer membranes were investigated with respect to their interaction with functional biomolecules.

The compression of polymer films at the air-water interface was monitored by BAM before transferring the films on solid support by the Langmuir–Blodgett technique as schematically illustrated in Figure 7A. The transfer to silica slides was performed at surface pressure (Π) values below the collapse pressure (26 mN m^{-1}). All polymer films were obtained with a transfer ratio of about 1. That means that the transfer yield was close to 100%, with uniform deposition of the polymer onto the silica support. During Langmuir compression the copolymer undergoes different phase transitions, starting with a “pancake” conformation (Figure 14 A), followed by “mushroom” and “brush-like” arrangements, in which small lateral interactions force the water soluble polymer blocks to coil (Figure 14 B, and E.a,b.c). At higher surface pressures, the

copolymers adopt a more ordered “cigar-like” conformation, and the final conformation corresponds to a highly packed monolayer film formed at the collapse point. This can be observed in Figure 14 C, and E.d. [101] To tune the interactions with enzymes, polymer films with different directions and transfer sequences were prepared. Indeed, different directions and transfer sequences are expected to induce formation of polymer films with different architectures, which will affect the properties of these films and the resulting entrapment and accessibility of the enzymes. Different transfer directions were used, “up” means the silicon substrate was moved up from the water subphase to the air subphase and the inverse direction is called “down” transfer. The resulting polymer films based on single transfers are labeled up and down, respectively, and combinations of two transfers are labeled accordingly down-down, up-down, down-up or up-up (Figure 15A).

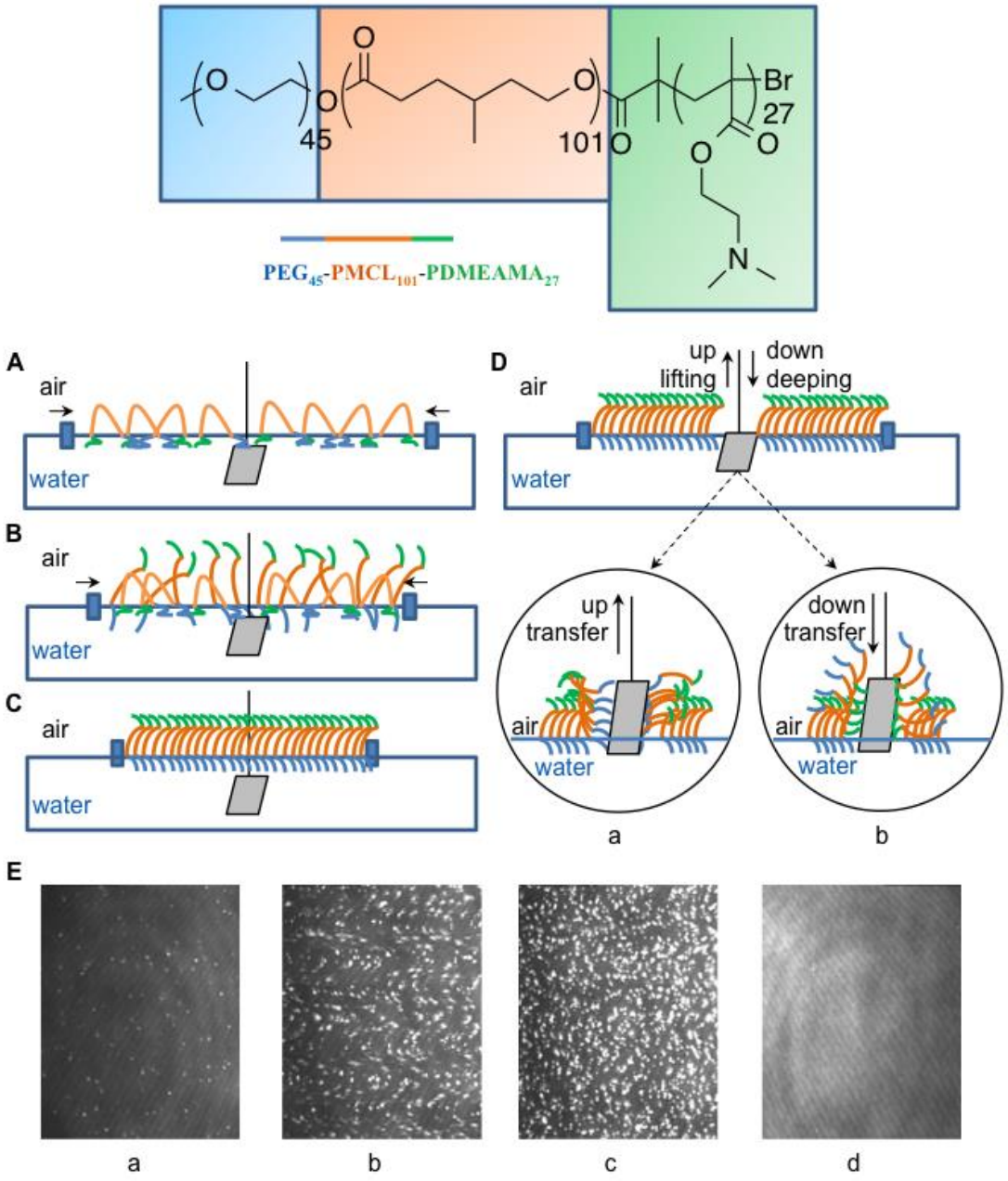

Figure 14. PEG_{45}-b-$PMCL_{101}$-b-$PDMAEMA_{27}$ copolymer used for solid supported membranes preparation. A to D – principle of the Langmuir–Blodgett transfer technique: A – polymer spread at air-water interface; B – polymer film organization at air-water interface; C – polymer film compressed at air-water interface; D – polymer transfer onto a hydrophilic solid support (a – up transfer, up lifting; b – down transfer, down dipping); E – Brewster angle microscopy (BAM) images with the polymer film organization at air-water interface (a – "mushroom" conformation,

at 12 mN m^{-1}; b and c – "brush-like" arrangements at 15 mN m^{-1} and at 16 mN m^{-1}, respectively; d – uniform film formed at collapse point, 26 mN m^{-1}).

After compression, the polymer layers were transferred onto the silica slide, receiving solid supported polymer films. The characterization of the formed films is described below. In the case of "up" transfer, the polished silica wafers were hooked on the dipper and placed in the water subphase before formation of the polymer layer at the air/water interface (Figure 14 D.a). For the "down" transfer, the silica slides were placed in the air subphase above the polymer layer (Figure 14 D.b). LB transfer technique allowed polymer film generation as monolayers or bilayers after two consecutive transfers (Figure 15B).

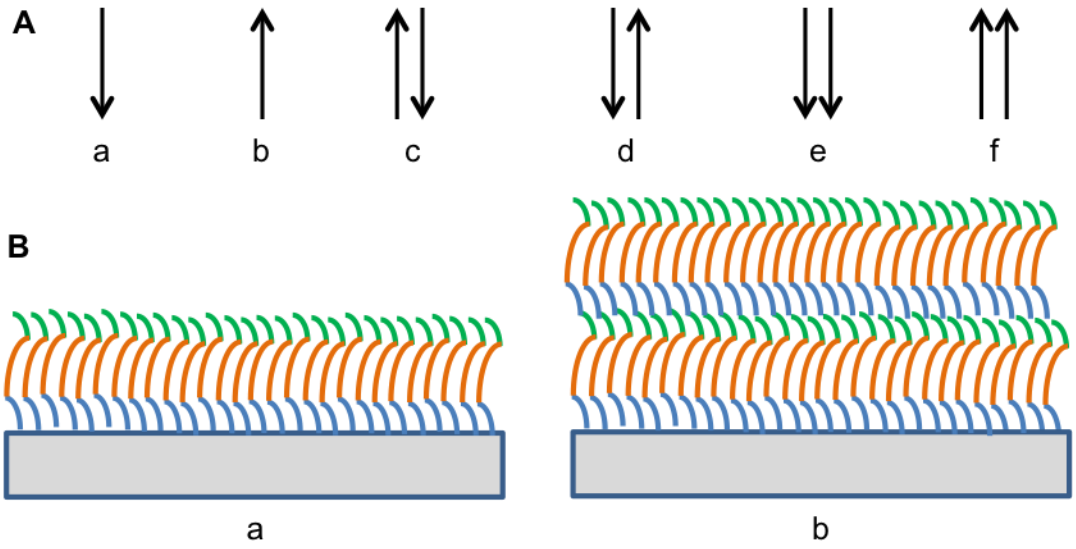

Figure 15. LB transfers to generate the polymer films: A – transfer directions (a – down transfer, down dipping; b – up transfer, up lifting; c – up-down transfer; d – down-up transfer; e – down-down transfer; f – up-up transfer); B – films resulting from specific transfers (a – monolayer film; b – bilayer film).

Earlier studies revealed that during "up" transfer the PEG block is adsorbed on the solid silica surface and the PDMAEMA block is oriented outside.[9] This equips the solid supported polymer

membranes with stimuli-responsive behaviour as PDMAEMA is pH responsive.[102] Additional interesting properties are expected for bilayer morphologies, where the monolayer acts as a new "substrate" for the second transfer, because it has been described that the interaction between such films leads to considerable rearrangements.[103] Hence, a detailed insight into the morphology of these mono- and bilayer polymer membranes is necessary in order to understand interaction of the films with enzymes.

The thickness of the A_{45}-B_{101}-C_{27} films is correlated with the number of layers and the type of transfer and thus thickness measurements can indicate successful transfer of the polymer to the substrate. The film thickness as determined by spectroscopic ellipsometry increased following the order of polymer transfers on the solid support: down-down transfer < up-down transfer < down-up transfer < up transfer (monolayer) < up-up transfer (bilayer) (**Figure 15 A**). In addition, the surface hydrophilicity was determined to ensure favorable conditions for interaction between enzymes and the A_{45}-B_{101}-C_{27} block copolymer films. Static water CA for all A_{45}-B_{101}-C_{27} films are below 90° (**Figure 16 A**), therefore all polymer films on silica slides possess a hydrophilic surface.[104] Further, these findings indicate that the triblock copolymer chains are arranged at the air-water interface with a hydrophilic block oriented towards air. Based on previous results that showed that the C block is oriented to the air subphase in up monolayers, it is deduced that the combined double transfers behave similarly and the PDMAEMA block is oriented upwards.[9] Moreover, the interaction of the polymer membranes with the enzymes is also governed by the surface roughness (**Figure 16 B**), a high roughness translates to a larger surface area available for interaction of biomolecules. The membrane topography and the RMS were determined by atomic force microscopy measurements. RMS was selected as it is more sensitive to large deviations with respect to the mean than other roughness parameters.[105] All polymer films except the down and down-down transfer formed membranes of a few nanometers roughness, increasing with the number and direction of Langmuir-Blodgett transfers (**Table 1**).

A

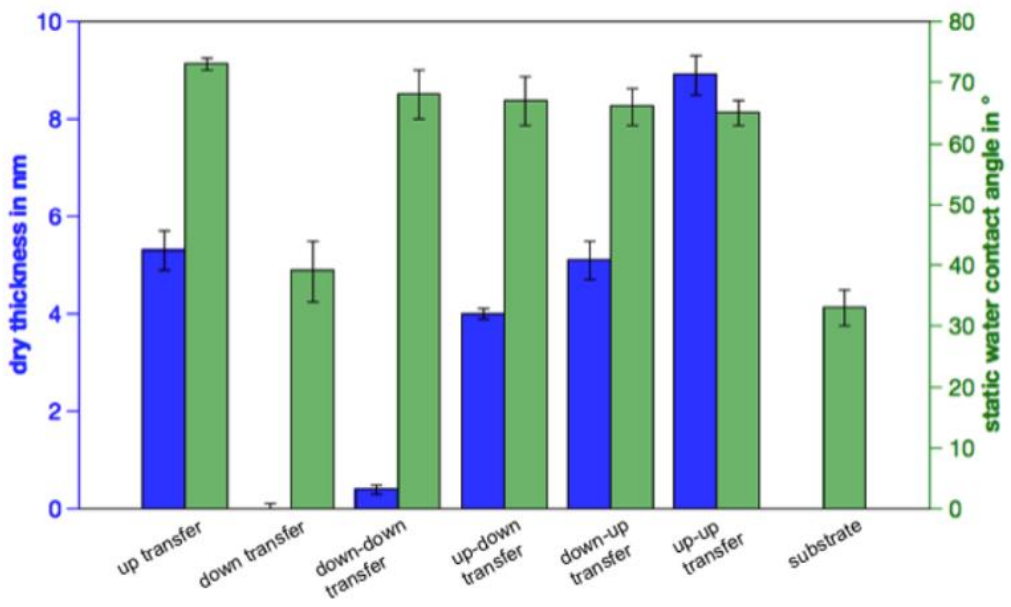
dry thickness in nm
static water contact angle in °
0
2
4
6
8
10
0
10
20
30
40
50
60
70
80
up transfer
down transfer
down-down transfer
up-down transfer
down-up transfer
up-up transfer
substrate

B

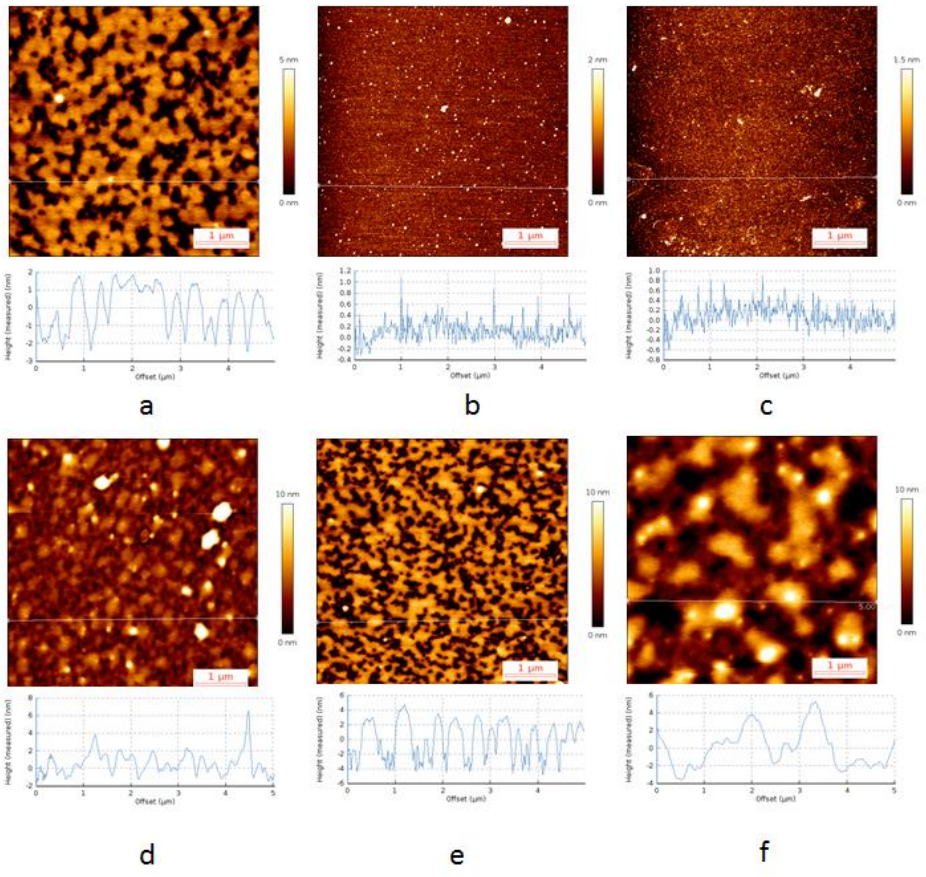
a
b
c
d
e
f

Figure 16.Characterization of different solid supported A_{45}-B_{101}-C_{27} copolymer films: A – thickness and wettability; B – AFM images (AC mode in air) with different transfer types and their height profiles (a – up transfer, monolayer film formed; b – down transfer, no film formation; c – down-down transfer, no film formation; d – down-up transfer, down-up monolayer film formed; e – up-down transfer, up-down monolayer film formed; f – up-up transfer, bilayer film formed).

Table 1 Roughness of the A_{45}-B_{101}-C_{27} monolayer and bilayer films.

Block copolymer films[a]	Roughness [nm][b]		
	1 day	1 week	3 months
Monolayer	1.08 ± 0.04	1.48 ± 0.11	0.94 ± 0.14
up-down monolayer	2.35 ± 0.07	2.05 ± 0.02	2.18 ± 0.13
Bilayer	4.30 ± 0.48	4.45 ± 0.37	4.67 ± 0.25

[a] all transfers were performed at 26 mN m^{-1}; [b] average values calculated from measurements taken on three different plates.

The stability of the mono- and bilayer polymer membranes was evaluated by comparison of the film topography of freshly prepared films with samples stored at room temperature in air for one week and three months, respectively. **Figure 17** shows the AFM micrographs and the cross-sections, respectively.

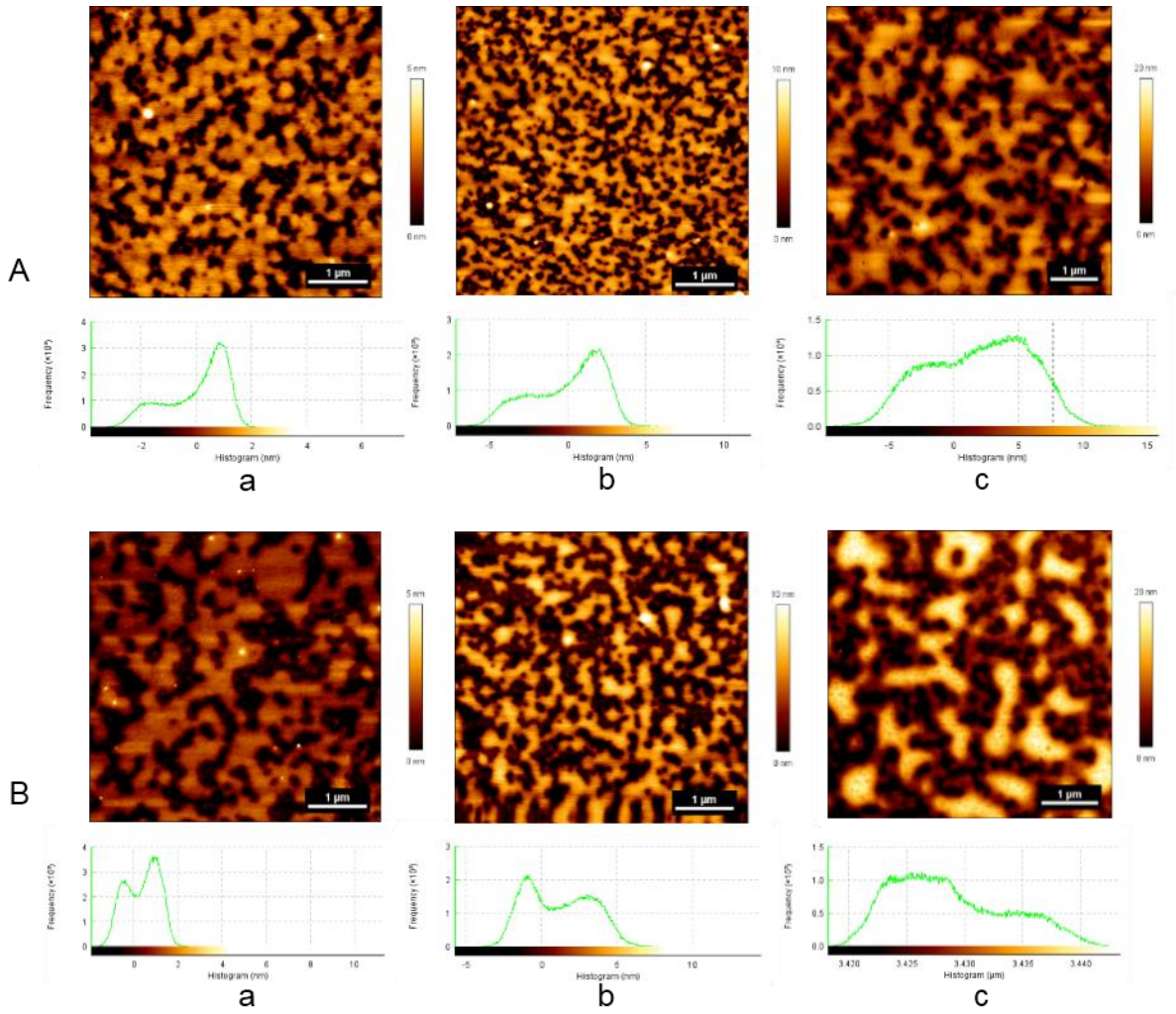

Figure 17. AFM images of the triblock copolymer film and the related histograms of the channel values: A – after 1 week; B – after 3 months; a – monolayer film; b – up-down monolayer film; c – bilayer film.

Importantly, no considerable topographical differences were detected for any of the transfer sequences, underlining the long-term stability and the application potential as long-lived soft synthetic surfaces.

The “up” transfer yielded a monolayer with a dry thickness of 5.3 ± 0.4 nm and a static water CA value of 73 ± 1°, which shows a clear change from a silica substrate (33± 3°) (Figure 16 A). That means that the surface became more hydrophobic compared to a bare silica slide. The surface roughness was determined as 1.08 ± 0.04 nm (Table 1). For “down” and “down-down” transfers the data indicates that polymer membranes could not be formed, the thickness was negligible (0-0.4 ± 0.1nm) and the contact angles were not significantly different after “down” transfer (39° ± 0.1°) compared to the bare silica substrate. This may be explained by the orientation of the polymer chains, since both B and C blocks will interact with the substrate (as opposed to the A block in “up” transfers). Hence, the interaction with the substrate is governed by repulsion from the B block and attraction from the C block, and it appears the repulsion was stronger than attractive forces and thus membranes could not be formed.

Polymer films obtained after “up-down” and “down-up” transfers possess a dry thickness of 4.0 ± 0.1 nm and 5.1 ± 0.4 nm, respectively. These values are similar to the thickness of the monolayer film, which suggests that a monolayer-based membrane was formed (up-down monolayer and down-up monolayer). This further emphasizes that only an “up” transfer leads to a successful membrane formation on silica support. However, the roughness of the membrane increases (2.35 ± 0.07 nm for up-down monolayer), suggesting interaction or rearrangements of the polymer membrane during a second transfer. Importantly, both up-down and down-up monolayers possess a hydrophilic surface as confirmed by their CA values of 66 ± 3° and 67 ± 4° respectively. In the case of the “up-up” transfer, the film thickness is almost twice (8.9 ± 0.4 nm) in comparison with the monolayer film, indicating formation of a bilayer membrane. This is further supported by the membrane wettability (65 ± 2°) and an increase in roughness (4.30 ± 0.48 nm).

We introduce the following terminology for the polymer membranes formed by the amphiphilic asymmetric block copolymer based on the preparation method and the results discussed above: monolayer for membranes prepared by "up" transfer, bilayer for "up-up" transfer, up-down monolayer ("up-down") and down-up monolayer ("down-up"). In contrary to z- and y-type lipid films, this terminology describes the preparation more precisely and allows to relate the preparation method directly with the interaction with the enzymes.[106]

3.4.2 Adsorption of Enzyme on Copolymer Membranes

The three most promising solid supported polymer membranes monolayer, up-down monolayer and bilayer were selected for further studies regarding adsorption of two different enzymes, laccase and tyrosinase. Laccase has a molecular weight of 96 kDa and dimensions of 4.5 nm × 5.5 nm × 6.5 nm,[107] while tyrosinase is larger with 120 kDa and is 10.4 nm x 10.45 nm x 10.84 nm in size.[108] Enzyme adsorption on the different types of solid supported polymer membranes was investigated by QCM-D (**Figure 18**), as this method allows calculation of the mass of adsorbed enzyme on the membrane surface.

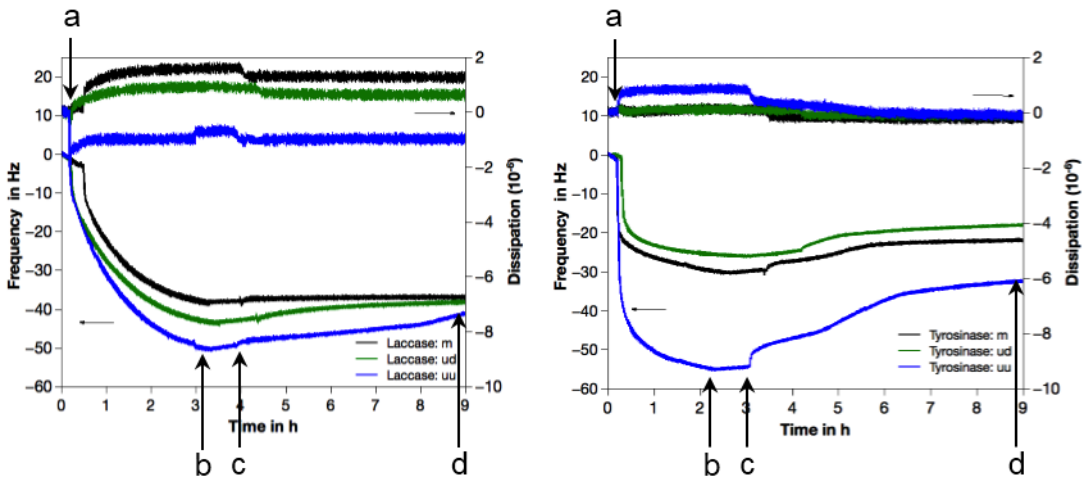

Figure 18. Changes in frequency (mass) and dissipation during the adsorption-incubation-desorption of laccase (left) and tyrosinase (right). Stages of enzymes adsorption: a – system stabilization (buffer flow); b – enzyme adsorption (enzyme flow); c – enzyme incubation (no flow);

d – enzyme desorption (buffer flow). Both enzymes (0.5 µg mL^{-1}) adsorbed on polymer membranes: monolayer (m); up-down monolayer (ud) or bilayer (uu). QCM graphs shown are from the 5th overtone.

The data was suitable for analysis with the Sauerbrey equation, as the change in dissipation was very small and the condition for dissipation (D) to frequency (F) ratio $\Delta D_n/(-\Delta F_n/n) \ll 4\ 10^{-7}$ Hz^{-1} is fulfilled (average value of ~ 0.04 10^{-7} Hz^{-1}, n=5, 5 MHz crystal).[98] Hence, the frequency difference is proportional to the adsorbed mass and the film is considered to be rigid.[109]

We evaluated the changes in frequency (F) during the enzyme adsorption on different polymer films in four stages as indicated by arrows in Figure 4: (a) system stabilization, with constant F under buffer flow (10-20 minutes), (b) enzyme adsorption, F decreases under enzyme flow (2-3 hours), (c) enzyme incubation without flow, F almost constant (30 minutes), (d) enzyme desorption, F increases under buffer flow until stable again, suggesting that no more enzyme is desorbing. The adsorption of laccase on monolayer (up and up-down) and bilayer (up-up) films occurred during 3 hours. After the incubation, less laccase was desorbed under buffer flow from monolayers than from the bilayer. No significant influence of the film type on the deposited mass of laccase was observed, the enzyme was adsorbed on all three types of polymer films in a range of 0.562-0.632 µg cm^{-2} (Table 2, Figure 19). Triplicate QCM-D measurements resulted in a standard deviation ranging between 2.08 – 8.52 Hz for laccase and between 0.87 – 10.21 Hz for tyrosinase. The high values of the standard deviation are due to several factors, such as the transfer of the block copolymer on the silica slides, QCM-D working regime, the ability of the enzymes to adsorb/desorb on the polymer film.

Table 2 . Adsorption of laccase and tyrosinase on three different types of A_{45}-B_{101}-C_{27} triblock copolymer films measured by QCM-D.

A_{45}-B_{101}-C_{27} block copolymer	Enzyme	Δf (Hz)*	Enzyme mass adsorbed (μg cm^2)	Surface coverage (μmol cm^{-2})	Number of enzymes/ cm^2 10^{-12}
monolayer	laccase	35.3	0.625	6.5	3.92
up-down monolayer	laccase	40.6	0.562	5.9	3.53
bilayer	laccase	35.7	0.632	6.6	3.96
monolayer	tyrosinase	38	0.672	4.7	2.81
up-down monolayer	tyrosinase	21.2	0.375	3.1	1.88
bilayer	tyrosinase	40	0.708	5.9	3.55

Enzyme molecular weights were taken into account to determine the surface coverage as *Δm/MW ratio*, and the number of enzymes adsorbed per area of polymer film.[110] For tyrosinase, adsorption ended earlier (2 hours) and less enzyme was adsorbed on the monolayer films, whilst considerably more was adsorbed on the bilayer film (0.708 μg cm^{-2}). After incubation, tyrosinase desorption under buffer flow was more prominent than for laccase, thus at the end less tyrosinase than laccase remained adsorbed on the films. The enzyme dimensions are expected to influence the adsorption-desorption process. Indeed, a lower quantity of the larger enzyme tyrosinase, was finally adsorbed on the polymer membrane surface, which may be explained by requiring more space per molecule on the synthetic membrane.

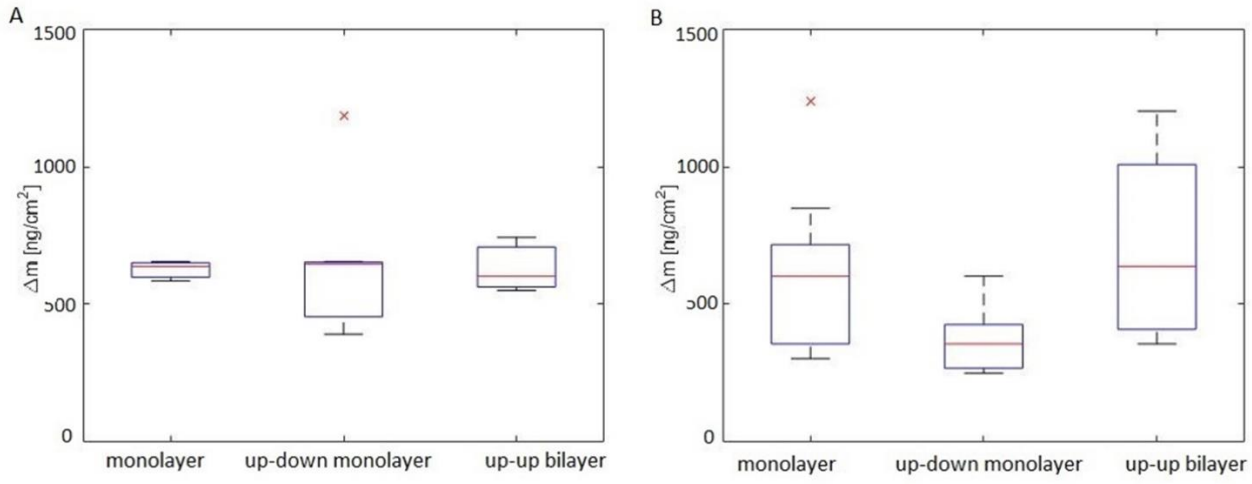

Figure 19. Amount of laccase (A) and tyrosinase (B) in ng/cm^2 calculated from QCM-D and shown in a boxplot with n=3-6.

Another factor affecting the enzyme immobilization process in the case of tyrosinase as compared to laccase is the tyrosinase tetramer structure, adopting a less compact configuration when adsorbing on the synthetic membrane.[108] This explains why the type of polymer film (mono/bilayer film, up/down transfer) influenced the enzyme immobilization for tyrosinase more than for laccase. The results are in agreement with studies where tyrosinase was deposited on lipid-based membranes prepared by Langmuir–Schaefer technique (horizontal lifting).[88]

The successful attachment of both enzymes on polymer films (monolayers and bilayer) is based on an electrostatic interaction between the enzymes and the exposed domain of the polymer films. PDMAEMA, which is the exposed C block of the polymer membranes, is positively charged at a pH between 5 and 8 due to protonation of the tertiary amino groups.[111] Both, laccase and tyrosinase are negatively charged in the pH range used, (laccase above pH 3.5 [107] and tyrosinase above pH 4.7, Sigma – Datasheet). Hence, it is deduced that the electrostatic interaction is key to the adsorption of these enzymes on the synthetic mono- and bilayers. An influence of the surface charge on the adsorption of laccase on positively charged methylene blue self-assembled monolayer films has been observed in other studies as well. [100] The adsorption-desorption behavior suggests that both adsorption and desorption of both enzymes differs with the

membrane type and enzyme. The adsorbed mass of laccase and tyrosinase on polymeric membranes remained stable for at least 18 h (**Figure 20**) at room temperature.

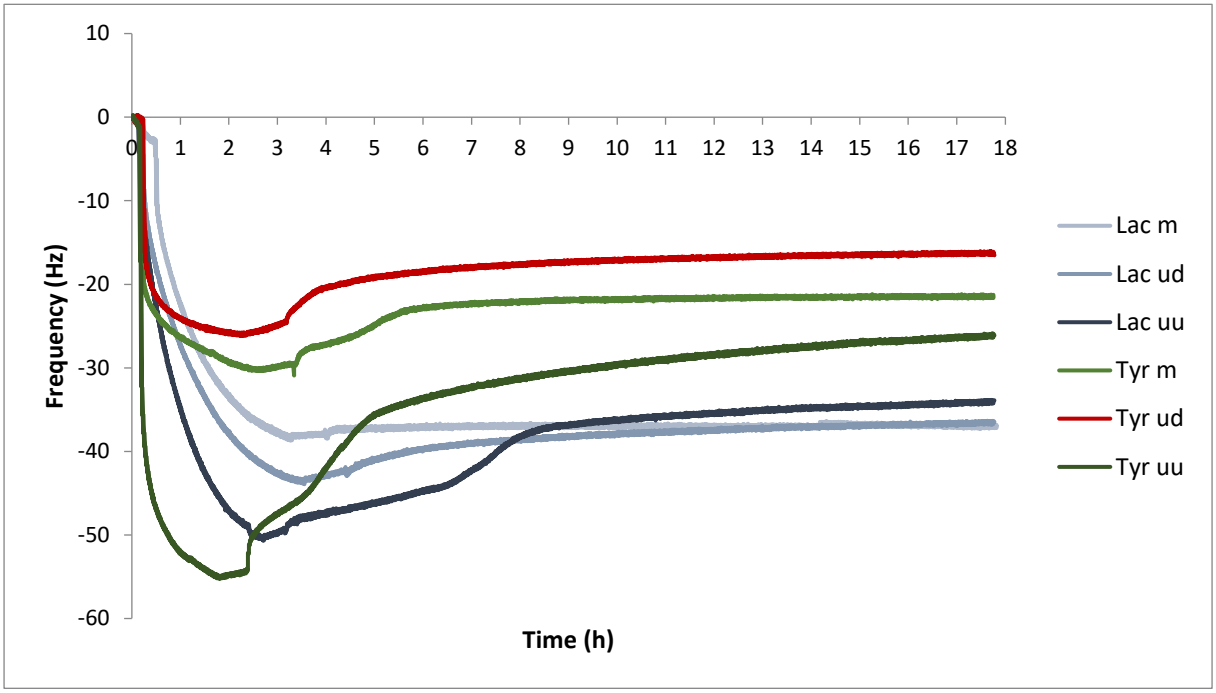

Figure 20. Changes in frequency (mass) during the adsorption of laccase and tyrosinase (both enzymes from 0.5 µg mL^{-1} solutions) on the copolymer membranes: monolayer (m); up-down monolayer (ud) or bilayer (uu); data of 5th overtone shown.

3.4.3 Active Surfaces Generation with Immobilized Enzymes on Copolymer Membranes

Enzyme adsorption on the polymer films for activity tests was performed by immersion of the A_{45}-B_{101}-C_{27} solid supported monolayer/bilayer films in enzyme solutions. AFM images of the $A_{45}B_{101}C_{27}$ triblock copolymer films with adsorbed laccase and tyrosinase, respectively, did not show significant differences when measured immediately, after 1 day and after 3 months (**Figure**

21). Long-term stability of these active surfaces supports their further application and is discussed below.

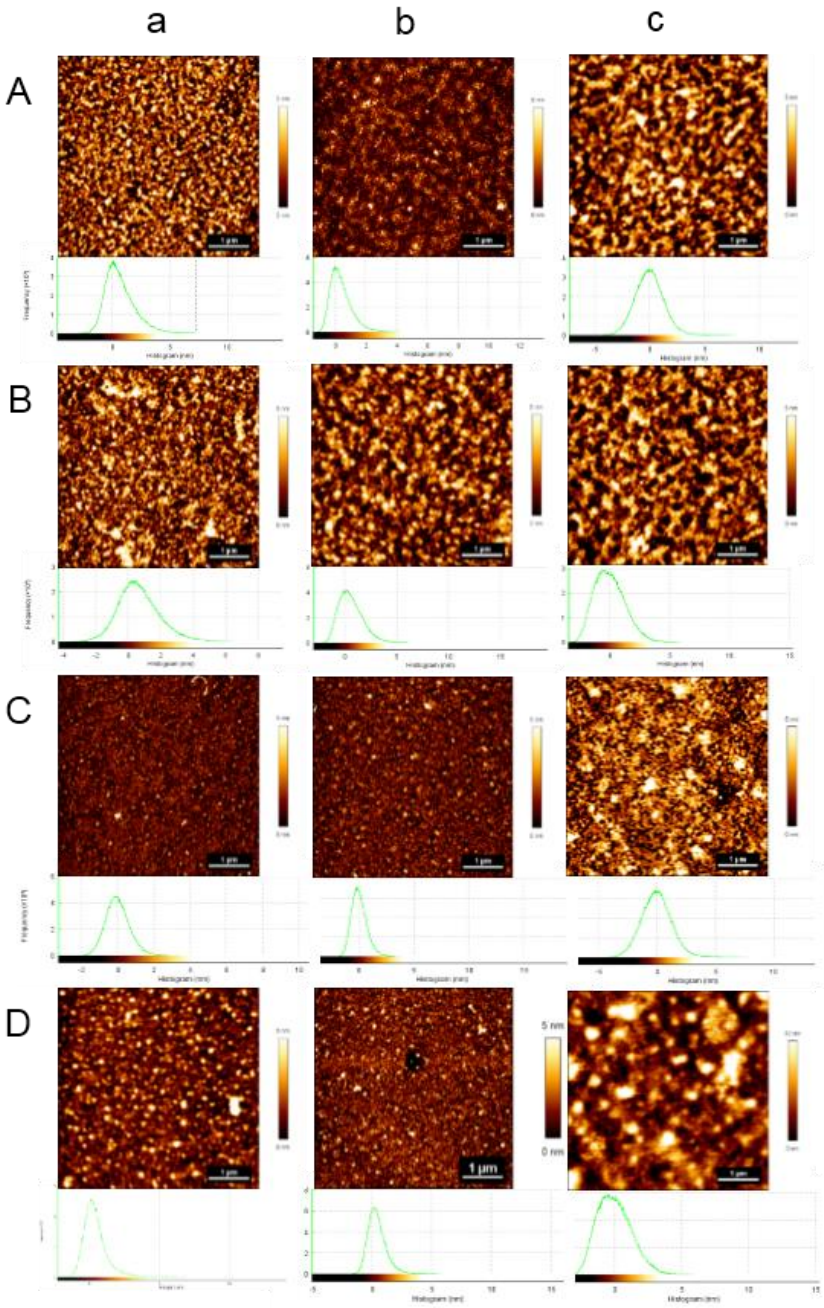

Figure 21. AFM images of the triblock copolymer films with adsorbed enzymes and the related histograms of the channel values: A – laccase after 1 day; B – laccase after 3 months; C – tyrosinase after 1 day; D – tyrosinase after 3 months; a – monolayer film; b – up-down monolayer film; c – bilayer film.

In order to determine the amount of the enzymes immobilized on the A_{45}-B_{101}-C_{27} solid supported copolymer films, the BCA assay was used. The BCA assay allows to quantify the amount of proteins in solution, hence the enzymes were first desorbed from the polymer films using SDS, contrary to the total enzyme amount adsorbed as determined by QCM-D. The concentration of SDS (5 wt%) used for enzyme desorption was in the range where the results obtained by the BCA assay are not affected, as stated by the supplier. The data obtained with BCA assay for both enzymes is presented in **Figure 22**. In the case of laccase, the amounts of desorbed enzyme available for BCA assay quantification are smaller than the amount of adsorbed laccase, probably due to incomplete removal of the enzyme by SDS. This indicates that not all laccase molecules are accessible, a fraction that cannot be removed remains embedded in the polymer film.

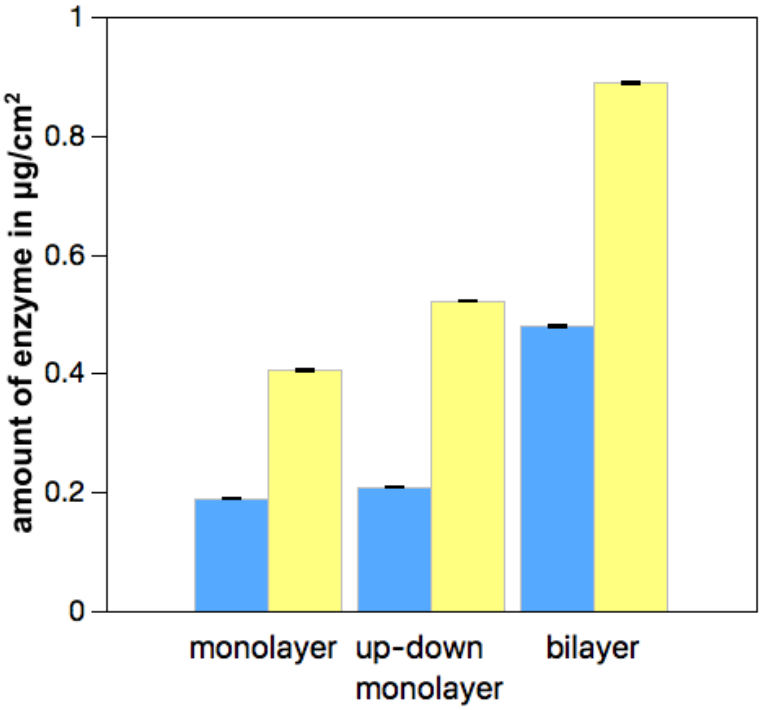

Figure 22. Amounts of laccase (blue) and tyrosinase (yellow) removed from the monolayer, up-down monolayer and bilayer polymer films, measured by BCA assay. The determined mass of the enzymes were expressed as mass per surface area (µg cm^{-2}).

Interestingly, whilst the amount of immobilized laccase is approximately similar for all layer types, as determined by QCM-D, the accessibility determined by the BCA assay varies with the type of polymer film. Both monolayers (monolayer and up-down monolayer) have lower concentrations of accessible laccase than the bilayer. For the monolayer films, the values of removed laccase of 0.189 ± 0.001 μg cm^{-2} (monolayer), and 0.209 ± 0.001 μg cm^{-2} (up-down monolayer) are significantly lower than what was obtained for the bilayer films (0.479 ± 0.003 μg cm^{-2}). A similar behavior has been observed for tyrosinase, with less enzyme detected in the case of monolayers (0.405 ± 0.002 μg cm^{-2} for monolayer and 0.521 ± 0.001 μg cm^{-2} for up-down monolayer) than in the case of the bilayer (0.888 ± 0.001 μg cm^{-2}). This observation can be explained by a higher roughness and therefore a larger surface area of the bilayer, which makes the immobilized biomolecules more accessible. A higher amount of tyrosinase was removed according to the BCA assay compared to what was obtained by QCM-D. This unexpected behavior might be related to differences in the adsorption-desorption procedures of these methods and intrinsic properties of tyrosinase (conformation, charge, interaction with the synthetic membrane). Besides, the measurement principles are very different and for the BCA assay also affected by the accessibility of the enzymes, complicating an immediate comparison. Importantly, both QCM-D and BCA assay confirm that laccase and tyrosinase adsorb on the different types of polymer films, a prerequisite for the development of a biosensors based on the specific enzyme activities.

3.4.4 Enzymatic Activity Free and on Polymer Membranes

The enzymatic activity of laccase and tyrosinase adsorbed on polymer monolayer and bilayer membranes was studied and compared with the activity of free enzymes. In a previous study, immobilized laccase was studied with 2,6-dimethoxyphenol (DMP) as substrate.[9] Since tyrosinase doesn´t convert DMP (**Appendix A1**) and I wanted to see the diversity of the method, the activities were studied with two different phenol derivatives as models to assess the biodetection of phenols by active surfaces. In case of laccase DMP (0.1 mM) was used and 4-methoxyphenol (4-MP, 0.2 mM) in case of tyrosinase. The activity of both enzymes free in solution increased with the enzyme concentration (0.1-0.3 μg mL^{-1}) (**Figure 23, Table 3**) and maximum activity of laccase

free in solution was reached after 24 h, while tyrosinase free in solution reached a maximum after 1 h

.

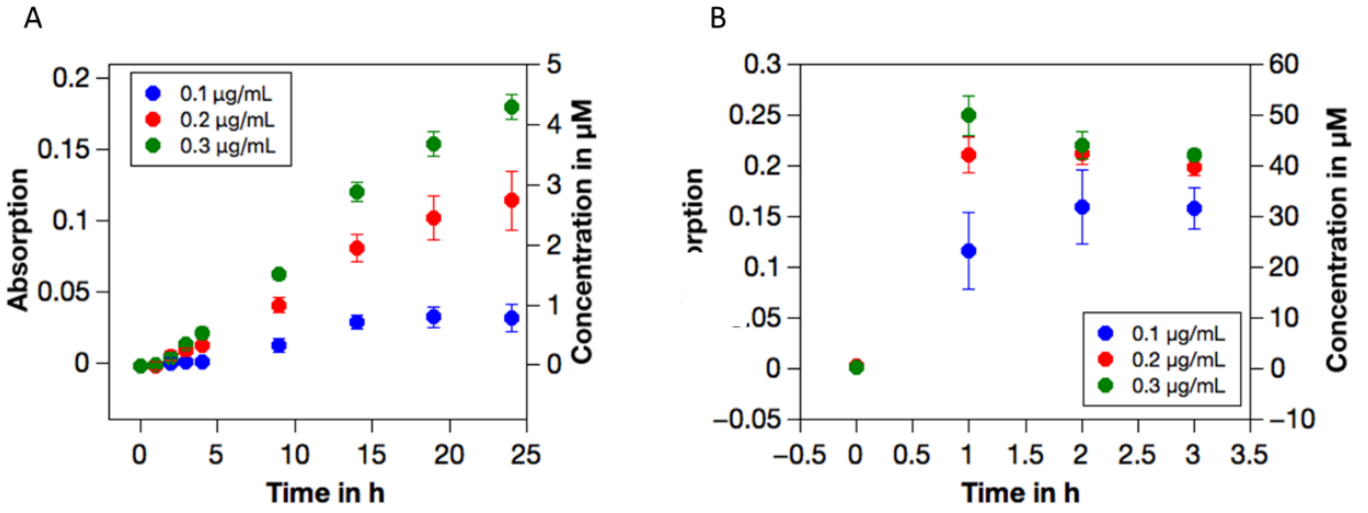

Figure 23. Activity of free (f) laccase (A) in the presence of DMP as substrate and tyrosinase (B) in the presence of 4-MP as substrate with different enzyme concentrations: 0.1 µg mL^{-1} (blue), 0.2 µg mL^{-1} (red), 0.3 µg mL^{-1} (green). The activity is shown as absorption intensity (left) and as product concentration (µM, right). The product concentration was calculated using the calibration curves shown in ***Appendix A2****. Therefore, the activity of the immobilized enzymes on the copolymer mono- and bilayer films was tested for different time periods, laccase for 24 h (with maximum activity at 19-24 h) and tyrosinase for 6 h (with maximum activity at 2-3 h).*

Table 3 Concentration of the oxidation product (µM) for free enzymes at different concentrations (0.1, 0.2 and 0.3 µg mL^{-1}).

Time (h)	0.1 µg mL^{-1} free enzyme Concentration of the oxidation product (µM)	0.2 µg mL^{-1} free enzyme Concentration of the oxidation product (µM)	0.3 µg mL^{-1} free enzyme Concentration of the oxidation product (µM)
Laccase (initial DMP concentration 0.1 mM)			
0	0	0	0
1	0	0	0.01±0.05
2	0.04±0.08	0.15±0.07	0.13±0.07
3	0.06±0.07	0.23±0.05	0.35±0.05
4	0.05±0.05	0.33±0.05	0.53±0.08
9	0.33±0.10	1.00±0.13	1.50±0.09
14	0.71±0.10	1.94±0.22	2.88±0.15
19	0.79±0.17	2.45±0.36	3.68±0.20
24	0.78±0.22	2.73±0.48	4.30±0.20
Tyrosinase (initital 4-MP concentration 0.2 mM)			
0	0.22±024	0.47±0.21	0.37±0.41
1	23.20±7.52	42.24±3.54	49.86±3.88
2	31.94±7.37	42.44±2.26	44.06±2.82
3	31.59±4.04	39.81±1.77	42.24±1.07

The activity increased starting from enzymes immobilized on monolayer to up-down monolayer, with the enzymes immobilized on bilayer showing the highest activity (Figure 24, Figure 25 A, B).

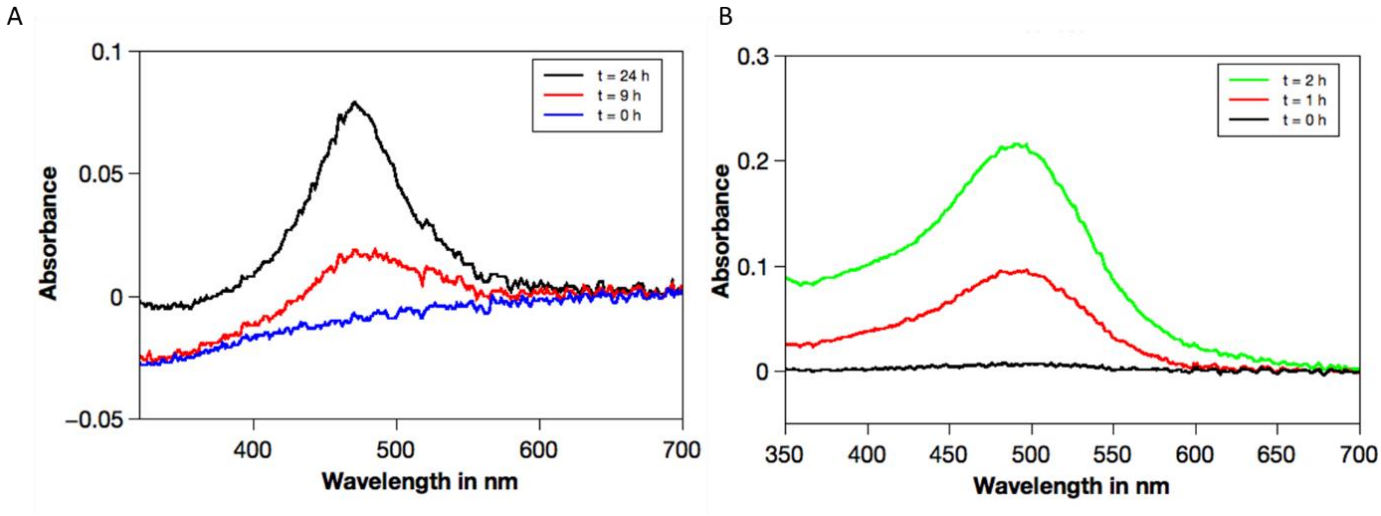

Figure 24.Absorption curves of A) laccase with DMP (0.1mM) and B) tyrosinase with 4-MP (0.2mM) on uu bilayer showing the change in peak intensity over reaction time due to product formation.

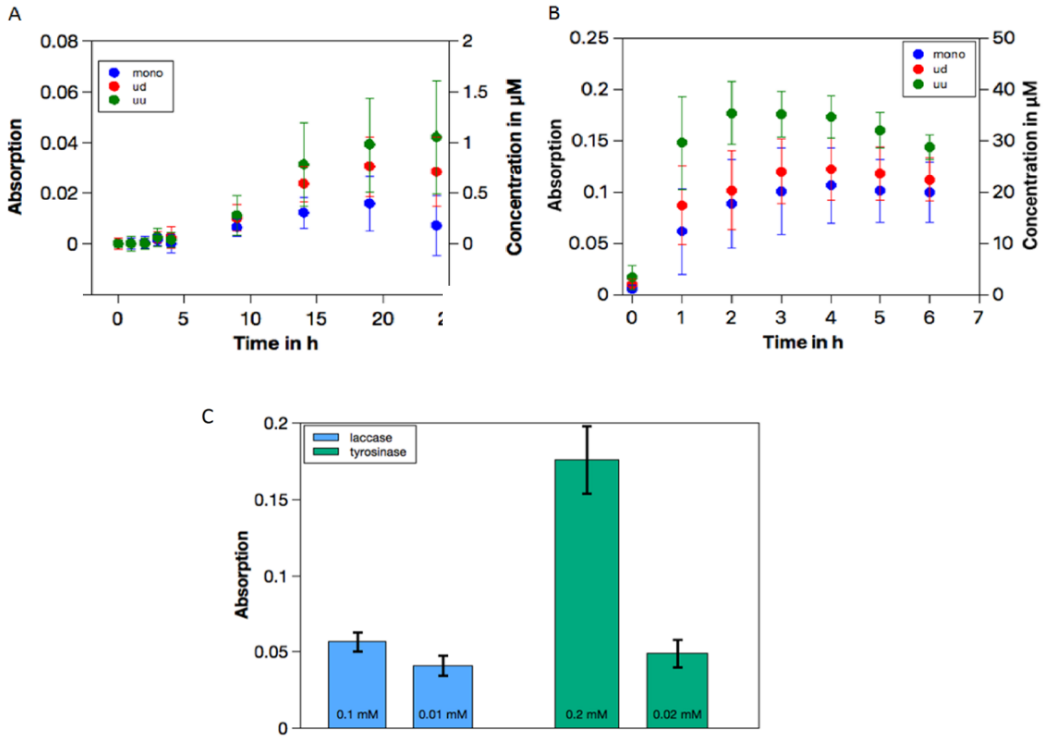

Figure 25.Activity of enzymes immobilized on the A_{45}-B_{101}-C_{27} block copolymer films as determined by oxidative product formation. (A) Laccase with 0.1 mM DMP as substrate which forms a product with a characteristic UV/vis absorption (λ = 470) (A), and (B) tyrosinase with 0.2 mM 4-MP as substrate forming a product that can be detected by UV/vis absorption at λ = 492). Curves are based on: monolayer (m, blue), up-down monolayer (ud, red), bilayer (uu, green), (lines added to guide the eye only). Activity of tyrosinase and laccase immobilized on the bilayer (uu) for two different concentrations of the enzyme substrates (C): DMP 0.1 mM and 0.01 mM (after 24 h), and 4-MP 0.2 mM and 0.02 mM (after 3 h). Enzymatic activity is shown via absorption intensity as measured and product concentration (µM) as calculated using the calibration curves in ***Appendix A2****. For all measurements, background correction has been performed by subtraction of the absorption intensity obtained when the enzyme substrate was added to the polymer membrane.*

Thereby, for laccase the maximum concentration for the product was detected after 24h on the bilayer (1.05±0.55 µM), compared to the monolayer, where the maximum was after 19 h (0.39±0.26 µM). For tyrosinase the highest concentration of formed product on the monolayer was detected after 4h (21.33±7.35 µM) and for the bilayer after 2h (35.38±6.09 µM) (Table 4).

In literature these reactions are well known and the mechanisms described. [112, 113] This activity behavior correlated well with the concentration of accessible enzymes on the bilayer film as determined by BCA assay.

Table 4 . Concentration of the oxidation product (μM) for immobilised laccase and tyrosinase.

Time (h)	Monolayer Concentration of the oxidation product (μM)	Up-down monolayer Concentration of the oxidation product (μM)	Up-up bilayer Concentration of the oxidation product (μM)
Laccase (initial DMP concentration 0.1 mM)			
0	0	0	0
1	0	0	0
2	0.01±0.05	0	0
3	0.04±0.05	0.06±0.05	0.06±0.08
4	0	0.06±0.11	0.04±0.06
9	0.15±0.08	0.25±0.13	0.27±0.19
14	0.30±0.15	0.59±0.17	0.78±0.41
19	0.39±0.26	0.75±0.29	0.97±0.45
24	0.18±0.29	0.71±0.34	1.05±0.055
Tyrosinase (initial 4-MP concentration 0.2 mM)			
0	1.18±0.72	2.08±1.06	3.43±2.31
1	12.33±8.29	17.48±7.73	29.63±9.07
2	17.68±8.62	20.43±7.63	35.38±6.09
3	20.13±8.48	23.98±6.29	35.23±4.47
4	21.33±7.35	24.43±6.06	34.58±4.14
5	20.28±6.17	23.58±5.18	32.03±3.44
6	19.98±5.80	22.48±4.16	28.73±2.42

As the highest activity of laccase and tyrosinase has been obtained for the enzymes immobilized on bilayer, we used the bilayer films to get more insight into the the phenol derivative detection range by decreasing 10-fold the concentration of the enzymes substrate (Figure 25 C). The autooxidation of the enzyme substrates has been taken into account as a background correction, that has been performed for all curves by subtraction of the absorption intensity obtained when the enzyme substrate was added to the polymer membrane. The 10-fold decrease of the enzyme substrates concentration decreased the enzymatic activity only slightly, indicating that lower concentrations of phenol derivatives can be efficiently detected by the functional surfaces (with 0.01 mM laccase substrate concentration and 0.02 mM tyrosinase substrate concentration). Importantly, the concentration of remaining substrate, which acts as a model for phenol contaminants, is reduced by 50% for tyrosinase and 10% for laccase. This further highlights the potential of the hybrid membranes for sensing and detection applications.

Enzymes immobilized on an up-down monolayer resulted in a more active surface than the monolayer. Different parameters may account for these differences in behavior, it may be related to the different roughness of these films, which affects the accesibility of the enzymes. In addtion, different enzyme conformations resulting in reduced conformational freedom of the enzyme that are affecting the mode of interaction between the enzyme and substrate may also affect the enzyme activity on the polymeric membranes. Importantly, both laccase and tyrosinase remained active upon adsorption on the polymer films as indicated by the increase in absorption. Yet, compared to free enzyme in solution the adsorbed enzymes have lower activity, which might be related to various molecular factors, as for example to the reduced acessibility of adsorbed enzymes or reduced conformational freedom of the enzyme. The stability of the films has been evaluated by preparing them two weeks and one day before the enzyme immobilization, respectively. As the activity for both laccase and tyrosinase did not change, it indicates that the films preserve their properties for at least two weeks (Figure 26).

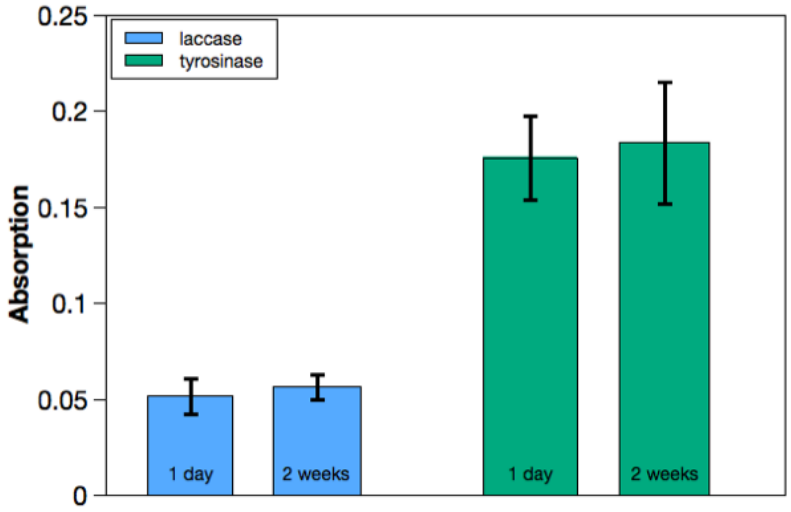

Figure 26. Activity of enzymes immobilized on the A_{45}-B_{101}-C_{27} block copolymer bilayer films with two weeks difference in preparation; laccase (blue) measured after 24 h with DMP as substrate (0.1 mM), λ_{max} = 470 nm, tyrosinase (green) measured after 3 h with 4-MP as substrate (0.2 mM), λ_{max} = 492 nm; averages of four measurements were used; error bars give standard deviation. The dispersity of the values for the immobilized enzymes activity are due to several factors: polymer transfer on the silica support, enzyme adsorption onto the polymer film, type of enzyme and substrate.

The measured activity was compared with the activity that is theoretically expected if the enzyme is fully accesible to the substrates (**Figure 27**). The theoretically expected and measured activity is very similar for tyrosinase immobilized on the bilayer polymer film (uu). For laccase, however, the measured activity is clearly lower than what would be exptected based on the amount of immobilized enzyme. This behavior is indicating a reduced accessibility of the enzyme after imobilization. Importantly, a comparison with surfaces that are not functionalized with polymer membranes further underlines the advantageous effect of the polymers as there is hardly any enzymatic activity observed on bare silica despite a higher amount of adsorbed enzyme (**Figure**

27). The reason is probably the fact that the enzyme is not able to adsorb to a smooth silica surface.

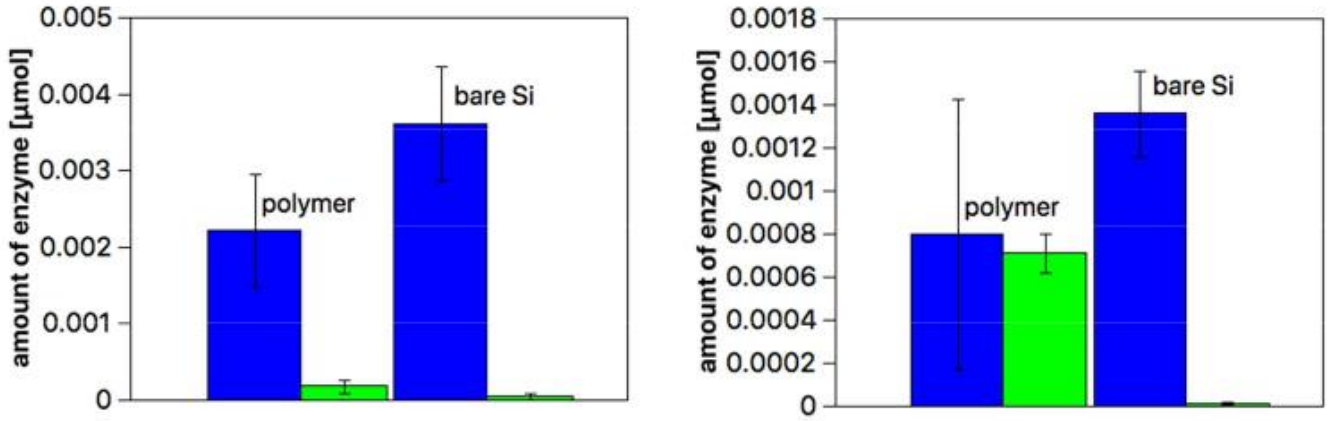

Figure 27. Determination of relative enzymatic activity of the enzymes laccase (left) and tyrosinase (right) on the bilayer polymer membrane (up-up) and on bare silicon wafer for comparison. The amount of enzyme on surface (blue) was calculated by subtracting the enzymatic activity determined in wash solutions from the washing solution used for immobilization. Hence, the reminder is assumed to be adsorbed on the surfaces. The result is compared to the experimentally determined result (green).

Together, the stability of the solid supported copolymer films and the preserved bioactivity indicate that these active surfaces have high potential upon optimization, for phenol and phenol derivatives biosensing.

3.5 Conclusion

The advantageous combination of the intrinsic bio-activity of the enzymes with the robustness and versatility of solid supported polymer membranes allows the creation of efficient “active surfaces”. In this respect, a systematic analysis of the effects of the molecular factors of the polymer membranes on the activity of the enzymes represents a crucial step that is necessary to control the efficacy of such functional planar membranes and advance their development for the production of desired compounds or for biosensing. In this project polymer membranes that provide a stable, solid-supported environment for the enzymes are reported. Interaction of both enzymes with different arrangements of the polymer films produced by LB transfer: mono- and bilayers with different morphology and properties (film thickness, wettability and roughness) were investigated. The three most promising polymer films (the monolayer, the up-down monolayer and the bilayer) were selected for enzyme adsorption and activity studies. It was observed that enzyme adsorption on the polymeric film is affected more by electrostatic interactions at enzyme/polymer interface than by surface roughness. Whilst both, laccase and tyrosinase preserved their enzymatic activity upon adsorption on the different types of polymer films, their activity was affected by the type of polymer film: bilayer films showed the highest activity for both enzymes. Therefore, bilayers are the most appealing candidates for combination with enzymes to sustain enzymatic reaction for sensing applications in aqueous environments. However, in order to advance towards potential applications of such functional planar bio-hybrid membranes further optimization is necessary to support scale-up as biosensors for the detection of phenol and its harmful derivatives, which are well known pollutants of drinking and natural water. The results of this work were also published in Langmuir.[74]

4 Chapter 2: The Influence of the Properties of Synthetic Planar Membranes on the Functional Insertion of Melittin

4.1 Introduction

4.1.1 Solid-supported planar membranes with Biopores

Transmembrane proteins have been incorporated into artificial polymer membranes for fundamental studies of their structures within synthetic membranes and especially for selective transport of molecules. Various applications exist for such systems which combine biomolecules and polymer membranes, such as water purification or sensing purposes. [114, 115, 116] These membrane proteins can be inserted in synthetic solid-supported membranes by different methods, specifically, (i) destabilisation of the membrane with an electric current, which favours protein insertion, and (ii) addition of detergent followed by its slow removal with biobeads, which drives protein insertion. Destabilisation of the membrane with an electric current has been used for water soluble biomolecules, for example the bacterial membrane polypeptide α-hemolysin (αHL). [117] Methods which are using biobeads have been used for insoluble membrane proteins, such as the potassium channel of the bacterium *Mesorhizobium loti*, MloK1. [32] Both reconstitution methods have their own challenges, since it is possible that the biomolecules are not only reconstituted in the membrane in a transverse active form, but also with another orientation, which results in non-functional membranes. [118]

4.1.2 Melittin and its interaction with membranes

Melittin is the main toxin of the bee venom and was discovered around 1970.[119] It has different effects on biological membranes, including cell lysis, antimicrobial activity and voltage-dependent ion conductance. [120] Among other membrane-active peptides, melittin is the most extensively studied. It is used in scientific research for cell and liposome lysis and as a model for pore-forming peptides, for example also in lipid bilayers.[121] The following model for the melittin actions was proposed by Terwilliger. According to his studies, melittin occupies space in the headgroup region of the hydrophilic molecules in the bilayer but does not extend all the way to the center of the bilayer. In order that there not be any empty space underneath the melittin molecule, the lipid chains must be distorted from the planar bilayer to fill the space, the so-called wedge effect. The amphipathic character also proposes that melittin could be stable at the edge of a planar bilayer, therefore being capable of generating membrane edges. At low concentrations in a membrane, melittin lies parallel to the membrane surface. This wedge effect increases the area of the outer leaflet relative to the unperturbed inner leaflet. As the melittin concentration increases, the area imbalance leads to the spontaneous formation of pores which are stabilized by melittin (the so-called edge effect). When the melittin concentration increases, the size of these pores increases until they connect and the membrane disintegrates, causing cell lysis.[120, 122]

4.2 Motivation

Pore-forming peptides are of interest due to their antimicrobial activity and ability to form gateways through lipid membranes.[123] In previous studies, pore-forming peptides were also used to investigate their pore formation inside polymer membranes.[117, 124] However, their interactions with polymer membranes are still poorly understood. Yet, this is an important piece of the puzzle on the way to further applications, such as sensors or medical devices. In this work a systematic investigation is carried out on how a model peptide interacts with and inserts into polymer membranes, to induce pore formation into planar membranes using the model peptide melittin. By varying selected molecular properties of block copolymers and resulting membranes (e.g. hydrophilic to hydrophobic block ratio, membrane thickness, surface roughness) and the stage at which the melittin was added to the polymer membranes a deeper understanding of melittin

insertion requirements is gained. The design of synthetic membranes permeabilized with melittin opens a new path toward the development of biosensors and catalytic compartments based on pore-forming peptides functionally inserted in planar polymer membranes.

4.3 Materials and Methods

4.3.1 Materials

All reported compounds were purchased from Sigma-Aldrich (USA) unless otherwise stated.

4.3.2 Synthesis of amphiphilic copolymers

A small library of amphiphilic PMOXAx-*b*-PDMSy-*b*-PMOXAx triblock copolymers was synthesized according to a reported synthesis procedure.[125-127]

Here a brief description of the synthesis of the copolymer $PMOXA_5$-b-$PDMS_{58}$-b-$PMOXA_5$ as an example. For this, the hydroxyl-terminated PDMS (OH-PDMS-OH) was synthesized by acid-catalyzed polycondensation. After purification, OH-PDMS-OH was stirred with trifluoromethanesulfonic acid in anhydrous hexane to form bitriflate-activated PDMS macroinitiator. After the filtration of the reaction mixture and evaporation of hexane, anhydrous ethyl acetate was added, in the presence of which the macroinitiator reacted with distilled 2-methyl-2-oxazoline (MOXA) in a symmetric cationic ringopening polymerization. After quenching the reaction with TEA/water (1:4 v/v), impurities were removed by ultrafiltration in water/EtOH (1:1 v/v). The solvent was removed by vacuum distillation and the resulting bihydroxyl-terminated triblock copolymer $PMOXA_5$-b-$PDMS_{58}$-b-$PMOXA_5$ was dried under vacuum.

For the CLSM experiments 5% of $PDMS_{37}$-b-$PMOXA_9$ copolymers were used that were labeled with the fluorescent dye, sulforodhamine B acid chloride (SRB). The dye was linked to the hydroxyl end group of the polymer.[41]

4.3.3 Langmuir-monolayers at air-water interface

Polymer films were formed at the air–water interface by closing the Langmuir trough barrier, which was monitored, as previously described, by an EP3SW system (Nanofilm Technologie GmbH, Göttingen, Germany) equipped with a Nd-YAG laser (λ = 532 nm), long-distance objective (Nikon, 10×), and monochrome CCD camera.3, 4 The size of the BAM image is 220 × 250 μm2, with a resolution of 1 μm.

4.3.4 Langmuir-Blodgett transfer of the copolymers

LB transfers of copolymer monolayers onto solid supports were performed using a mini-trough (KSV Instruments, Finland) with surface area of 242 cm2. For the transfer, glass slides were placed in the water subphase. The copolymers were then dissolved in chloroform at a concentration of 1 mg ml-1 and spread on the water surface. The film was formed at the air–water interface, while concomitantly measuring the associated Langmuir isotherms. The mini-trough barriers were stopped at a surface pressure lower than that corresponding to the film collapse. This surface pressure was determined during the recording of the Langmuir isotherms. For all four copolymers, a surface pressure of 38 mN m-1 was chosen. At that surface pressure, monolayers of copolymers were transferred to the previously submerged glass slides or silica plates by lifting the dipper at a constant rate of 0.5 mm min-1.

4.3.5 Alizarin Red S staining

Glass and silica slides were sequentially rinsed with chloroform and ethanol, and then dried with nitrogen gas. Afterwards, an oxygen plasma cleaner (Harrick Plasma, Ithaca) was used to remove the undesired contaminates on the slides and to activate the surfaces of the slides for the amination at maximum radiofrequency power for 3 min. After cleaning and activation, the slides were placed in a glass petri-dish filled with a solution containing 15 mL dry toluene under argon atmosphere, 100 μL aminopropyltriethoxysilane (APTES) and 50 μL dry trimethylamine. This solution was kept overnight under argon atmosphere. Next day, the silanized slides were sequentially washed with toluene and methanol and then 5 mL of 4-formylphenylboronic acid

(concentration of 1 mg ml-1) was added followed by gentle shaking overnight. After 24 hours, the slides were washed with methanol and a solution of Alizarin Red S (1 mg dissolved in 5 mL methanol) was added to the slides. After a last methanol-washing step, the slides were kept under dark until the copolymer membranes were transferred to Alizarin Red S-treated glass slides.

4.3.6 CA measurements

Once transferred, the wetting properties of the copolymer membranes were determined with a contact angle goniometer CAM 100 (LOT quantum design), using a CDD camera with 50 mm optics. Droplets of ultrapure water were placed with a micro-syringe on the supported-polymer membranes. The recorded images were analyzed by automatic curve fitting (Young-Laplace equation) performed by the instrument software. The droplet volume was kept constant for all measurements; measurements were taken on five different areas on each slide, and average values and standard deviation were calculated.

4.3.7 AFM

The surface topography of the copolymer membranes was monitored by AFM before and after deposition of the copolymers by using a JPK NanoWizard 3 AFM (JPK Instruments AG). All measurements were performed in the AC mode in air, using silicon cantilevers (Tap150 Al-G, Budget Sensors) with a nominal spring constant of 10–130 N m^{-1} and a resonance frequency of 300 kHz. The images were analyzed with the data analysis software JPK Data Processing (v. 5.0).[74]

4.3.8 QCM-D monitoring

A Q-sense E1 instrument (Biolin Scientific, Sweden) was used to monitor adsorption of melittin by recording changes in frequency and dissipation as a function of time. Silicon oxide coated QCM-D sensors (model no: QSX303) were rinsed with water and ethanol. After gentle drying, oxygen plasma was used for 3 min at the maximum radiofrequency power to remove additional contaminants from the sensor's surface. Subsequent to plasma cleaning, the block copolymer films were transferred to silicon dioxide sensors by LB technique using the mini-trough, which lead to the formation of a planar copolymer membrane on the silicon oxide. The membrane coated silicon oxide was placed in the QCM-D measurement chamber. Then, PBS buffer was injected into the chamber and the measurement baseline was established under continuous flow of 100 µl min^{-1} until the frequency signal fluctuation was below ±1 Hz. Then, 15 µM melittin (in PBS, pH 7) was injected to the chamber for different periods of time (30 min to 2 hours). After the frequency and dissipation signals reached a minimum fluctuation, the membranes were rinsed with PBS. For all experiments, liquid samples were added under continuous flow at a rate of 100 µl min^{-1} as regulated by a Reglo digital peristaltic pump (Ismatec, Glattbrug). The QCM-D measurement data were collected at 3^{rd}, 5^{th}, 7^{th}, 9^{th}, and 11^{th} odd overtones and the reported QCM-D data were obtained at 5^{th} overtone due to stability of the obtained signal. In order to estimate the adsorbed mass of melittin, the Sauerbrey equation was applied.[60] This equation converts frequency shifts into mass density values as follows: $\Delta m = -C\Delta f$, where Δm is the adsorbed mass, C is the proportionality constant (17.7 ng cm^{-2}), Δf is the frequency shift.

4.3.9 Functionality of melittin upon insertion into planar membranes

Melittin was added to the planar copolymer membranes in two different ways: I) before the membrane transfer and II) after the membrane transfer. Using the first approach, the barriers in the LB trough were closed until surface pressure 30 mN m^{-1} was reached, then 20 µl of 15 µM melittin in PBS was added while stirring. After 10 min, the barriers were closed until the final surface pressure was reached and then transferred on the solid support. Using the second

approach, the 15 µM in PBS solution of melittin was added after the film transfer and incubated for 1h.

In order to check the functionality of melittin, CLSM was employed. The samples were examined with a Zeiss 880 CLSM (Zeiss, Germany) on a water-immersion objective (C-Apochromat 40x/1.2 W Korr FCS M27). For the CLSM, we used copolymers labeled with a fluorescent dye (SRB) which was linked to the hydroxyl end group of the copolymer to observe the fluorescence of the resulting copolymer membrane. For the channel analyzing the SRB labeled copolymer membrane, a 561 nm DPSS 5561-10 laser with 645-704 nm filter was used. For the channel analyzing FITC labeled melittin, a 488 nm argon laser was used, with 493-629 nm filters. In order to monitor the exchange between Alizarin Red S and glucose, CLSM was used with a 488 nm argon laser with 499-643 nm filters. The data were analyzed by ImageJ in order to calculate the fluorescence intensity: the fluorescence intensity of the whole image was captured and calculated with the program.

4.4 Results and Discussion

4.4.1 An integrative approach for understanding the effect of molecular factors on functional insertion of biopores in synthetic membranes

To investigate the interaction and insertion of melittin into the copolymer membranes, four $PMOXA_x$-*b*-$PDMS_y$-*b*-$PMOXA_x$ triblock copolymers were selected,[125, 126] further called $A_3B_{22}A_3$, $A_6B_{34}A_6$, $A_6B_{44}A_6$, and $A_5B_{56}A_5$, as membrane forming block copolymers. Here, A represents the PMOXA domain, while B represents the PDMS domain, with x as the number of repeating units in the A block (3, 5 and 6, respectively) and y as the number of repeating units in the B block (22, 34, 44 and 56, respectively)(Table 5). These block copolymers have different characteristics in terms of the molecular weight, ratio between the hydrophilic domain and the copolymer domain (f-fraction) and dispersity, molecular factors that influence the resulting properties of the copolymer membrane. Using these block copolymers, a polymer membrane platforms were created: Solid supported polymer membranes.

Solid-supported polymer membranes were used to analyse the effects of copolymer molecular parameters (e.g. f-fraction and dispersity) and derived membrane properties (e.g. surface

roughness and membrane thickness) on interaction and insertion of melittin. Melittin, an amphiphilic peptide composed of 26 amino acids was selected as a model pore forming peptide due to its conformational change from random coil in solution to amphiphilic α-helical bent rod when interacts with lipid bilayers[128, 129] or cell membranes, resulting in a bilayer perforation and thus a loss of ions and small molecules. As the composition of the lipid bilayer influences the interaction with melittin,[120, 130, 131] we expect that this effect will be significant when the membrane is synthetic. In addition, when the concentration of melittin, present in the lipid membranes increases, it was shown that the peptides undergo a dynamic reorientation eventually producing pores with a diameter ranging from 1.3 nm to 5 nm.

Table 5. Library of amphiphilic triblock copolymers with their respective characteristics (molecular weight (M_n), dispersity (Đ), f-fraction)

Code	Block length	M_n (g mol^{-1})	Đ	f-fraction
$A_3B_{22}A_3$	$PMOXA_3$-$PDMS_{22}$-$PMOXA_3$	2300[126]	1.75[126]	0.22[126]
$A_6B_{34}A_6$	$PMOXA_6$-$PDMS_{34}$-$PMOXA_6$	3750[126]	1.67[126]	0.27[126]
$A_6B_{44}A_6$	$PMOXA_6$-$PDMS_{44}$-$PMOXA_6$	4500[126]	1.71[126]	0.23[126]
$A_5B_{56}A_5$	$PMOXA_5$-$PDMS_{56}$-$PMOXA_5$	6750[125]	2.4[125]	0.13[125]

4.4.2 Solid supported polymer membranes

Planar copolymer membranes were created on solid supports by LB- method (named solid-supported polymer membranes) to evaluate their interaction with melittin. First, the behavior of the copolymers at the air-water interface was investigated by compression of Langmuir monolayers, in order to determine the transfer point for the preparation of a solid supported membrane. The clean silica substrate was immersed in water and then the polymer dissolved in chloroform was spread on the air-water interface in the trough. Once the chloroform was evaporated, two barriers compressed the copolymer resulting in highly stable two-dimensional monolayers at the air-water interface. The same procedure, without the transfer was used to obtain the Langmuir isotherms of the distinct copolymers (**Figure 28 A**). The Langmuir isotherms had similar aspect, with a distinct plateau zone where the copolymers rearranged at the air-water interface until the monolayers collapsed. For example, the $A_5B_{56}A_5$ copolymer had a lift-off area at 1448 $Å^2$ and its collapse point was reached at a surface pressure of 44 mN m^{-1}, at the mean molecular area of 75 $Å^2$. The Langmuir isotherm of $A_5B_{56}A_5$ showed the longest plateau compared to other polymers. That means that the transition from a liquid-expanded to a liquid-

condensed state occurred more slowly, due to the higher molecular weight and length of the polymer. Also, the copolymer covered less area per polymer chain when PDMS domain was smaller, leading to a thicker packing. All four polymers formed homogenous monolayers throughout the whole compression as shown by BAM images (Figure 28 B).[74]

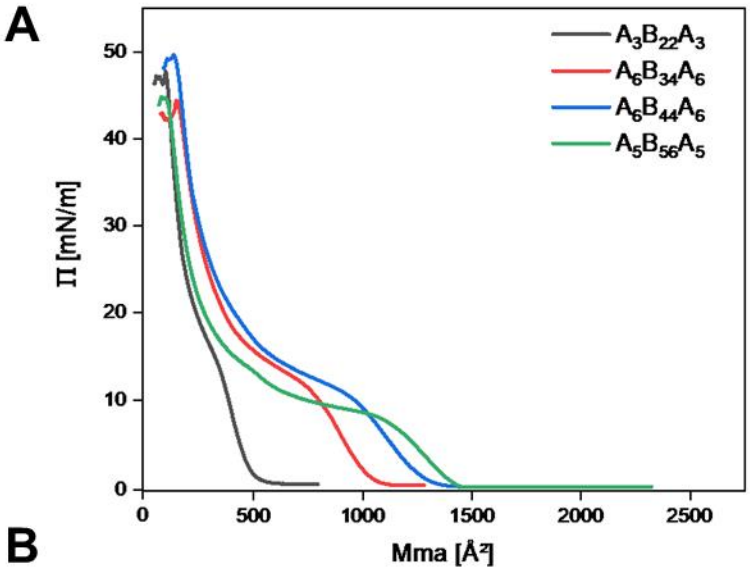
A
50
40
30
20
10
0
Π [mN/m]
0
500
1000
1500
2000
2500
Mma [Å²]
A3B22A3
A6B34A6
A6B44A6
A5B56A5

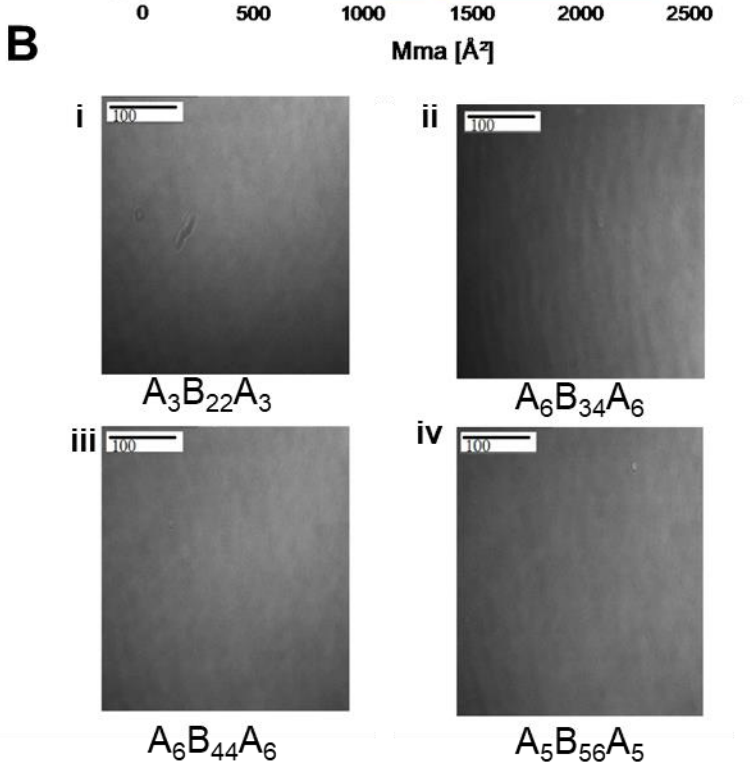
B
i
100
A3B22A3
ii
100
A6B34A6
iii
100
A6B44A6
iv
100
A5B56A5

Figure 28. A) Langmuir-Isotherms of the four polymers $A_6B_{44}A_6$, $A_6B_{34}A_6$,$A_3B_{22}A_3$ and $A_5B_{56}A_5$. B) BAM micrographs for the four polymers: i) $A_6B_{44}A_6$, ii) $A_6B_{34}A_6$,iii) $A_3B_{22}A_3$ and iv) $A_5B_{56}A_5$ at the surface pressures (38 mN m^{-1}) used for transfer. The scale bar (100 µm) is the same for all images.

In addition, both, stability and elasticity for one model polymer ($A_3B_{22}A_3$) were measured. The stability of monolayers at the air-water interface was assessed by measuring the surface pressure of the monolayer compressed to a surface pressure of 38 mN m^{-1} over 100 minutes. At this high surface pressure, the well-packed monolayer is already formed and the slow decrease of the surface pressure in time indicates that the monolayer is stable enough to be transferred to a solid substrate (**Figure 29A**). The elasticity was evaluated by recording four reversible compression-expansion cycles (**Figure 29 B**). No relevant hysteresis was observed, the block copolymer did not dissolve in water, and its monolayer can therefore be considered elastic.

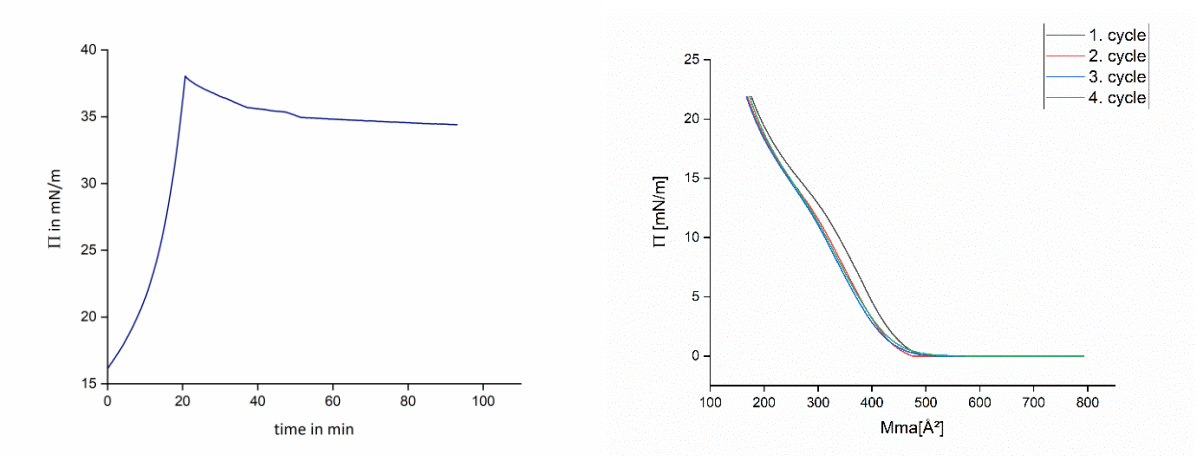

Figure 29. $A_3B_{22}A_3$ stability measurements over time. B) $A_3B_{22}A_3$ elasticity measurements shown in four cycles.

Afterwards, the monolayers were transferred from the air-water interface to silica slides at a surface pressure of 38 mN m^{-1} to obtain defect-free copolymer membranes. The surface pressure of 38 mN m^{-1} was chosen according to the Langmuir isotherms, since it showed a solid-like state of the copolymer monolayer, while being still flexible enough to allow the insertion of

biomolecules. In order to understand the effect on melittin insertion, the membrane properties before insertion were examined by ellipsometry (membrane thickness), contact angle (the hydrophilic/hydrophobic balance), and atomic force microscopy (for the surface topography and roughness) (Table 6).

Table 6. Properties of planar polymer membranes on solid support.

Code	Planar membrane thickness (nm)[a]	Contact angle (°)	RMS (nm)[b]
$A_3B_{22}A_3$	2.7 ± 0.1	52 ± 0.1	0.47 ± 0.14
$A_6B_{34}A_6$	3.6 ± 0.1	57 ± 0.1	0.69 ± 0.04
$A_6B_{44}A_6$	3.7 ± 0.1	55 ± 0.2	0.45 ± 0.16
$A_5B_{56}A_5$	4.7 ± 0.2	55 ± 0.1	0.96 ± 0.32

[a]The membrane thickness was obtained by ellipsometry. [b]Root mean square (RMS, roughness) of the membrane was determined by AFM.

The thickness of the synthetic membrane increased, with increasing number of PDMS units in the hydrophobic domain and molecular weight of the copolymer. As expected, the copolymer with the lowest M_n and the shortest PDMS domain ($A_3B_{22}A_3$) formed the thinnest membrane (2.7 ± 0.1 nm), while the copolymer with the longest PDMS domain and the highest M_n ($A_5B_{56}A_5$) formed the thickest membrane (4.7 ± 0.2 nm); the increase was less noticeable between $A_6B_{34}A_6$ and $A_6B_{44}A_6$, possibly due to the higher surface roughness of the former. Furthermore, contact angle measurements showed an increase of that the contact angle from 29 ± 2° of non-treated surfaces to 52-57° after the transfer of the copolymer membranes, indicating that the polymer chains exhibited similar directional arrangements, regardless of the copolymers, with the hydrophilic PMOXA domain oriented towards water and silica. We then investigated the surface topography of the different polymer membranes by AFM. All copolymers formed smooth

membranes on silica (Figure 30), as indicated by the values of the Root Mean Square (RMS) roughness (Table 6). Compared to the roughness of the bare silica (0.14 ± 0.01 nm), the copolymer with the longest PDMS domain led to the highest roughness of the solid-supported membrane (0.96 ± 0.32 nm) while the copolymer with shortest PDMS domain induced formation of solid-supported membranes with the least roughness (0.47 ± 0.14 nm).

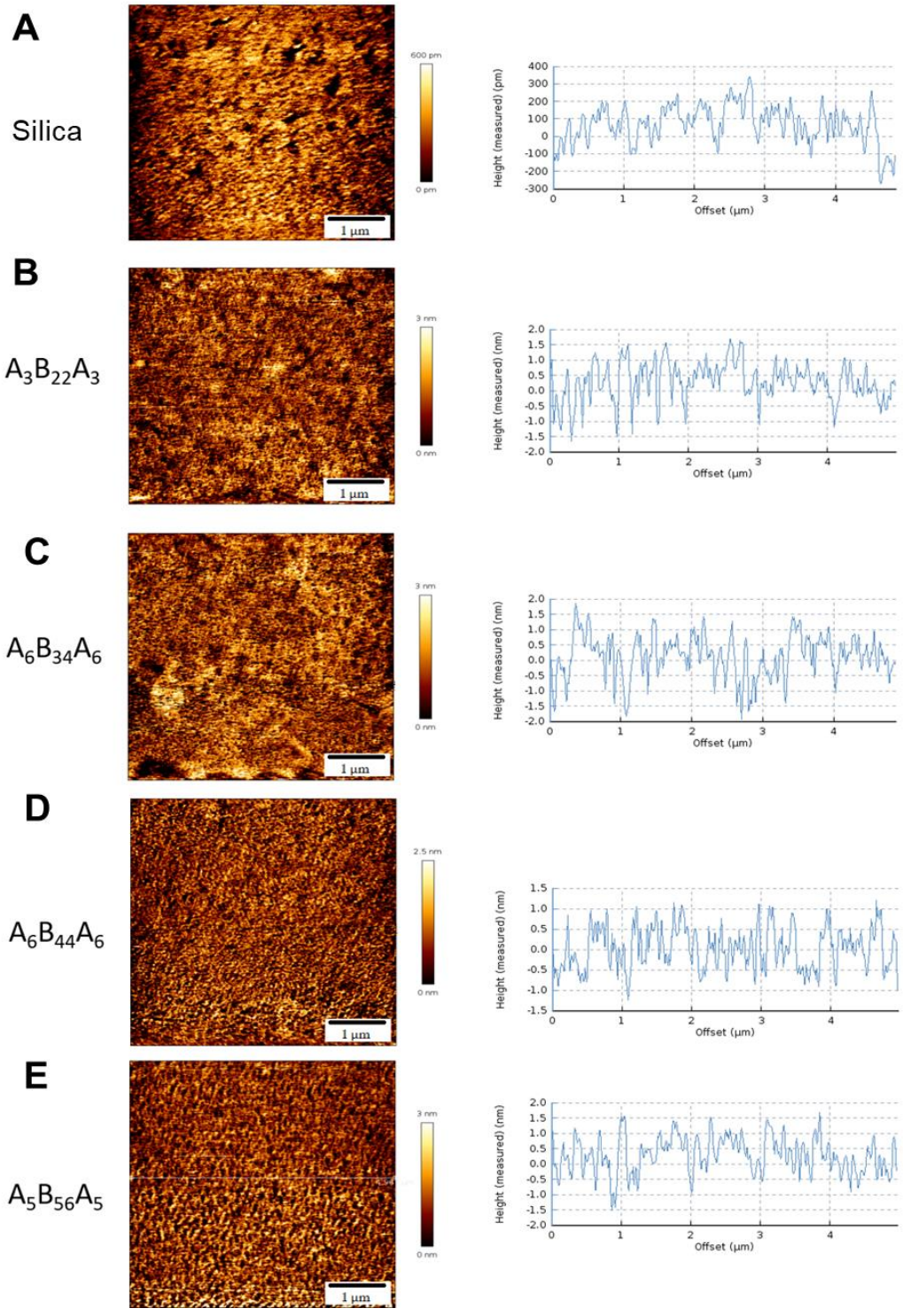
A
Silica
600 pm
0 pm
1 µm
Height (measured) (pm)
Offset (µm)
B
$A_3B_{22}A_3$
3 nm
0 nm
1 µm
Height (measured) (nm)
Offset (µm)
C
$A_6B_{34}A_6$
3 nm
0 nm
1 µm
Height (measured) (nm)
Offset (µm)
D
$A_6B_{44}A_6$
2.5 nm
0 nm
1 µm
Height (measured) (nm)
Offset (µm)
E
$A_5B_{56}A_5$
3 nm
0 nm
1 µm
Height (measured) (nm)
Offset (µm)

Figure 30. AFM micrographs and their respective cross sections for silica (A) and after deposition of $A_3B_{22}A_3$ (B), $A_6B_{34}A_6$ (C), $A_6B_{44}A_6$ (D) and $A_5B_{56}A_5$ (E) on silica.

4.4.3 Interaction of melittin with the solid-supported planar copolymer membranes

The interaction of melittin was monitored within supported polymer membranes using QCM-D.[132] Simultaneous changes in the resonance frequency (ΔF_n) and energy dissipation (ΔD_n) were recorded as a function of time, and with that reflecting the mass and viscoelastic properties of the adsorbed material, respectively, upon addition of melittin(**Figure 31**).

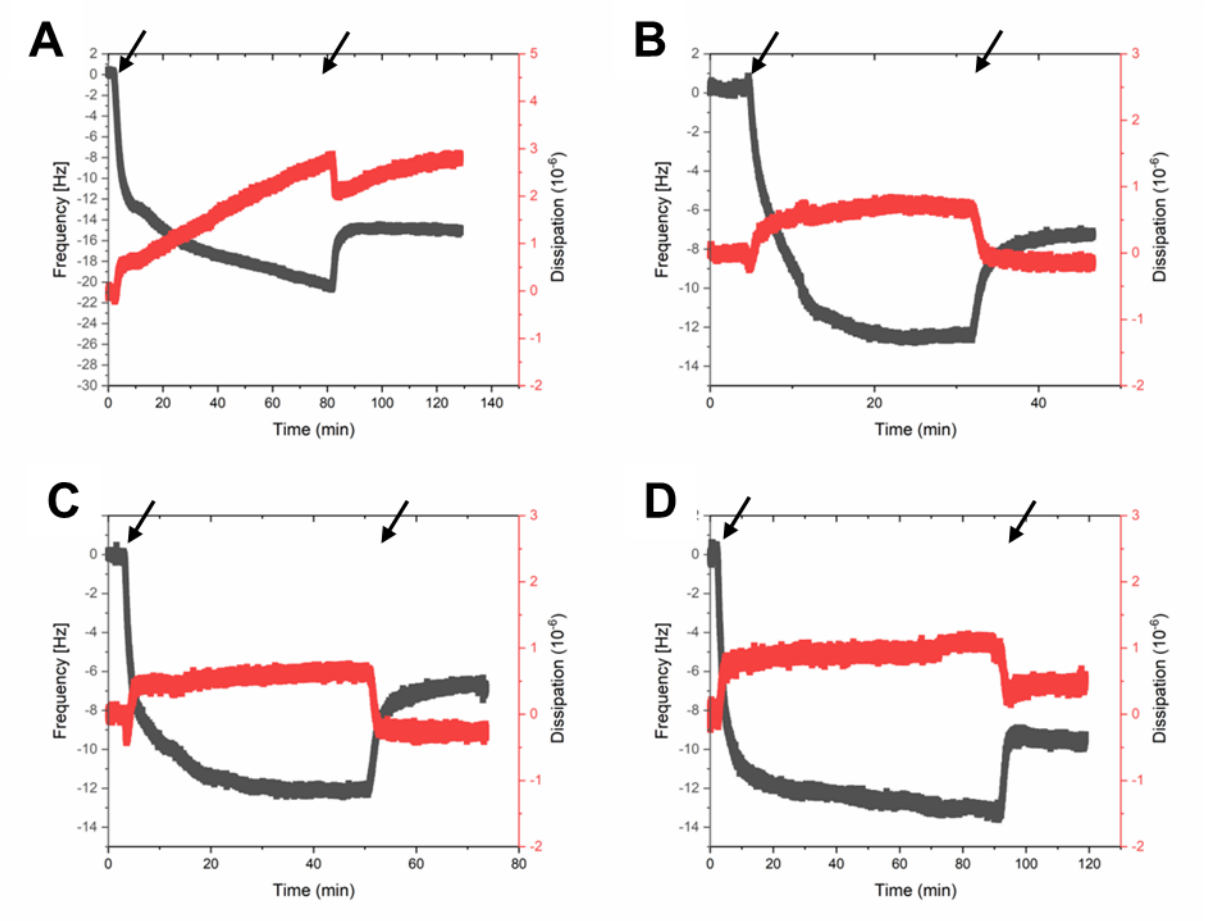

Figure 31. Changed in frequency and dissipation shift upon addition of 15 μM melittin to solid supported polymer membrane made of $A_3B_{22}A_3$ (A), $A_6B_{34}A_6$ (B), $A_6B_{44}A_6$ (C) and $A_5B_{56}A_5$ (D). The arrows sequentially indicate addition of melittin and rinsing with buffer solution.

Melittin adsorption led to a negative frequency shift, which represents an increase of adsorbed melittin mass on the sensor. Additionally, by taking into account the molecular weight of melittin, the average surface density of melittin monomers was determined using the Sauerbrey equation. Using this equation, it was determined that the average surface density of melittin monomers on solid-supported polymer membrane of $A_2B_{22}A_3$ corresponds to 70 ± 9 ×10^{12} cm^{-2}, a higher value compared to the other copolymer membranes (**Figure 32A**).[32, 74] However, taking into account only the average surface density of the melittin monomers is not sufficient to explain their interaction with solid-supported polymer membranes, as parameters of the copolymer chains (dispersity and f-fraction) and properties of the resulting membranes (surface roughness) should be considered. For example, dispersity of the copolymers affects the interaction of melittin because a higher value increases the probability of the peptide interaction with copolymer chains of optimal length, whilst the f-fraction can influence the electrostatic interactions between the polymer membrane and melittin. In addition, a higher roughness of the membrane means a larger interface for the melittin interaction. Therefore, the melittin surface density together with these molecular factors was included in a more appropriate model and calculated the volumetric density (ρ_{eff}) of melittin inside solid-supported polymer membranes with the equation:

$$\rho_{eff} = \frac{\sigma \times f \times Đ}{RMS}, \qquad [7]$$

where ρ_{eff} is the volumetric density of melittin, σ is the surface density of melittin, f is the ratio between the molar mass of the hydrophilic block and total molar mass of the block copolymer, Đ is the dispersity of the block copolymer, defined as the ratio of the weight to number average molar masses, and RMS is the root mean square roughness obtained from AFM measurements.

Furthermore, the relationship between ρ_{eff} and membrane thickness (θ) shows an exponential decay (**Figure 32B**), equal to:

$$\rho_{eff} = 6.20 \times e^{0.03(\frac{-\theta}{1.11})}, (r^2=0.99), \qquad [8]$$

where Θ is the membrane thickness (in nm). The trend, an exponential decay, suggests that the ability of melittin to insert into the synthetic membranes drops sharply with increasing membrane thicknesses (from 0.57 melittin monomers nm^{-3} for a thickness of 2.7 nm to 0.12 melittin monomers nm^{-3} for 4.7 nm). Overall, the interaction and adsorption of melittin on planar membranes is favored for membranes with a higher roughness (higher surface area), whereas melittin insertion is favored for membranes with a lower thickness (ease of penetration). This model is the first molecular description of the interface interaction between copolymer membranes and peptides, providing information of the complex scenario of molecular factors influencing the insertion in planar membranes and thus how a peptide interacts with a synthetic membrane. If the interaction between melittin and the membrane is affected by the membrane characteristics, it also has an influence on the ability of the peptide to stably insert within the polymer membrane.

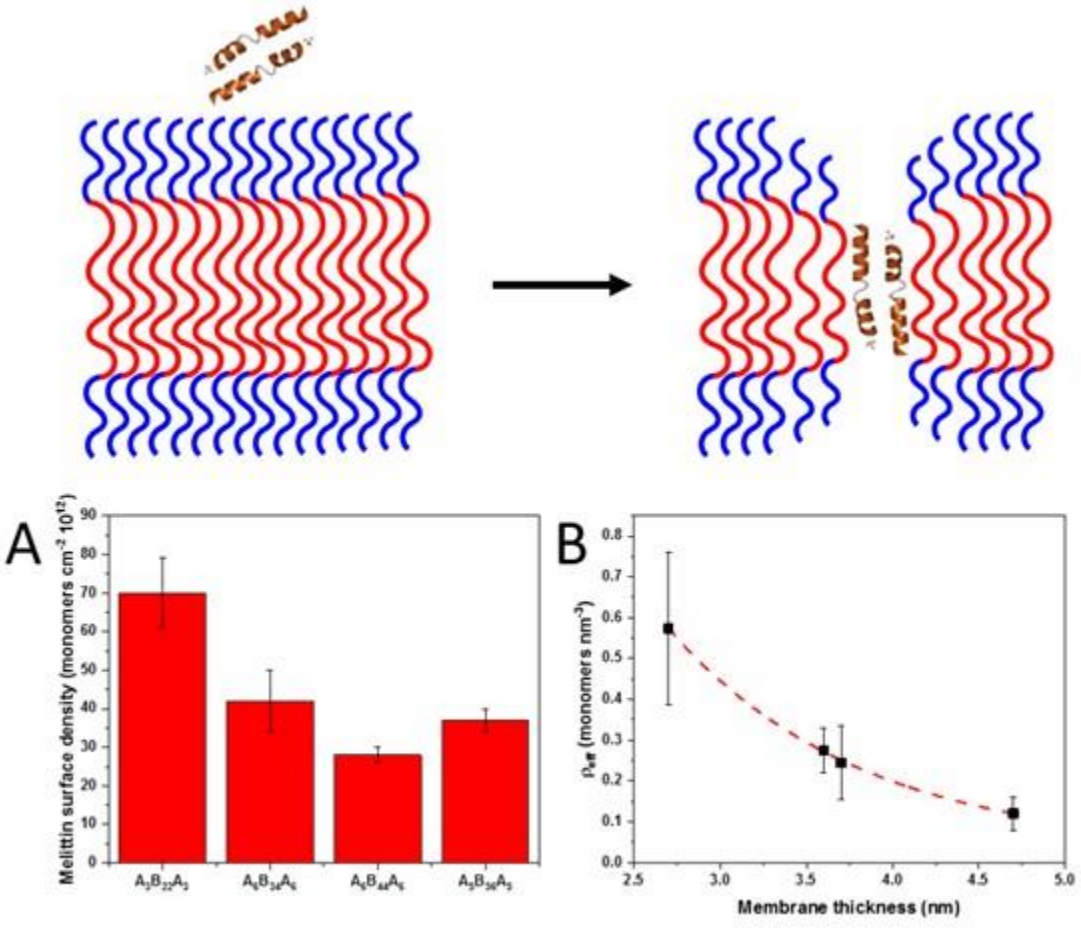

Figure 32. (A) Number of melittin monomers cm^{-2} 10^{-12}. (B) ρ_{eff} dependence of membrane thickness, which follows an exponential decay as the membrane thickness increases.

4.4.4 Functionality of the melittin pores inside the solid-supported planar polymer membranes

In order to test the functionality of the melittin pores inside the planar membranes, I prepared glass slides functionalized with a fluorescent complex, formed by Alizarin Red S and boronic acid. This complex is well-known for being fluorescent in the absence of glucose. Once added, glucose substitutes Alizarin in the complex causing a drop in the fluorescence intensity (**Figure 33**).[133]

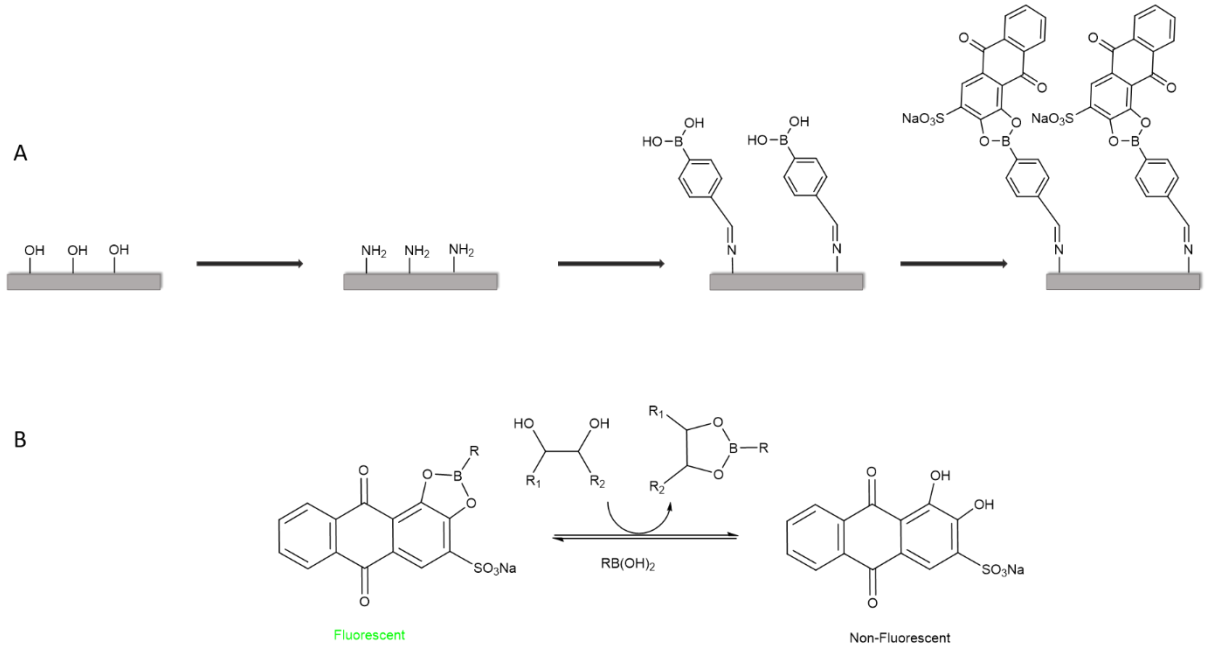

Figure 33. A) Functionalization of a glass slide with a boronic acid- Alizarin Red S complex, and B) Mechanism of Alizarin Red S/ cis-diol exchange.

The synthesis steps were followed up by measuring CA and ellipsometry. The results are shown in **Figure 34**. The thickness is rising with each synthesis step between approximately 1-1.5 nm. The hydrophilicity is changing after each step. While the surface is quite hydrophilic after amination and the addition of boronic acid, the addition of Alizarin Red S makes it more hydrophobic.

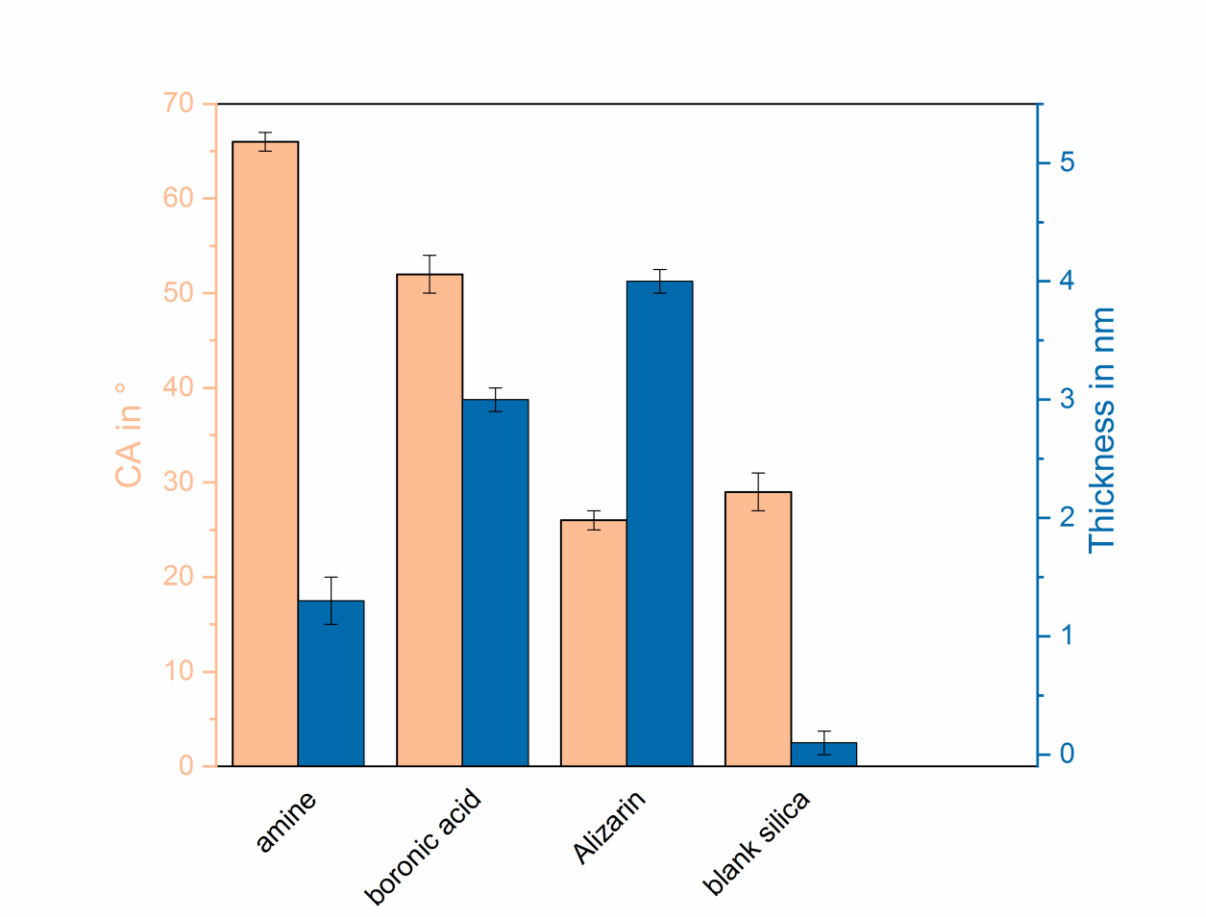

Figure 34. Contact angle and ellipsometry measurements for the alizarin slide preparation.

The idea behind this assay was that, when a homogeneous membrane is transferred on top of the Alizarin Red S complex, there would be no observable drop in the fluorescence intensity after addition of glucose, since the membrane shields the complex. When pores are formed by melittin insertion inside the planar copolymer membrane, glucose is expected to diffuse through and exchange with Alizarin in the complex, resulting in a drop in the fluorescence intensity. Thus, glucose was added to various Alizarin-modified surfaces: I) surfaces with no copolymer membrane, II) surfaces with copolymer membranes without melittin, III) surfaces with copolymer membranes with melittin, which was added before the membrane formation and IV) surfaces with copolymer membranes and melittin added after the membrane transfer.

The fluorescence intensity associated with Alizarin Red S was monitored by CLSM (**Figures 35-37, Appendix A3**).

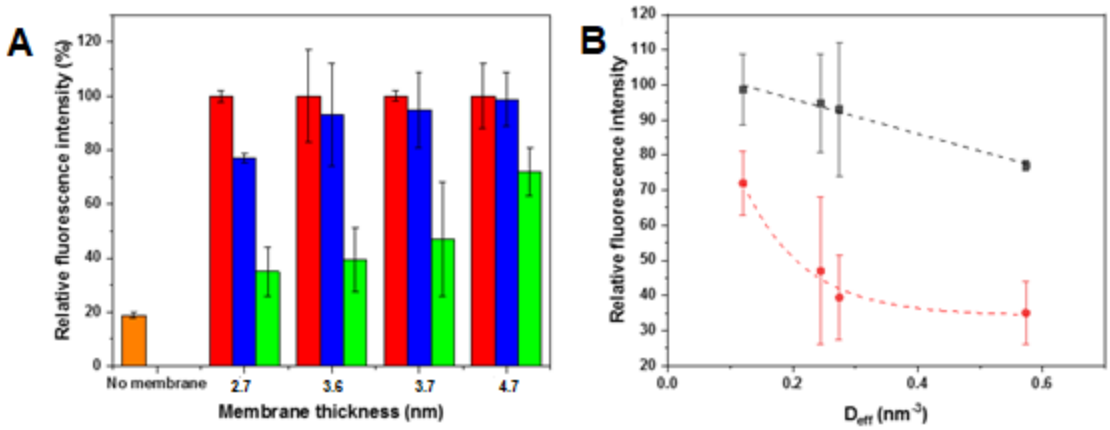

Figure 35. A) Remaining mean relative fluorescence intensity of the Alizarin Red S-boronic acid complex, after addition of glucose to Alizarin-functionalized surfaces: without a membrane (orange), with a copolymer membrane without melittin (red), with a copolymer membrane to which melittin was added after the membrane transfer (blue) and with a copolymer membrane to which melittin was added before the membrane transfer (green). A lower relative intensity corresponds to a higher glucose permeation. B) Relative fluorescence intensity dependence to ρ_{eff}*, for melittin added: before the polymer membrane transfer (red) and after the polymer membrane transfer (black). The starting relative fluorescence intensity was normalized to 100 % for each sample. Error bars shown as ± SD, n = 3.*

In order to compare the effect of glucose addition on different membranes with and without melittin, the initial fluorescence intensity was normalized to 100%. The fluorescence intensity decreased dramatically for Alizarin Red S-based surfaces without membranes, down to 18% in 1h, due to the unhindered diffusion of glucose and exchange with Alizarin. No decay in fluorescence intensity was obtained for any polymer membranes without melittin, indicating that the membranes were stable and without defects, thus preventing the passage of glucose. When melittin was added before the copolymer membrane transfer, the thinnest membrane showed the lowest residual fluorescence (35% after 1 h), while the thickest membrane retained most of the fluorescence intensity (73% after 1 h). The membranes with intermediate thickness allowed a mean decrease in the fluorescence intensity to 39% and 47%, respectively (Figure 35A). These

results show that melittin added before the transfer of the copolymer membranes remained functional and the insertion efficiency decreased with the increase of the membrane thickness. The thinner membrane led to the highest number of functionally inserted melittin peptides and favored the formation of pores.

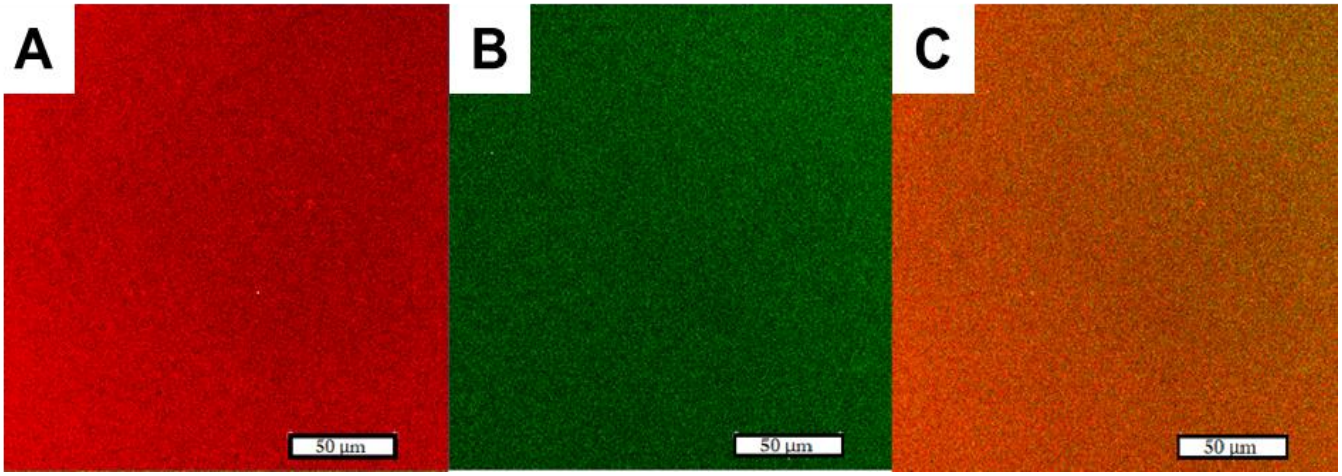

Figure 36. CLSM micrographs of a solid supported polymer membrane made of $A_3B_{22}A_3$ block copolymers with FITC labeled-melittin added before transfer A) the SRB labeled-polymer channel (Red) , B) the FITC labeled-melittin channel (green) and C) the combination of both channels. The scale bar is the same for all images (50 µm).

A different behavior was obtained for the planar membranes when melittin was added after their transfer on solid support: only the thinnest membrane exhibited a significant decrease in the fluorescence intensity of Alizarin Red S due to the glucose diffusion through (77% in 1 h). For all other thicker membranes, no significant decrease in the fluorescence intensity of Alizarin Red S complex was observed after 1 h ($A_6B_{34}A_6$: 93%; $A_6B_{44}A_6$: 95%; $A_5B_{56}A_5$: 98%). Therefore, the insertion of melittin is more difficult in a less dynamic state of the membrane, as is the case after the membrane transfer on a solid substrate. Interestingly, a linear correlation between ρ_{eff} and the membrane thickness for melittin added before the transfer and an exponential correlation when melittin was added afterwards (r^2 = 99 for both) was observed (Figure 35 B).

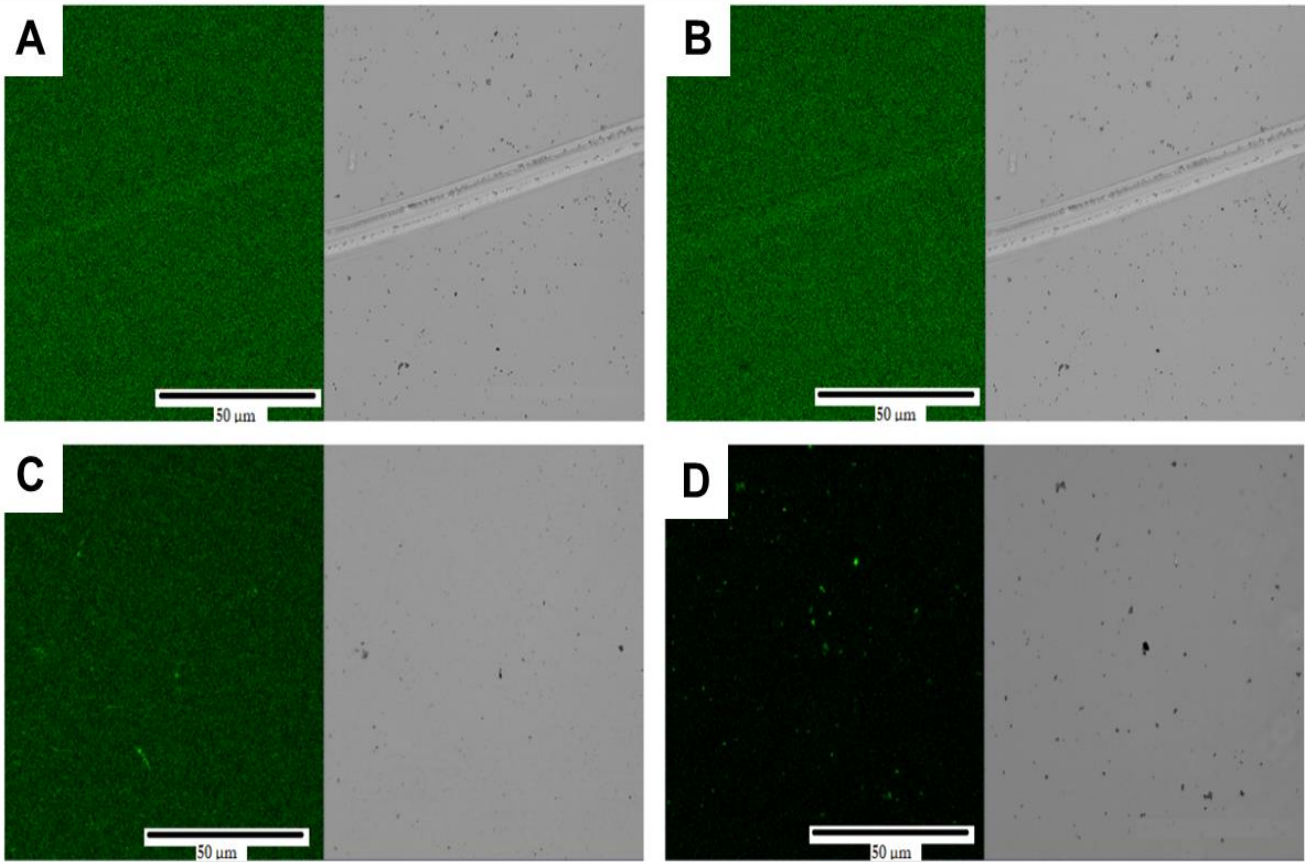

Figure 37. CLSM micrographs of polymer membranes made of $A_3B_{22}A_3$ on alizarin (green channel) containing glass slides. A) No melittin, before glucose addition, B) no melittin, 1h after glucose addition, C) melittin was added before transfer, before glucose addition, D) melittin was added before transfer, 1h after glucose addition.The scale bar is the same for all images (50 µm).

4.5 Conclusion and Outlook

The insertion of biopores and membrane proteins in planar polymer membranes is a more complex scenario than the insertion in lipid membranes. The reason is due to the significant difference in membrane properties, such as thickness. In this thesis, the molecular factors influencing the interactions and functional insertion of biopores in synthetic planar membranes were investigated. In this regard, melittin was used as a model peptide to elucidate the molecular factors (characteristics of the copolymer chains and properties of the membranes) that affect a functional insertion into PMOXA-*b*-PDMS-*b*-PMOXA membranes. The insertion strongly depended on inherent copolymer characteristics (hydrophilic ratio, dispersity) and membrane properties (thickness and roughness). In addition, it was shown that the induced pore-formation led to functional surfaces which could be used to transport glucose through the membrane. This work shows the insertion into planar membranes, in addition in a collaborative work, Andrea Belluati also investigated GUVs and small vesicles, where also the influence of curvature on the insertion was investigated. A combined paper about all architectures was published in 2020. [134] There it was shown that the addition of melittin to pre-formed planar membranes, vesicles or GUVs resulted in different permeabilization outcomes, with the planar membranes not favoring functional insertion. It is thus presumed that the membrane curvature should be considered too. As an outlook it would be interesting to investigate the influence of similar peptides and also other parameters, such as polymer composition.

5 Overall Conclusion and Outlook

In this thesis two different projects are presented. Their common goal was the development of biomimetic solid-supported membranes based on amphiphilic block copolymers. Through the preparation of different systems, it was shown that amphiphilic block copolymers are able to form uniform and reproducible membranes, when deposited on solid supports and that they can successfully perform as platforms for active biological compounds. In the first project, the morphology and properties of the mono- and bilayer polymer membranes were investigated with respect to their interaction with functional biomolecules. Firstly, the behavior of the block copolymer PEG_{45}-*b*-$PMCL_{101}$-*b*-$PDMAEMA_{27}$ the was studied at the air-water interface. After it was shown that the copolymer was able to form stable monolayers at the air-water interface, it was transferred using the Langmuir-Blodgett technique in different directions (up, down or both), which resulted in well-organized and defect-free films deposited on solid supports. Thereby, different architectures were achieved. They were characterized by AFM, contact angle and ellipsometry measurements. The three most promising polymer films (the monolayer, the up-down monolayer and the bilayer) were selected for enzyme adsorption and activity studies with phenolic compounds. These membranes composed of this triblock copolymer were used as cushions for immobilization of respectively laccase and tyrosinase. In addition, they were investigated in terms of homogeneity of the formed monolayer and bilayer. By using QCM-D, it was observed that enzyme adsorption on the polymeric film was affected more by electrostatic interactions at enzyme/polymer interface than by surface roughness. Both, laccase and tyrosinase preserved their enzymatic activity upon adsorption on the different types of polymer films. However, their activity was affected by the type of polymer film. Bilayer films showed the highest activity for both enzymes. Therefore, bilayers were proven to be the most appealing candidates for combination with enzymes to sustain enzymatic reaction for sensing applications in aqueous environments. A successful sensor for phenols was established during this project. As an outlook, several applications are possible, such as medical or environmental sensors with specific enzymes. However, in order to advance further optimization is necessary, for example to support scale-up of the sensor production process.

In the second project, the insertion of a model pore-forming peptide melittin in planar polymer membranes was investigated. The main goal was to study the molecular factors which were supporting the insertion. For this, a small library of PMOXA-*b*-PDMS-*b*-PMOXA of different lengths were first investigated at the air-water interface by BAM and then transferred by Langmuir Blodgett as bilayers to solid supports (glass or silica). The membranes were characterized by AFM, contact angle, LSM and ellipsometry. All of the polymers formed homogeneous membranes. Afterwards, two different techniques were used to insert melittin pores into the bilayers: Before transfer and after transfer techniques. Both techniques lead to melittin insertion, however the before transfer technique was by far more promising. The reason for that is most probably the flexibility of the chains at the air-water interface, when melittin was added. The insertion is in addition dependent on inherent copolymer characteristics (hydrophilic ratio, dispersity) and membrane properties (thickness and roughness). In addition, it was shown that the induced pore-formation led to functional surfaces which could be used to transport glucose through the membrane. As an outlook these surfaces can be used as glucose sensors or even medical devices.

In this thesis biofunctional membranes prepared from block copolymers were presented. They showed promising stability, diversity, and possibility of adjusting their properties to the desired functionality. It was shown that these robust membranes can successfully act as platforms for insertion of the biomolecules, such as membrane proteins and the decoration with enzymes. Most interestingly, it was shown that the biomolecules preserved their activity after being combined with the planar polymer membranes. With this, the great potential of the amphiphilic block copolymers in the development of systems mimicking biological membranes can be applied to applications in various fields, such as medicine, environment, sensing and others. Even if the great goal to develop an artificial cell is still far away, with these results we made a step closer to this achievement.

6 Appendix

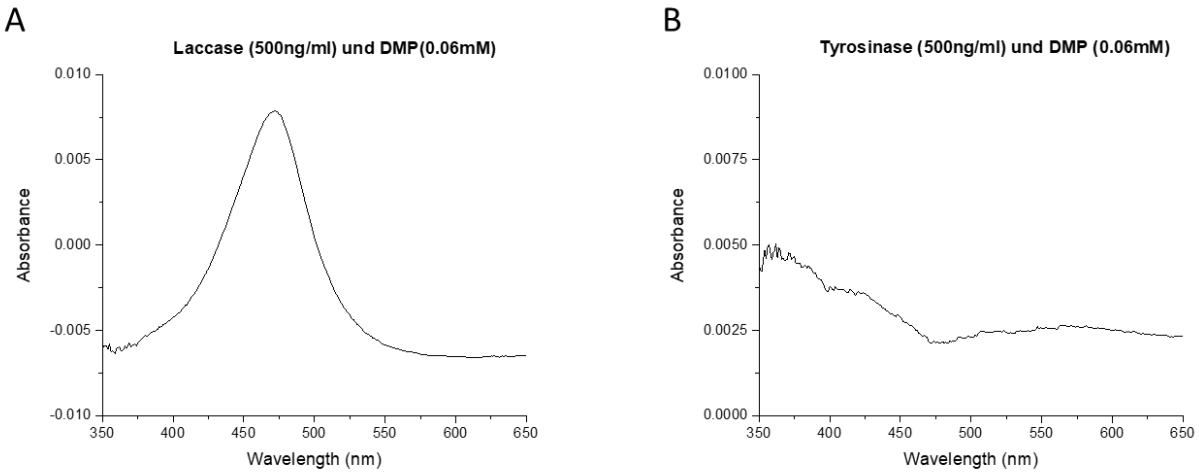

Figure A1. Activity of free (f) laccase (500ng/ml) (A) in the presence of DMP (0.06mM) as substrate and tyrosinase (500ng/ml) (B) also with DMP (0.06 mM) as substrate. The activity is shown as absorption intensity (left) and the wavelength (nm, right). The measurement was conducted 3 min after the substrate addition.

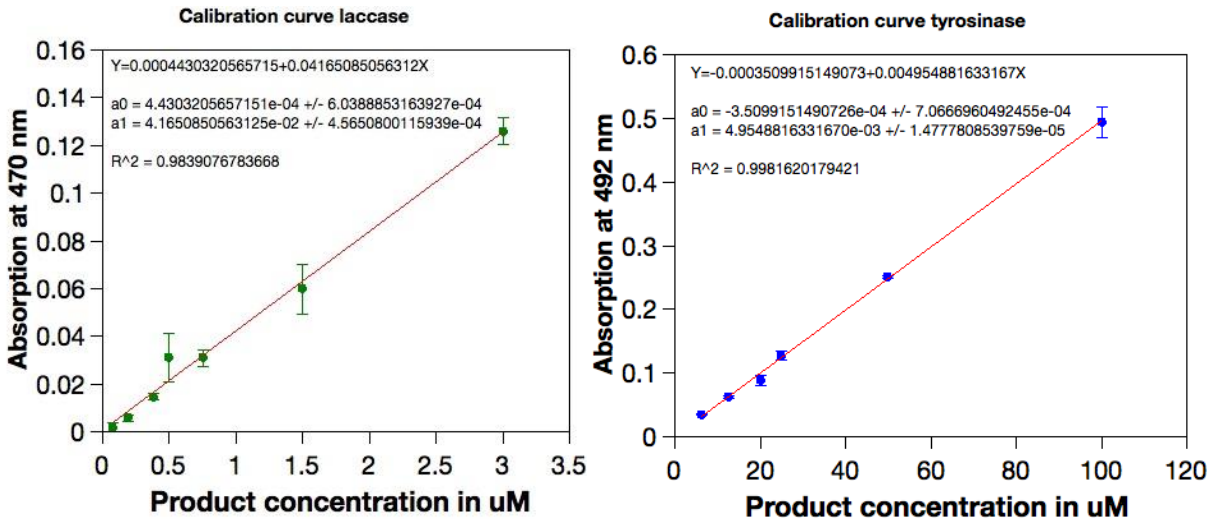

Figure A2. Calibration curves for enzymatic reactions. Left: Conversion of DMP by Laccase, Right: Conversion of 4-MP and subsequent reaction with MBTH by Tyrosinase.

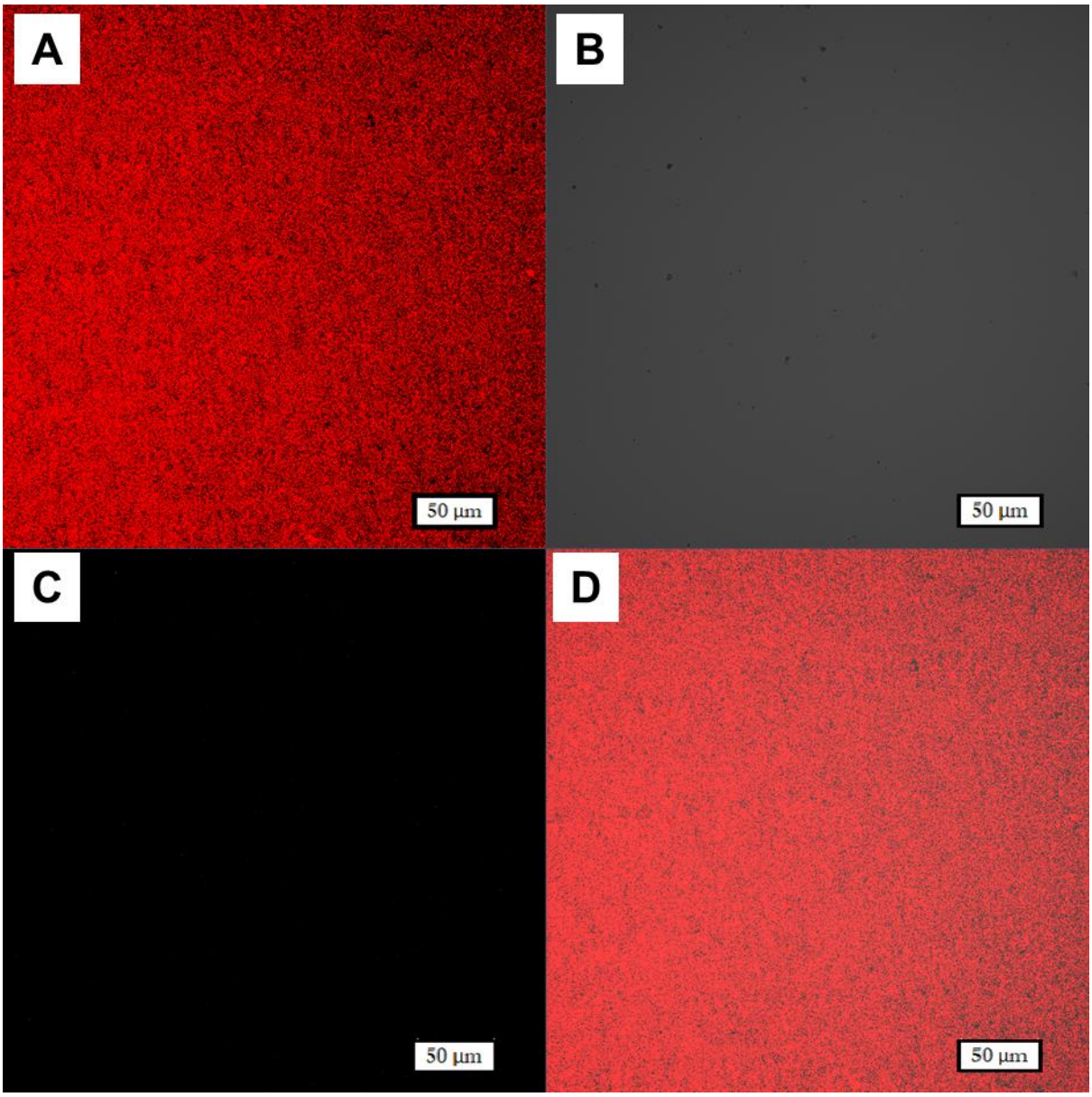

Figure A3. CLSM micrograph of a labelled $A_5B_{56}A_5$ membrane with the melittin/Alizarin Red S with A) labelled membrane (red), B) transmission channel, C) Alizarin Red S channel (green) and D) the combined channel for the labelled membrane and Alizarin Red S. The scalebar is the same for all images (50 µm).

7 References

1. Watson, H., Biological membranes. *Essays Biochem* 2015, *59*, 43-69.

2. Singer, S. J.; Nicolson, G. L., The Fluid Mosaic Model of the Structure of Cell Membranes. 1972, *175* (4023), 720-731.

3. Tanford, C., The Hydrophobic Effect. Formation of Micelles and Biological Membranes. *Science* 1974, *184* (4136), 559.

4. Lombard, J. J. B. D., Once upon a time the cell membranes: 175 years of cell boundary research. 2014, *9* (32).

5. Lehninger, A. L., Nelson, D. L. 1., Cox, M. M, *Lehninger principles of biochemistry*. New York ; New Delhi: W.H. Freeman 2008; Chapter 11, 372.

6. Cooper, G. M., The Cell: A Molecular Approach. *Sunderland (MA): Sinauer Associates* 2000, (2nd edition), 1.

7. Yin, H.; Flynn, A. D., Drugging Membrane Protein Interactions. *Annual review of biomedical engineering* 2016, *18*, 51-76.

8. Smith, J. S.; Kosusnik, A. R.; Mochel, J. P., A Retrospective Clinical Investigation of the Safety and Adverse Effects of Pantoprazole in Hospitalized Ruminants. *Frontiers in Veterinary Science* 2020, *7* (97).

9. Draghici, C.; Kowal, J.; Darjan, A.; Meier, W.; Palivan, C. G., "Active Surfaces" Formed by Immobilization of Enzymes on Solid-Supported Polymer Membranes. *Langmuir* 2014, *30* (39), 11660-11669.

10. Wah, T. Y., Nature-inspired membrane set to reduce purification costs. *Membrane Technology* 2016, *2016* (5), 7.

11. Messager, L.; Gaitzsch, J.; Chierico, L.; Battaglia, G., Novel aspects of encapsulation and delivery using polymersomes. *Current Opinion in Pharmacology* 2014, *18*, 104-111.

12. Letchford, K.; Burt, H., A review of the formation and classification of amphiphilic block copolymer nanoparticulate structures: micelles, nanospheres, nanocapsules and polymersomes. *Eur. J. Pharm. Biopharm.* 2007, *65* (3), 259-269.

13. Yorulmaz Avsar, S.; Kyropoulou, M.; Leone, S.; Schoenenberger, C.-A.; Meier, W.; Palivan, C., Biomolecules Turn Self-Assembling Amphiphilic Block Co-polymer Platforms Into Biomimetic Interfaces. *Frontiers in Chemistry* 2019, *6*, 645.

14. Klok, H.-A.; Lecommandoux, S., Supramolecular materials via block copolymer self-assembly. *Adv. Mater.* 2001, *13* (16), 1217-1229.

15. Kowal, J.; Zhang, X.; Dinu, I. A.; Palivan, C. G.; Meier, W., Planar Biomimetic Membranes Based on Amphiphilic Block Copolymers. *ACS Macro Lett.* 2014, *3* (1), 59-63.

16. Viktoria Mikhalevich, C. Z., Anja Car, Cornelia Palivan, Wolfgang Meier, *Bio-inspired polymers*. RSC: 2016; p 221-258.

17. Marguet, M.; Bonduelle, C.; Lecommandoux, S., Multicompartmentalized polymeric systems: towards biomimetic cellular structure and function. *Chem. Soc. Rev.* 2013, *42* (2), 512-529.

18. Zhang, X.; Tanner, P.; Graff, A.; Palivan, C. G.; Meier, W., Mimicking the cell membrane with block copolymer membranes. *J. Polym. Sci., Part A: Polym. Chem.* 2012, *50* (12), 2293-2318.

19. Bello, O. S.; Adegoke, K. A.; Oyewole, R. O., Biomimetic materials in our world: a review. *IOSR J. Appl. Chem.* 2013, *5* (3), 22-35, 14 pp.

20. Itel, F.; Najer, A.; Palivan, C. G.; Meier, W., Dynamics of membrane proteins within synthetic polymer membranes with large hydrophobic mismatch. *Nano Lett.* 2015, *15* (6), 3871-3878.

21. Chen, Q.; Schönherr, H.; Vancso, G. J., Mechanical properties of block copolymer vesicle membranes by atomic force microscopy. *Soft Matter* 2009, *5* (24), 4944-4950.

22. Jaskiewicz, K.; Larsen, A.; Lieberwirth, I.; Koynov, K.; Meier, W.; Fytas, G.; Kroeger, A.; Landfester, K., Probing Bioinspired Transport of Nanoparticles into Polymersomes. 2012, *51* (19), 4613-4617.

23. Jaskiewicz, K.; Makowski, M.; Kappl, M.; Landfester, K.; Kroeger, A., Mechanical Properties of Poly(dimethylsiloxane)-block-poly(2-methyloxazoline) Polymersomes Probed by Atomic Force Microscopy. *Langmuir* 2012, *28* (34), 12629-12636.

24. Garni, M.; Thamboo, S.; Schoenenberger, C.-A.; Palivan, C. G., Biopores/membrane proteins in synthetic polymer membranes. *Biochimica et Biophysica Acta (BBA) - Biomembranes* 2017, *1859* (4), 619-638.

25. Yan, Y.; Xiong, W.; Li, X.; Lu, T.; Huang, J.; Li, Z.; Fu, H., Molecular Packing Parameter in Bolaamphiphile Solutions: Adjustment of Aggregate Morphology by Modifying the Solution Conditions. *The Journal of Physical Chemistry B* 2007, *111* (9), 2225-2230.

26. Jagoda, A., Kowal, J. , Delcea, M. , Palivan, C. G., Meier, W., Polymer Vesicles on Surfaces. In *Biomaterials Surface Science*, A. Taubert, J. F. M. a. J. C. R. C., Ed. Wiley: 2013.

27. LoPresti, C.; Lomas, H.; Massignani, M.; Smart, T.; Battaglia, G., Polymersomes: nature inspired nanometer sized compartments. *J. Mater. Chem.* 2009, *19* (22), 3576-3590.

28. Egli, S.; Schlaad, H.; Bruns, N.; Meier, W., Functionalization of block copolymer vesicle surfaces. *Polymers* 2011, *3* (1), 252-280.

29. Hirano-Iwata, A.; Aoto, K.; Oshima, A.; Taira, T.; Yamaguchi, R.-t.; Kimura, Y.; Niwano, M., Free-Standing Lipid Bilayers in Silicon Chips−Membrane Stabilization Based on Microfabricated Apertures with a Nanometer-Scale Smoothness. *Langmuir* 2010, *26* (3), 1949-1952.

30. Housecroft, C. E.; Palivan, C. G.; Gademann, K.; Meier, W.; Calame, M.; Mikhalevich, V.; Zhang, X.; Piel, E.; Szponarski, M.; Wiesler, A.; Lanzilotto, A.; Constable, E. C.; Fanget, A.; Stoop, R. L., 'Active Surfaces' as Possible Functional Systems in Detection and Chemical (Bio) Reactivity. *CHIMIA International Journal for Chemistry* 2016, *70* (6), 402-412.

31. Zhang, X.; Fu, W.; Palivan, C. G.; Meier, W., Natural channel protein inserts and functions in a completely artificial, solid-supported bilayer membrane. *Scientific Reports* 2013, *3*, 2196.

32. Kowal, J. Ł.; Kowal, J. K.; Wu, D.; Stahlberg, H.; Palivan, C. G.; Meier, W. P., Functional surface engineering by nucleotide-modulated potassium channel insertion into polymer membranes attached to solid supports. *Biomaterials* 2014, *35* (26), 7286-7294.

33. Itel, F.; Chami, M.; Najer, A.; Lorcher, S.; Wu, D.; Dinu, I. A.; Meier, W., Molecular Organization and Dynamics in Polymersome Membranes: A Lateral Diffusion Study. *Macromolecules* 2014, *47* (21), 7588-7596.

34. Baumann, P.; Tanner, P.; Onaca, O.; Palivan, C. G., Bio-decorated polymer membranes: a new approach in diagnostics and therapeutics. *Polymers* 2011, *3* (1), 173-192.

35. Kim, Y.-R.; Jung, S.; Ryu, H.; Yoo, Y.-E.; Kim, S. M.; Jeon, T.-J., Synthetic biomimetic membranes and their sensor applications. *Sensors* 2012, *12*, 9530-9550.

36. Belegrinou, S.; Dorn, J.; Kreiter, M.; Kita-Tokarczyk, K.; Sinner, E.-K.; Meier, W., Biomimetic supported membranes from amphiphilic block copolymers. *Soft Matter* 2010, *6* (1), 179-186.

37. Krywko-Cendrowska, A.; di Leone, S.; Bina, M.; Yorulmaz-Avsar, S.; Palivan, C. G.; Meier, W., Recent Advances in Hybrid Biomimetic Polymer-Based Films: from Assembly to Applications. *Polymers (Basel)* 2020, *12* (5), Recent Advances in Hybrid Biomimetic Polymer-Based Films: from Assembly to Applications.

38. Puiggalí-Jou, A.; del Valle, L. J.; Alemán, C., Biomimetic hybrid membranes: incorporation of transport proteins/peptides into polymer supports. *Soft Matter* 2019, *15* (13), 2722-2736.

39. Edmondson, S.; Osborne, V. L.; Huck, W. T. S., Polymer brushes via surface-initiated polymerizations. *Chemical Society Reviews* 2004, *33* (1), 14-22.

40. Tabaei, S. R.; Vafaei, S.; Cho, N.-J., Fabrication of charged membranes by the solvent-assisted lipid bilayer (SALB) formation method on SiO2 and Al2O3. *Physical Chemistry Chemical Physics* 2015, *17* (17), 11546-11552.

41. Kowal, J.; Wu, D.; Mikhalevich, V.; Palivan, C. G.; Meier, W., Hybrid Polymer–Lipid Films as Platforms for Directed Membrane Protein Insertion. *Langmuir* 2015, *31* (17), 4868-4877.

42. Langmuir, I., THE CONSTITUTION AND FUNDAMENTAL PROPERTIES OF SOLIDS AND LIQUIDS. II. LIQUIDS.1. *Journal of the American Chemical Society* 1917, *39* (9), 1848-1906.

43. Langmuir, I., The mechanism of the surface phenomena of flotation. *Transactions of the Faraday Society* 1920, *15* (June), 62-74.

44. Ariga, K.; Yamauchi, Y.; Mori, T.; Hill, J. P., 25th Anniversary Article: What Can Be Done with the Langmuir-Blodgett Method? Recent Developments and its Critical Role in Materials Science. *Advanced Materials* 2013, *25* (45), 6477-6512.

45. Dynarowicz-Łątka, P.; Dhanabalan, A.; Oliveira, O. N., Modern physicochemical research on Langmuir monolayers. *Advances in Colloid and Interface Science* 2001, *91* (2), 221-293.

46. Ybert, C.; Lu, W.; Möller, G.; Knobler, C. M., Collapse of a Monolayer by Three Mechanisms. *The Journal of Physical Chemistry B* 2002, *106* (8), 2004-2008.

47. Peterson, I. R., Langmuir-Blodgett films. *Journal of Physics D: Applied Physics* 1990, *23* (4), 379.

48. Daear, W.; Mahadeo, M.; Prenner, E. J., Applications of Brewster angle microscopy from biological materials to biological systems. *Biochimica et Biophysica Acta (BBA) - Biomembranes* 2017, *1859* (10), 1749-1766.

49. Hoenig, D.; Moebius, D., Direct visualization of monolayers at the air-water interface by Brewster angle microscopy. *The Journal of Physical Chemistry* 1991, *95* (12), 4590-4592.

50. Hénon, S.; Meunier, J., Microscope at the Brewster angle: Direct observation of first-order phase transitions in monolayers. *Review of Scientific Instruments* 1991, *62*, 936-939.

51. Meunier, J., Why a Brewster angle microscope? *Colloids and Surfaces A: Physicochemical and Engineering Aspects* 2000, *171* (1), 33-40.

52. Ogieglo, W.; Wormeester, H.; Eichhorn, K.-J.; Wessling, M.; Benes, N. E., In situ ellipsometry studies on swelling of thin polymer films: A review. *Progress in Polymer Science* 2015, *42*, 42-78.

53. https://www.pi1.uni-stuttgart.de/research/methods_overview/ellipsometry/. (accessed 14.06.2020, 16:11p.m.).

54. Negara, C., *Fast Polarization State Detection by Division-of-Amplitude in a Simple Configuration Setup*. 2016.

55. Binnig, G.; Quate, C. F.; Gerber, C., Atomic Force Microscope. *Physical Review Letters* 1986, *56* (9), 930-933.

56. Gerber, C.; Lang, H. P., How the doors to the nanoworld were opened. *Nature Nanotechnology* 2006, *1* (1), 3-5.

57. Dufrêne, Y. F.; Ando, T.; Garcia, R.; Alsteens, D.; Martinez-Martin, D.; Engel, A.; Gerber, C.; Müller, D. J., Imaging modes of atomic force microscopy for application in molecular and cell biology. *Nature Nanotechnology* 2017, *12* (4), 295-307.

58. Möller, C.; Allen, M.; Elings, V.; Engel, A.; Müller, D. J., Tapping-Mode Atomic Force Microscopy Produces Faithful High-Resolution Images of Protein Surfaces. *Biophysical Journal* 1999, *77* (2), 1150-1158.

59. Tomasz Tański, B. Z., Paweł Jarka and Marcin Staszuk, Introductory Chapter: Why Atomic Force Microscopy (AFM) is One of the Leading Methods of Surface Morphology Research of all Engineering Material Groups, Atomic-force Microscopy and Its Applications. *IntechOpen* 2018.

60. Sauerbrey, G., Verwendung von Schwingquarzen zur Wägung dünner Schichten und zur Mikrowägung. *Zeitschrift für Physik* 1959, *155* (2), 206-222.

61. Nomura, T.; Okuhara, M., Frequency shifts of piezoelectric quartz crystals immersed in organic liquids. *Analytica Chimica Acta* 1982, *142*, 281-284.

62. Liu, G.; Zhang, G., Basic Principles of QCM-D. In *QCM-D Studies on Polymer Behavior at Interfaces*, Liu, G.; Zhang, G., Eds. Springer Berlin Heidelberg: Berlin, Heidelberg, 2013; pp 1-8.

63. Sakai, K., Quartz Crystal Microbalance with Dissipation Monitoring (QCM-D). In *Measurement Techniques and Practices of Colloid and Interface Phenomena*, Abe, M., Ed. Springer Singapore: Singapore, 2019; pp 45-50.

64. Meiron, T. S.; Marmur, A.; Saguy, I. S., Contact angle measurement on rough surfaces. *Journal of Colloid and Interface Science* 2004, *274* (2), 637-644.

65. Huhtamäki, T.; Tian, X.; Korhonen, J. T.; Ras, R. H. A., Surface-wetting characterization using contact-angle measurements. *Nature Protocols* 2018, *13* (7), 1521-1538.

66. Teng, X.; Li, F.; Lu, C., Visualization of materials using the confocal laser scanning microscopy technique. *Chemical Society Reviews* 2020, *49* (8), 2408-2425.

67. Mallya, L.; Mala, K.; Jathanna, V., Confocal LASER Scanning Microscopy (CLSM) for Evaluation of Endodontic Microflora-A Review. *Indian Journal of Public Health Research & Development* 2019, *10*, 69.

68. Lomora, M.; Itel, F.; Dinu, I. A.; Palivan, C. G., Selective ion-permeable membranes by insertion of biopores into polymersomes. *Phys. Chem. Chem. Phys.* 2015, *17* (24), 15538-15546.

69. Wang, H.; Chung, T. S.; Tong, Y. W.; Jeyaseelan, K.; Armugam, A.; Chen, Z.; Hong, M.; Meier, W., Highly Permeable and Selective Pore-Spanning Biomimetic Membrane Embedded with Aquaporin Z. *Small* 2012, *8* (8), 1185-1190.

70. Duong, P. H.; Chung, T.-S.; Jeyaseelan, K.; Armugam, A.; Chen, Z.; Yang, J.; Hong, M., Planar biomimetic aquaporin-incorporated triblock copolymer membranes on porous alumina supports for nanofiltration. *Journal of Membrane Science* 2012, *409*, 34-43.

71. Balasubramanian, V.; Herranz-Blanco, B.; Almeida, P. V.; Hirvonen, J.; Santos, H. A., Multifaceted polymersome platforms: Spanning from self-assembly to drug delivery and protocells. *Progress in Polymer Science* 2016, *60*, 51-85.

72. Hammer, D. A.; Kamat, N. P., Towards an artificial cell. *FEBS Lett* 2012, *586*.

73. Adhikari, B.; Majumdar, S., Polymers in sensor applications. *Progress in Polymer Science* 2004, *29* (7), 699-766.

74. Draghici, C.; Mikhalevich, V.; Gunkel-Grabole, G.; Kowal, J.; Meier, W.; Palivan, C. G., Biomimetic Planar Polymer Membranes Decorated with Enzymes as Functional Surfaces. *Langmuir* 2018, *34* (30), 9015-9024.

75. Idrissi, M. E.; Meyer, C. E.; Zartner, L.; Meier, W., Nanosensors based on polymer vesicles and planar membranes: a short review. *Journal of Nanobiotechnology* 2018, *16*, 63.

76. Kim, Y.-R.; Jung, S.; Ryu, H.; Yoo, Y.-E.; Kim, S. M.; Jeon, T.-J., Synthetic Biomimetic Membranes and Their Sensor Applications. *Sensors (Basel, Switzerland)* 2012, *12* (7), 9530-9550.

77. Jung, S.-H.; Choi, S.; Kim, Y.-R.; Jeon, T.-J., Storable droplet interface lipid bilayers for cell-free ion channel studies. *Bioprocess and Biosystems Engineering* 2012, *35* (1), 241-246.

78. William W. Anku, M. A. M. a. P. P. G., Phenolic Compounds in Water: Sources, Reactivity, Toxicity and Treatment Methods, Phenolic Compounds - Natural Sources, Importance and Applications. *IntechOpen* 2017.

79. Villegas, L. G. C.; Mashhadi, N.; Chen, M.; Mukherjee, D.; Taylor, K. E.; Biswas, N., A Short Review of Techniques for Phenol Removal from Wastewater. *Curr. Pollut. Rep.* 2016, *2* (3), 157-167.

80. Janusz, G.; Pawlik, A.; Świderska-Burek, U.; Polak, J.; Sulej, J.; Jarosz-Wilkołazka, A.; Paszczyński, A., Laccase Properties, Physiological Functions, and Evolution. *Int J Mol Sci* 2020, *21* (3), 966.

81. Yoon, J.; Fujii, S.; Solomon, E. I., Geometric and electronic structure differences between the type 3 copper sites of the multicopper oxidases and hemocyanin/tyrosinase. *Proceedings of the National Academy of Sciences* 2009, *106* (16), 6585.

82. Zolghadri, S.; Bahrami, A.; Hassan Khan, M. T.; Munoz-Munoz, J.; Garcia-Molina, F.; Garcia-Canovas, F.; Saboury, A. A., A comprehensive review on tyrosinase inhibitors. *J Enzyme Inhib Med Chem* 2019, *34* (1), 279-309.

83. Kim, J. H.; Lim, S. Y.; Nam, D. H.; Ryu, J.; Ku, S. H.; Park, C. B., Self-assembled, photoluminescent peptide hydrogel as a versatile platform for enzyme-based optical biosensors. *Biosens. Bioelectron.* 2011, *26* (5), 1860-1865.

84. Pang, R.; Li, M.; Zhang, C., Degradation of phenolic compounds by laccase immobilized on carbon nanomaterials: Diffusional limitation investigation. *Talanta* 2015, *131*, 38-45.

85. Qu, Y.; Ma, M.; Wang, Z.; Zhan, G.; Li, B.; Wang, X.; Fang, H.; Zhang, H.; Li, C., Sensitive amperometric biosensor for phenolic compounds based on graphene–silk peptide/tyrosinase composite nanointerface. *Biosens. Bioelectron.* 2013, *44*, 85-88.

86. Hanifah, A. S.; Lee, Y.; Musa, A., Effects of Gold Nanoparticles on the Response of Phenol Biosensor Containing Photocurable Membrane with Tyrosinase. *Sensors* 2008, *8* (10), 6407.

87. Cabaj, J.; Sołoducho, J.; Chyla, A.; Bryjak, J.; Zynek, K., The characterization of ordered thin films built of immobilized phenoloxidases. *Sens. Actuators, B* 2009, *136* (2), 425-431.

88. Cabaj, J.; Sołoducho, J.; Świst, A., Active Langmuir–Schaefer films of tyrosinase—Characteristic. *Sens. Actuators, B* 2010, *150* (2), 505-512.

89. Cabaj, J.; Sołoducho, J.; Nowakowska-Oleksy, A., Langmuir–Blodgett film based biosensor for estimation of phenol derivatives. *Sens. Actuators, B* 2010, *143* (2), 508-515.

90. Böyükbayram, A. E.; Kıralp, S.; Toppare, L.; Yağcı, Y., Preparation of biosensors by immobilization of polyphenol oxidase in conducting copolymers and their use in determination of phenolic compounds in red wine. *Bioelectrochemistry* 2006, *69* (2), 164-171.

91. Ameer, Q.; Adeloju, S. B., Development of a potentiometric catechol biosensor by entrapment of tyrosinase within polypyrrole film. *Sens. Actuators, B* 2009, *140* (1), 5-11.

92. Pavinatto, F. J.; Fernandes, E. G. R.; Alessio, P.; Constantino, C. J. L.; de Saja, J. A.; Zucolotto, V.; Apetrei, C.; Oliveira Jr, O. N.; Rodriguez-Mendez, M. L., Optimized architecture for

Tyrosinase-containing Langmuir-Blodgett films to detect pyrogallol. *Journal of Materials Chemistry* 2011, *21* (13), 4995-5003.

93. Apetrei, C.; Rodríguez-Méndez, M. L.; De Saja, J. A., Amperometric tyrosinase based biosensor using an electropolymerized phosphate-doped polypyrrole film as an immobilization support. Application for detection of phenolic compounds. *Electrochimica Acta* 2011, *56* (24), 8919-8925.

94. Govindhan, M.; Lafleur, T.; Adhikari, B.-R.; Chen, A., Electrochemical Sensor Based on Carbon Nanotubes for the Simultaneous Detection of Phenolic Pollutants. *Electroanalysis* 2015, *27* (4), 902-909.

95. Benítez-Martínez, S.; Valcárcel, M., Graphene quantum dots as sensor for phenols in olive oil. *Sens. Actuators, B* 2014, *197*, 350-357.

96. Rodríguez-Delgado, M. M.; Alemán-Nava, G. S.; Rodríguez-Delgado, J. M.; Dieck-Assad, G.; Martínez-Chapa, S. O.; Barceló, D.; Parra, R., Laccase-based biosensors for detection of phenolic compounds. *TrAC, Trends Anal. Chem.* 2015, *74*, 21-45.

97. Matter, Y.; Enea, R.; Casse, O.; Lee, C. C.; Baryza, J.; Meier, W., Amphiphilic PEG-b-PMCL-b-PDMAEMA Triblock Copolymers: From Synthesis to Physico-Chemistry of Self-Assembled Structures. *Macromol. Chem. Phys.* 2011, *212* (9), 937-949.

98. Vogt, B. D.; Lin, E. K.; Wu, W.-l.; White, C. C., Effect of Film Thickness on the Validity of the Sauerbrey Equation for Hydrated Polyelectrolyte Films. *J. Phys. Chem. B* 2004, *108* (34), 12685-12690.

99. Gunkel, G.; Huck, W. T. S., Cooperative Adsorption of Lipoprotein Phospholipids, Triglycerides, and Cholesteryl Esters Are a Key Factor in Nonspecific Adsorption from Blood Plasma to Antifouling Polymer Surfaces. *J. Am. Chem. Soc.* 2013, *135* (18), 7047-7052.

100. Qiu, H.; Xu, C.; Huang, X.; Ding, Y.; Qu, Y.; Gao, P., Immobilization of Laccase on Nanoporous Gold: Comparative Studies on the Immobilization Strategies and the Particle Size Effects. *J. Phys. Chem. C* 2009, *113* (6), 2521-2525.

101. Haefele, T.; Kita-Tokarczyk, K.; Meier, W., Phase Behavior of Mixed Langmuir Monolayers from Amphiphilic Block Copolymers and an Antimicrobial Peptide. *Langmuir* 2006, *22* (3), 1164-1172.

102. Vasquez, D.; Einfalt, T.; Meier, W.; Palivan, C. G., Asymmetric Triblock Copolymer Nanocarriers for Controlled Localization and pH-Sensitive Release of Proteins. *Langmuir* 2016, *32* (40), 10235-10243.

103. Kita-Tokarczyk, K.; Junginger, M.; Belegrinou, S.; Taubert, A., Amphiphilic Polymers at Interfaces. In *Self Organized Nanostructures of Amphiphilic Block Copolymers II*, Müller, A. H. E.; Borisov, O., Eds. Springer Berlin Heidelberg: Berlin, Heidelberg, 2011; pp 151-201.

104. Förch, R.; Schönherr, H.; Jenkins, A. T. A., *Surface design: applications in bioscience and nanotechnology*. John Wiley & Sons: 2009.

105. Raposo, M.; Ferreira, Q.; Ribeiro, P., A guide for atomic force microscopy analysis of soft-condensed matter. *Modern research and educational topics in microscopy* 2007, *1*, 758-769.

106. Girard-Egrot, A. P.; Godoy, S.; Blum, L. J., Enzyme association with lipidic Langmuir–Blodgett films: Interests and applications in nanobioscience. *Adv. Colloid Interface Sci.* 2005, *116* (1), 205-225.

107. Piontek, K.; Antorini, M.; Choinowski, T., Crystal Structure of a Laccase from the FungusTrametes versicolor at 1.90-Å Resolution Containing a Full Complement of Coppers. *J. Biol. Chem.* 2002, *277* (40), 37663-37669.

108. Ismaya, W. T.; Rozeboom, H. J.; Weijn, A.; Mes, J. J.; Fusetti, F.; Wichers, H. J.; Dijkstra, B. W., Crystal Structure of Agaricus bisporus Mushroom Tyrosinase: Identity of the Tetramer Subunits and Interaction with Tropolone. *Biochemistry* 2011, *50* (24), 5477-5486.

109. Reviakine, I.; Johannsmann, D.; Richter, R. P., Hearing What You Cannot See and Visualizing What You Hear: Interpreting Quartz Crystal Microbalance Data from Solvated Interfaces. *Anal. Chem.* 2011, *83* (23), 8838-8848.

110. Mazur, M.; Krysiński, P.; Michota-Kamińska, A.; Bukowska, J.; Rogalski, J.; Blanchard, G. J., Immobilization of laccase on gold, silver and indium tin oxide by zirconium–phosphonate–carboxylate (ZPC) coordination chemistry. *Bioelectrochemistry* 2007, *71* (1), 15-22.

111. Mahltig, B.; Gohy, J.-F.; Antoun, S.; Jérôme, R.; Stamm, M., Adsorption and structure formation of the weak polyelectrolytic diblock copolymer, PVP-b-PDMAEMA. *Colloid Polym. Sci.* 2002, *280* (6), 495-502.

112. Espín, J. C.; varon-castellanos, R.; Tudela, J.; Canovas, G., *Kinetic study of the oxidation of 4-hydroxyanisole catalyzed by tyrosinase*. 1997; Vol. 41, p 1265-76.

113. Kudanga, T.; Nemadziva, B.; Le Roes-Hill, M., Laccase catalysis for the synthesis of bioactive compounds. *Appl. Microbiol. Biotechnol.* 2017, *101* (1), 13-33.

114. http://www.aquaporin.dk/, 02.02.2016, 10:38.

115. http://www.sterlitech.com/membrane-process-development/flat-sheet-membranes/forward-osmosis-membranes.html, 02.02.2016,10:40.

116. Welch, M. E.; Doublet, T.; Bernard, C.; Malliaras, G. G.; Ober, C. K., A glucose sensor via stable immobilization of the GOx enzyme on an organic transistor using a polymer brush. *J. Polym. Sci., Part A: Polym. Chem.* 2015, *53* (2), 372-377.

117. Zhang, X.; Fu, W.; Palivan, C. G.; Meier, W., Natural channel protein inserts and functions in a completely artificial, solid-supported bilayer membrane. *Scientific Reports* 2013, *3* (1), 2196.

118. Mikhalevich, V.; Zelmer, C.; Car, A.; Palivan, C.; Meier, W., Chapter 6 Bio-inspired Polymer Membranes. In *Bio-inspired Polymers*, The Royal Society of Chemistry: 2017; pp 221-258.

119. Habermann, E., Bee and Wasp Venoms. *Science* 1972, *177* (4046), 314-322.

120. Lee, M.-T.; Sun, T.-L.; Hung, W.-C.; Huang, H. W., Process of inducing pores in membranes by melittin. *Proceedings of the National Academy of Sciences* 2013, *110* (35), 14243-14248.

121. Lin, J.-H.; Baumgaertner, A., Stability of a Melittin Pore in a Lipid Bilayer: A Molecular Dynamics Study. *Biophysical Journal* 2000, *78* (4), 1714-1724.

122. Terwilliger, T. C.; Weissman, L.; Eisenberg, D., The structure of melittin in the form I crystals and its implication for melittin's lytic and surface activities. *Biophys J* 1982, *37* (1), 353-61.

123. Unwin, A. P.; Hine, P. J.; Ward, I. M.; Fujita, M.; Tanaka, E.; Gusev, A. A., Templated Assembly of Pore-forming Peptides in Lipid Membranes. *Chimia (Aarau)* 2019, *73* (1), 59.

124. Lomora, M.; Garni, M.; Itel, F.; Tanner, P.; Spulber, M.; Palivan, C. G., Polymersomes with engineered ion selective permeability as stimuli-responsive nanocompartments with preserved architecture. *Biomaterials* 2015, *53*, 406-14.

125. Najer, A.; Wu, D.; Bieri, A.; Brand, F.; Palivan, C. G.; Beck, H.-P.; Meier, W., Nanomimics of Host Cell Membranes Block Invasion and Expose Invasive Malaria Parasites. *ACS Nano* 2014, *8* (12), 12560-12571.

126. Lörcher, S.; Meier, W., Cosolvent fractionation of PMOXA-b-PDMS-b-PMOXA: Bulk separation of triblocks from multiblocks. *European Polymer Journal* 2017, *88*, 575-585.

127. Nardin, C.; Hirt, T.; Leukel, J.; Meier, W., Polymerized ABA Triblock Copolymer Vesicles. *Langmuir* 2000, *16* (3), 1035-1041.

128. Terwilliger, T. C.; Eisenberg, D., The structure of melittin. I. Structure determination and partial refinement. *J. Biol. Chem.* 1982, *257* (11), 6010-6015.

129. Haldar, S.; Raghuraman, H.; Chattopadhyay, A., Monitoring Orientation and Dynamics of Membrane-Bound Melittin Utilizing Dansyl Fluorescence. *J. Phys. Chem. B* 2008, *112* (44), 14075-14082.

130. Popplewell, J.; Swann, M.; Freeman, N.; McDonnell, C.; Ford, R., Quantifying the effects of melittin on liposomes. *Biochim. Biophys. Acta (BBA) - Biomembranes* 2007, *1768* (1), 13-20.

131. Allende, D.; Simon, S.; McIntosh, T. J., Melittin-induced bilayer leakage depends on lipid material properties: evidence for toroidal pores. *Biophys. J.* 2005, *88* (3), 1828-1837.

132. Yorulmaz, S.; Jackman, J. A.; Hunziker, W.; Cho, N.-J., Supported Lipid Bilayer Platform To Test Inhibitors of the Membrane Attack Complex: Insights into Biomacromolecular Assembly and Regulation. *Biomacromolecules* 2015, *16* (11), 3594-3602.

133. Springsteen, G.; Wang, B., Alizarin Red S. as a general optical reporter for studying the binding of boronic acids with carbohydrates. *Chem. Commun.* 2001, (17), 1608-1609.

134. Belluati, A.; Mikhalevich, V.; Yorulmaz Avsar, S.; Daubian, D.; Craciun, I.; Chami, M.; Meier, W. P.; Palivan, C. G., How Do the Properties of Amphiphilic Polymer Membranes Influence the Functional Insertion of Peptide Pores? *Biomacromolecules* 2020, *21* (2), 701-715.